THIXOTROPIC-VISCOELASTIC RHEOLOGICAL FINGERPRINTS IN LARGE AMPLITUDE OSCILLATORY SHEAR

BY

BRENDAN C. BLACKWELL

THESIS

Submitted in partial fulfillment of the requirements
for the degree of Master of Science in Mechanical Engineering
in the Graduate College of the
University of Illinois at Urbana-Champaign, 2013

Urbana, Illinois

Adviser:

Professor Randy H. Ewoldt

Abstract

In this work we demonstrate the use of large-amplitude oscillatory shear (LAOS) as a tool to characterize the behavior of constitutive models that exhibit both thixotropic and viscoelastic phenomena. We demonstrate this use of LAOS by first examining the strain controlled LAOS (LAOStrain) response of a Thixoelastic Jeffreys model. First, this canonical model is defined for capturing both viscoelasticity and thixotropy with a minimum number of model parameters. Then the use of LAOS is demonstrated as we explore this model response as a function of four dimensionless parameters: two LAOStrain deformation parameters (the Deborah number and the Wiessenberg number) and two material parameters (the ratio of viscoelastic to thixotropic timescales and the ratio of solvent viscosity to aggregate viscosity).

We present an analytical solution for the asymptotic nonlinearities of this model in LAOS, as well as numerical results for the full nonlinearities. We present these results in a manner that eases the challenges of visualizing a response to four independent parameters. This canonical thixotropic-viscoelastic constitutive model, containing the minimum number of parameters required to capture both thixotropic and viscoelastic phenomena, predicts that short thixotropic timescales can be experimentally observed with nonlinear oscillatory deformation. This is relevant to recent suggestions in classifying thixotropic versus “simple” yield stress fluids with no observable thixotropy.

Having established the signature of the simplest model that exhibits the features of interest, we then proceed to make two modifications, focusing on the fundamental characteristics of the kinetic rate equation. Expanding on the minimalist constitutive model that contains only

five material parameters, we first examine the distinct rheological material function signatures produced when kinetic structure breakdown is dictated either by stress or by strain rate. We compare and contrast the behavior of these closely related models using asymptotic nonlinearities in LAOS. We also explore the differences between model responses in LAOStrain and in controlled stress oscillations (LAOStress). We then observe the effects of a sixth model parameter (the most common addition to simple models in the literature), introduced to govern the order of reaction of the kinetic rate equation. Finally, we give broader context as to where these models fit into the bigger picture by presenting a chart that summarizes models that are commonly used to describe yield-stress fluids in the literature.

Overall, we show that LAOS provides a useful fingerprint for these thixotropic and viscoelastic models. Our analysis of the Thixoelastic Jeffreys model indicates that asymptotic scaling with respect to the amplitude of the input signal can identify the order of reaction. Furthermore it suggests that the amplitude-intrinsic nonlinearities are capable of identifying timescales that cannot be observed by step tests due to experimental limitations. Ultimately, these data can be used to inform constitutive model selection and therefore improve the accuracy of flow modeling of thixotropic viscoelastic fluids.

Table of Contents

Chapter 1

Introduction

The phenomenon of thixotropy first appeared in the literature in 1923 [1], originally defined as a reversible transition from a solid to a liquid induced by physical agitation. Current definitions identify thixotropy as a time-dependence of microstructure that ties viscosity to flow history, commonly using the terms ‘aging’ (increase in viscosity as the fluid lies undisturbed) and ‘rejuvenation’ (increase in fluidity as the fluid is sheared) [1]. Fluids that exhibit thixotropy have been studied in relation to many different applications, including medicine [2–5], biology [6,7], and manufacturing [8,9]. Much current study is devoted to experimental observation of microstructural evolution during thixotropic transients [10–12]. Thixotropic models may also be the key to conquering unsolved problems in modeling yield stress fluids [13,14]. These fluids are commonly modeled by coupling a tensorial rheological constitutive equation to a scalar variable to track the ‘structure’ of the fluid with the structure evolving by a kinetic rate equation. A precursor to this type of constitutive model was introduced by Goodeve in 1938 [15], while the earliest example to take the currently common form was proposed by Moore in 1959 [16]. Since then a multitude of unique constitutive models have been written and much study has been devoted to understanding thixotropy, connecting microstructural behavior to macro level properties, and accurately modeling rheological phenomena on a continuum level.

Thixotropy is closely related to yield-stress fluids. The general problem of accurately modeling yield-stress fluids remains difficult in part due to the interplay of thixotropy and the yield stress [13]. Recent work used thixotropic timescales to distinguish the two categories of

"thixotropic" and "simple" yield-stress fluids, defining simple yield-stress fluids as those without thixotropy (aging or rejuvenation) in response to step inputs [17]. This categorization has proved useful in several other works, such as those exploring shear banding [18–23], and helps frame some of the remaining unanswered questions about yield stress fluids [24]. However, a definition based on the presence or absence of observable thixotropy does not account for thixotropic timescales shorter than can be imposed as a step on a rheometer. Yet, many interesting flows and processes (e.g. fluid droplet impacts) take place on shorter timescales. It is therefore important to consider the existence of thixotropic timescales even when they are too short for standard measurement techniques to detect, or difficult to distinguish from viscoelastic timescales. In this work, we will show that the canonical Thixoelastic Jeffreys model we define in Chapter 2 predicts a possibility of measuring very short timescales using asymptotic LAOStrain.

In creating this model we strive to write the simplest possible expression that captures the features of interest. By identifying and exploring the minimalist form of a model that captures the phenomena of both thixotropy and viscoelasticity we seek to characterize and understand the fundamental trends of this diverse class of constitutive models, thereby gaining insight into material behavior, and also anchoring future exploration of more complex models. Having selected our simplest possible constitutive model, we proceed to probe this model first by subjecting it to simplified input flows. We consider steady simple shear flow (which is nonlinear, but lacks transients) as well as linear viscoelastic oscillatory shear (which is transient, but lacks nonlinearities). These simple tests will prove insufficient to fit all of the model parameters or fully characterize the behavior of the model. A test that is both transient and nonlinear is required, and we will demonstrate that large-amplitude oscillatory shear (LAOS) is a promising option. Specifically, LAOS performs a more systematic exploration of the deformation space

than step tests [25], and experimentally lends the ability to probe shorter thixotropic timescales than step tests because a short timescale oscillatory input is easier to experimentally apply than a step input.

After exploring the simplest form of our canonical model, we will explore two variations that are representative of common types of more complex thixotropic constitutive models. We will examine the consequences of whether kinetic structure breakdown is dictated by stress or by strain rate, as well as the addition of a sixth model parameter that governs the order of reaction of structure breakdown. We will use the rheological fingerprints of asymptotic nonlinearities to compare the responses of these model variations to the canonical form. These two modifications serve as an example of how the signatures we employ here can be used to characterize and compare further alterations and more complex variants of thixotropic models.

Finally, we give this exploration a broader context by surveying the constitutive modeling of yield stress fluids. Many different constitutive models are in common use in the study of yield stress fluids, yet there remain unsolved problems, and flows for which no constitutive model has accurately predicted experimentally observations. We present a summary chart that details a representative sampling of models that are applied to yield stress fluids in the literature, including various thixotropic models that are similar the Thixoelastic Jeffreys model.

Chapter 2

Thixoelastic Jeffreys Model Definition – Simplest Form

Moore's kinetic structure equation

$$\frac{d\xi}{dt} = \kappa_A(1-\xi) - \kappa_D\xi\,|\dot{\gamma}\,| \tag{1}$$

serves as a base case for more complex models. Many subsequent models use more complex kinetic equations, but most can be characterized as a modification of this simplest form (through the addition of another term or the inclusions of a power-function exponent to an existing term). To limit the number of model parameters, in this work we will exclusively examine the simplest first-order kinetic equation [16]. We use the variable ξ for the dimensionless structure parameter. (The variable λ is commonly used for the structure parameter in the literature [1], however we reserve this for the viscoelastic relaxation time.) The form of Eq. (1) bounds ξ between zero and one. Some models allow ξ to grow unbounded [26], but employing finite limits on the structure parameter is more common. Different exponents (orders of reaction) can also be considered [27–30].

Equation (1) contains two thixotropic timescales: the destruction timescale $|\kappa_D\dot{\gamma}_0|^{-1}$ and the aggregation timescale κ_A^{-1}. While the earliest thixotropic constitutive models were all purely viscous, a convenient framework for incorporating elasticity, and a viscoelastic timescale λ, was detailed by Quemada in 1999 [31]. The model that we examine in depth in this work is a reframing of Quemada's model, which we will call the Thixoelastic Jeffreys model. For our

constitutive model we employ a 3-element viscoelastic fluid model, the simplest viscoelastic fluid model with both a relaxation timescale and a retardation timescale. We write this as a solvent viscosity in parallel with a viscoelastic Maxwell element (Figure 1).

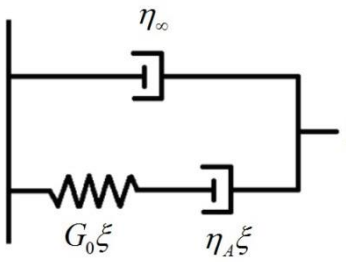

Figure 1 Diagram of the canonical 3-element viscoelastic thixotropic fluid

The solvent viscosity is assumed constant, whereas the elasticity and the viscosity of the Maxwell element are dependent upon the structure parameter. The abstraction of a Maxwell element represents viscoelastic behavior that could arise from various material classes, such as associating polymers, aggregating colloids, evolving droplets, or other structures that result in viscoelastic fluid behaviors. Of course, a superposition of multiple relaxation times can be used to generalize the model show in Figure 1, but here we consider the fundamental features of a single relaxation timescale, $\lambda_1 = \eta_A / G_0$, and a single retardation timescale $\lambda_2 = \lambda_1 \eta_\infty / \left(\eta_\infty + \eta_A \xi \right)$. It is worth noting that the relaxation timescale is not dependent upon the structure (both the modulus and viscosity have the same dependence on the structure, hence it cancels out), while the retardation timescale does change with changing ξ. A similar model has recently been explored by de Souza Mendes, in his work employing a larger number of parameters and more complex functional dependencies [32]. An alternative method to include elastic effects is to independently track elastic strain [27,30]. Again in order to keep the number of model parameters manageable and explore the most fundamental trends, we employ only the

three-element fluid to track elasticity, and we choose the simplest forms for the functional dependence of rheological model parameters on the structure parameter (linear dependence with a constant coefficient). More complex variants present potential for future study.

The canonical model of Figure 1 results in the constitutive equation

$$\frac{\dot{\sigma}}{G_0} + \frac{\sigma}{\eta_A} = \left(\xi + \frac{\eta_\infty}{\eta_A} \right) \dot{\gamma} + \frac{\eta_\infty}{G_0} \ddot{\gamma} \tag{2}$$

which couples with Eq. (1) to fully define the response. The above representation gives the constitutive equation in scalar form, which is tantamount to assuming one-dimensional homogeneous shear flow. Derivatives in this one-dimensional representation are with respect to dimensional time.

Various approaches to writing constitutive laws in three-dimensional form have been explored in the literature. Several models maintain the structure parameter as a scalar, employing a material derivative in the kinetic equation, Eq (1). Purely viscous models (without elasticity) that take this approach simply couple the structure to a tensor representation of a generalized Newtonian fluid [29,33,34], while other scalar structure models have employed an upper-convected Maxwell constitutive equation to incorporate viscoelasticity [35,36]. Several others choose to represent the structure itself as a tensor, employing a corotational [37,38] or Gordon-Schowalter [39] derivative in the kinetic equation. We continue to strive for simplicity in writing our model, so we elect to follow a path similar to that detailed by Bautista [35], tracking the structure as a scalar with a material derivative, and achieving material-frame invariance in our constitutive equation with upper convected time derivatives. The three dimensional representation is therefore

$$\frac{D\xi}{Dt} = \kappa_A(1-\xi) - \kappa_D \xi \,|\, \dot{\gamma} \,| \tag{3}$$

$$\frac{\underline{\underline{\sigma}}_{(1)}}{G_0} + \frac{\underline{\underline{\sigma}}}{\eta_A} = \left(\xi + \frac{\eta_\infty}{\eta_A} \right) \underline{\underline{\gamma}}_{(1)} + \frac{\eta_\infty}{G_0} \underline{\underline{\gamma}}_{(2)} \tag{4}$$

where $\dot{\gamma}$ is the second invariant of the rate of strain tensor $\underline{\underline{\gamma}}_{(1)} = \underline{\nabla v} + \left(\underline{\nabla v}\right)^{\mathrm{T}}$,

$$\dot{\gamma} = \sqrt{\frac{1}{2} \sum_i \sum_j \dot{\gamma}_{ij} \dot{\gamma}_{ji}} \tag{5}$$

The model has five parameters ($\kappa_A, \kappa_D, G_0, \eta_A, \eta_\infty$). We will be examining the response of the model to a homogeneous strain-controlled oscillatory input, thus we also must account for two input parameters (the amplitude γ_0 and the frequency ω of the simple shear strain waveform). This yields a total of 7 parameters that we must consider, with two linearly independent dimensions (all have units of either Pa, s^{-1}, or Pa.s). Hence by the Buckingham pi theorem the behavior can be characterized by 5 dimensionless parameters in oscillatory shear deformation [40].

Two previously published models are degenerate limits of this Thixoelastic Jeffreys model. In the limit of $\eta_\infty \to 0$ (i.e. removing the solvent viscosity) it is equivalent to the Thixoelastic Maxwell model explored by Quemada [31]. In the limit of $G_0 \to \infty$ (i.e. removing elastic strain), it is equivalent to the purely viscous thixotropic Moore model [16]. These two degenerate models could each therefore be characterized by only 4 dimensionless parameters in oscillatory shear, but would not capture basic viscoelastic features (relaxation and retardation timescales).

The number of parameters included in a model is a delicate balance. More values that can be changed allows a more diverse space of model responses and lends the ability to fit more varied

behavior, but it also makes analysis much more difficult. Some published thixotropic models have as many as a dozen dimensional parameters [32], at which point fitting all of the parameters and understanding their impacts on the model response is very challenging. As a starting point to understanding this diverse class of constitutive models, here we examine the simplest model that exhibits both viscoelasticity and thixotropy, which is the model described by Eq. (3) and (4), or in one-dimensional simple shear by Eq. (1) and (2). In large-amplitude oscillatory shear (LAOS) deformation there are three dimensionless model parameters (comparison of viscoelastic relaxation to thixotropic aggregation $\eta_A\kappa_A/G_0$, viscosity ratio η_∞/η_A, and thixotropic destruction constant κ_D), and two dimensionless input parameters (Deborah number based on viscoelastic relaxation time $\eta_A\omega/G_0$, and Weissenberg number based on thixotropic rates $\gamma_0\omega\kappa_D/\kappa_A$).

For numerical simulations we proceed with a nondimensionalized version of the governing equations. Times are scaled by κ_A, and stress can be normalized by either $\eta_A\dot{\gamma}_{char}$ or G_0. The choice is somewhat arbitrary, and the final stress expression can easily be transformed from one framing to another. Definitions of the dimensionless variables in the viscous nondimensionalization are

$$t^* = \kappa_A t \tag{6}$$

$$\sigma^* = \frac{\sigma}{\eta_A\dot{\gamma}_{char}} \tag{7}$$

$$\dot{\sigma}^* = \frac{\sigma}{\eta_A\dot{\gamma}_{char}\kappa_A} \tag{8}$$

$$\dot{\gamma}^* = \frac{\dot{\gamma}}{\dot{\gamma}_{char}} \tag{9}$$

$$\ddot{\gamma}^* = \frac{\ddot{\gamma}}{\dot{\gamma}_{char}\kappa_A} \tag{10}$$

where $\dot{\gamma}_{char}$ is the characteristic strain rate of whatever flow is imposed. Later when we examine large-amplitude oscillatory shear strain (LAOStrain), which imposes a sinusoidal strain $\gamma = \gamma_0 \sin(\omega t)$, the characteristic strain rate will be

$$\dot{\gamma}_{char} = \gamma_0 \omega \tag{11}$$

and hence the dimensionless strain rate input

$$\dot{\gamma}^*\left(t^*\right) = \cos\left(\frac{\mathrm{De}}{\lambda\kappa_A} t^*\right). \tag{12}$$

The five dimensionless input parameters for LAOStrain include three model parameters

$$\lambda\kappa_A = \frac{\eta_A}{G_0}\kappa_A, \quad \eta_\infty^* = \frac{\eta_\infty}{\eta_A}, \quad \kappa_D\,. \tag{13}$$

and two imposed deformation parameters

$$\mathrm{De} = \frac{\eta_A}{G_0}\omega, \quad \mathrm{Wi} = \frac{\kappa_D}{\kappa_A}\dot{\gamma}_{char}\,. \tag{14}$$

De is only well defined for an oscillatory or other transient input; a flow such as steady shear would be completely characterized by $\lambda\kappa_A, \eta_\infty^*$, Wi, and κ_D alone. This makes the dimensionless governing equations

$$\lambda\kappa_A\dot{\sigma}^* + \sigma^* = \left(\xi + \eta_\infty^*\right)\dot{\gamma}^* + \eta_\infty^*\lambda\kappa_A\ddot{\gamma}^* \tag{15}$$

$$\frac{d\xi}{dt^*} = \left(1-\xi\right) - \mathrm{Wi}\xi\,|\,\dot{\gamma}^*\,|\,. \tag{16}$$

The derivatives in the governing equation are with respect to dimensionless time t^* as defined in Eq. (10). We choose to operate primarily with the viscous scaling, because interestingly the dependence on κ_D disappears in this framing, and the governing equations contain only four dimensionless parameters (De, Wi, η_∞^*, and $\lambda\kappa_A$), as shown in Eq. (15) and (16). If the alternate elastic scaling

$$\sigma^* = \frac{\sigma\kappa_A}{G_0\dot{\gamma}_{char}} = \sigma^* \frac{\eta_A\kappa_A}{G_0} \tag{17}$$

is applied, then all five dimensionless parameters appear in the governing equations.

Chapter 3

Basic Model Responses

3.1 The Pipkin space

The space of deformations which a constitutive model (or material) undergoes can be characterized with two parameters: one describing the flow strength, and another the flow timescale [41]. For this model in oscillatory shear strain these two dimensionless parameters are the Wiessenberg number and the Deborah number, respectively, as defined in Eq. (13). A visual representation is shown in Figure 2(b). Each parameter can be similarly defined for other flows by replacing $\dot{\gamma}_0$ with the appropriate characteristic flow strength and replacing ω with the appropriate characteristic timescale. Two well-defined limits of this space are De→0, which is the steady flow regime, and Wi→0, which is the linear viscoelastic regime. As we explore these responses we will show that these two limits are not sufficient to fit all model parameters, or to fully explore the model response. A complete exploration and characterization will require a test that is both transient and nonlinear.

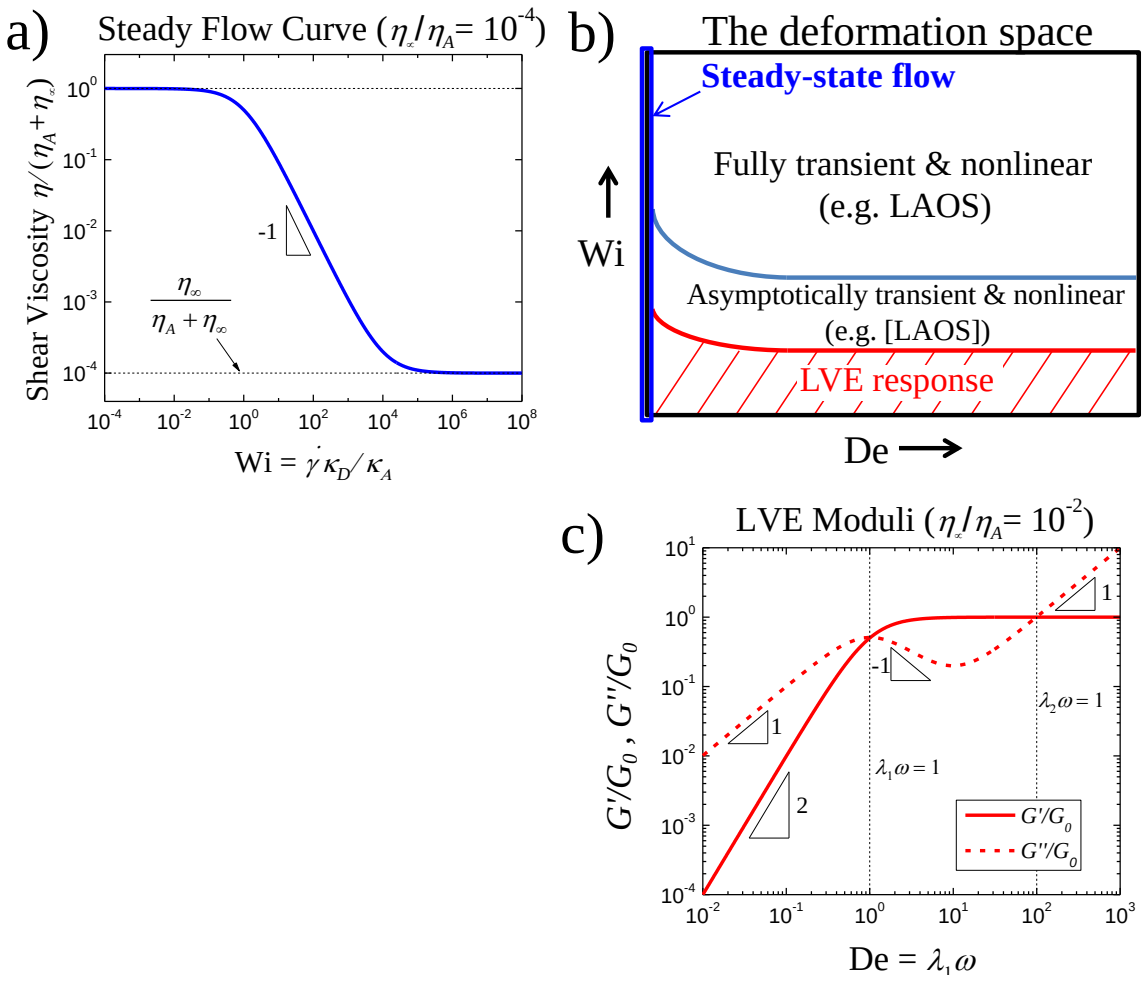

Figure 2 a) Flow curve showing steady-state viscosity as a function of Weissenberg number. b) Visual representation of the Pipkin space. c) Plot of the linear viscoelastic moduli as a function of Deborah number.

3.2 Steady-state and LVE Responses (Nonlinear or Transient)

First we examine the steady-state flow curve of this model, which is shown in Figure 2(a). When Eq. (1) and (2) are solved for a constant shear rate ($\dot{\gamma}^* = 1$ by definition) at long times, the structure tends to a steady state value of

$$\xi_{SS} = \xi(t \to \infty) = \frac{1}{1+\mathrm{Wi}}. \tag{18}$$

Recall $\mathrm{Wi} = \dot{\gamma}\kappa_D/\kappa_A$. The expression for viscosity is

$$\eta \equiv \frac{\sigma_{SS}}{\dot{\gamma}} \tag{19}$$

$$\eta(\mathrm{Wi}) = \eta_\infty + \eta_A \xi_{SS} . \tag{20}$$

Therefore as shear rate goes to zero ($\mathrm{Wi} \to 0$) the steady-state viscosity goes to $\eta_\infty + \eta_A$, and as shear rate goes to infinity the steady-state viscosity goes to η_∞. The ratio of κ_D / κ_A determines the value of $\dot{\gamma}$ at which the viscosity drops, hence steady flow can be used to fit η_∞, η_A, and the ratio κ_D / κ_A (but not κ_D and κ_D separately).

A transient test is required to characterize elasticity, so we examine the small amplitude oscillatory shear response of the model, shown in Figure 2(c). At $\mathrm{Wi} \to 0$, the structure is fully formed and $\xi \approx 1$, so the linear viscoelastic response is simply that of the Jeffreys model (Eq. (2) with $\xi = 1$). These curves can therefore be used to fit η_∞, η_A, and G_0.

The edges of the Pipkin space cannot fit all model parameters for the canonical thixotropic-viscoelastic model. Of the five model parameters, the low De limit (the "west coast" of the Pipkin space, which contains no transients) can fit η_∞, η_A, and the ratio of κ_D/κ_A (but not the individual values of κ_D and κ_A), while the low Wi limit (the "southern coast," which contains no nonlinearities) can fit η_∞, η_A, G_0. To identify κ_D and κ_A separately, one must measure a material function that is both transient and nonlinear (i.e. move away from the "coasts"). We will consider step-rate tests, then demonstrate the advantages of LAOS for this purpose.

3.3 Startup of Steady Shear (Transient and Nonlinear)

One potential test that meets the criterion of being both nonlinear and transient is startup of steady shear. Consider a step shear rate $\dot{\gamma} = \dot{\gamma}_0 H(t)$, where $H(t)$ is the Heaviside step function. The transient structure parameter is directly solved from Eq. (1) with initial condition $\xi(t=0) = \xi_0$

$$\xi(t) = \xi_{ss} + \left(\xi_0 - \xi_{ss}\right) e^{-t\kappa_A(1+Wi)} \tag{21}$$

$$\xi_{ss} = \left(1 + \mathrm{Wi}\right)^{-1} \tag{22}$$

with $\mathrm{Wi} = \dot{\gamma}_0 \, \kappa_D / \kappa_A$.

The structure evolution is governed by a first order ODE, hence $\xi(t)$ is a simple exponential decay which proceeds with a time constant given by $\left[\kappa_A \left(1+Wi\right)\right]^{-1}$. Later we will use this quantity as a measure of how quickly ξ responds to a strain rate input to help interpret the various other model responses. Using the solution for $\xi(t)$ from Eq. (21) and the governing equation for stress Eq. (2), the full stress response in startup of steady shear can then be solved analytically to give the transient shear viscosity

$$\eta^+(t,\dot{\gamma}_0) \equiv \frac{\sigma(t,\dot{\gamma}_0)}{\dot{\gamma}_0} \tag{23}$$

$$\eta^+(t,\dot{\gamma}_0) = \eta_A \xi_{ss} + \eta_\infty + \frac{\eta_A \left(\xi_0 - \xi_{ss}\right)}{\lambda \kappa_A \left(1+\mathrm{Wi}\right) - 1}\left[e^{-t\kappa_A(1+Wi)} - e^{-t/\lambda}\right]. \tag{24}$$

with ξ_{SS} given by Eq. (22). The appearance of κ_A decoupled from κ_D in this expression means that this test can be used to complete the fitting of the model parameters. Similarly, tests such as

creep and stress relaxation can be used if the input stress or strain is large enough to elicit a nonlinear response.

A major challenge with step tests is the experimental application of a discontinuous input; such tests are limited physically by how quickly a rheometer can apply a step in strain rate, which in turn limits how short of a timescale $\left[\kappa_A\left(1+Wi\right)\right]^{-1}$ can be fit. Using step tests Mewis and Wagner were able to fit timescales on the order of 0.1 seconds with experimental step times of roughly the same magnitude [42]. Shorter timescales are beyond observation with step-rate tests and current technology, but may be highly relevant in real materials, especially those subjected to rapidly varying deformations such as droplet impacts. The absence of thixotropy has been suggested for categorizing yield-stress fluids, but this definition is influenced by experimental limitations for observing short thixotropic timescales.

Oscillatory tests can accurately achieve experimental times an order of magnitude smaller than step tests (typically reliable to at least 100 rad/s, hence a timescale on the order of 0.01 seconds). Furthermore, we will also show that the Thixoelastic Jeffreys model predicts that thixotropic timescales, no matter how short, are accessible with oscillatory material functions at lower frequencies, making the fitting of these parameters easier.

Chapter 4

LAOS (Transient and Nonlinear)

4.1 Why LAOS?

Large-amplitude oscillatory shear presents several advantages over transient step tests including access to shorter thixotropic timescales as mentioned above. One significant experimental advantage is the nature of the input signal. A sinusoidal input strain (or stress) is easily and accurately achievable on a rheometer, while an instantaneous step in strain or in strain rate is not. Greater precision of the input signal allows for more precise analysis of the output signal. This also allows LAOS to probe shorter timescales than step tests. The oscillatory input also allows probing large strain rates without accumulating very large strains that may cause edge failure in a sample, as opposed to a startup of steady shear test which would very quickly accumulate large strains at high values of $\dot{\gamma}$ due to its unidirectionality.

LAOS also has several analytical advantages over step tests. First, due to the orthogonality of strain and strain rate for a sinusoidal input, it allows the decomposition of the signal into viscous and elastic components. This aids the intuitive interpretation of the model response and engenders a better understanding of the system. The oscillatory input also enables the harmonic decomposition of the signal by a Fourier transform, yielding material functions that are not dependent on time. This provides a simpler framework for analyzing and characterizing results than is available for any of the step tests. Furthermore, there exists a mathematical framework in the asymptotically nonlinear, low strain amplitude regime that reduces the dimensionality of the

material functions, which can be greatly advantageous when dealing with a model that has a large number of parameters (as the dimensionality of the space to explore can be high). We will begin our exploration of the response of our model to LAOS by examining the evolution of the structure parameter under oscillatory shear, which is the source of all nonlinearities in this model, then survey several different ways to represent the stress response.

4.2 Time-varying Structure During Oscillation

When structure evolution is strain rate driven (Eq. (1)), and the input is strain controlled (Eq. (12)), ξ is a function of only *t*, κ_A, and κ_D (only the thixotropic parameters). If the input was stress controlled or structure kinetics were stress driven (but not both), then ξ would also be a function of viscoelastic parameters. Figure 3 shows a sampling of time-periodic $\xi(t)$ curves for various values of 'aggregation rate' κ_A and 'destruction rate' $\kappa_D\dot{\gamma}_0$ for LAOStrain. These rates define the nonlinearity by the Weissenberg number $\mathrm{Wi} = \dot{\gamma}_0 \kappa_D / \kappa_A$. When aggregation significantly outweighs destruction (i.e. $\mathrm{Wi} \ll 1$), $\xi \approx 1$ throughout the cycle (this is the linear viscoelastic regime). When breakdown significantly outweighs buildup (i.e. $\mathrm{Wi} \gg 1$), $\xi \approx 0$ throughout. If the two are roughly balanced, then ξ oscillates about an intermediate value, with greater variation from its mean value at larger values of both κ_A and $\kappa_D\dot{\gamma}_0$. It is these oscillations of structure $\xi(t)$ from which the nonlinearities in the model response arise, in Eq. (4).

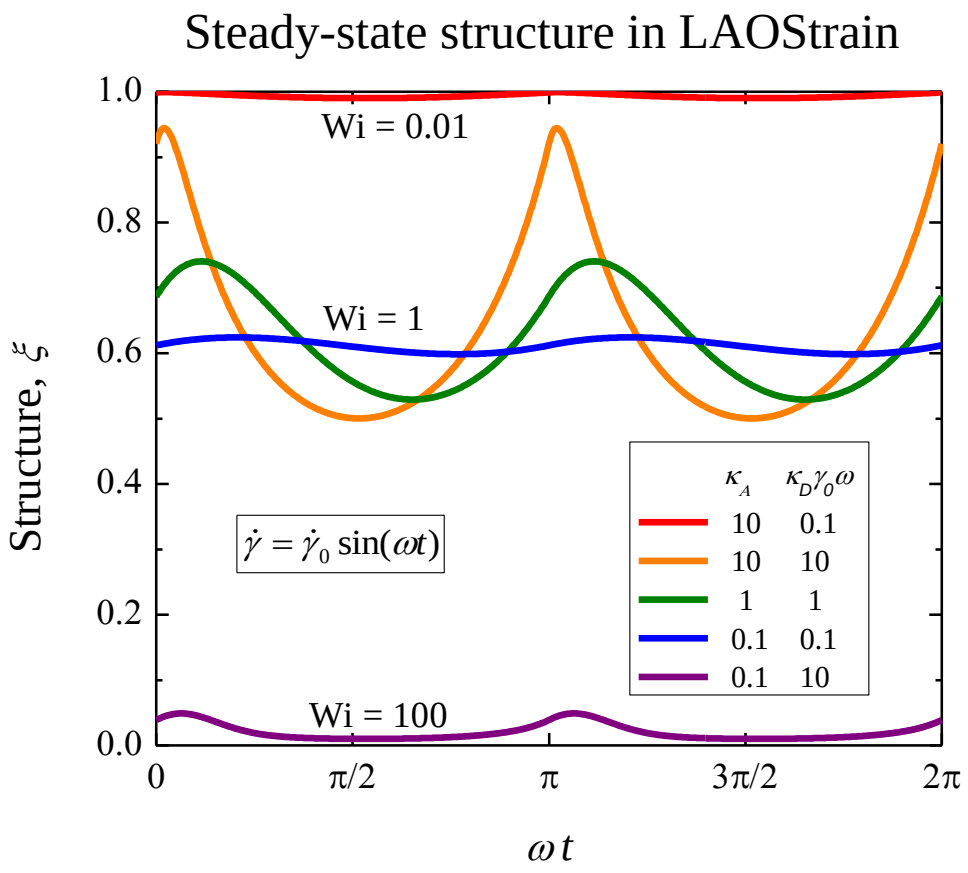

Figure 3 Steady-state oscillation of the structure parameter for varying values of buildup and breakdown parameters, from Eq. (1) with LAOStrain input of $\dot{\gamma} = \dot{\gamma}_0 \sin(\omega t)$,. $Wi = \dot{\gamma}_0 \kappa_D / \kappa_A$.

4.3 Asymptotic Nonlinearities ([LAOS])

Here we present the first analytical solution for a thixotropic-viscoelastic constitutive model subject to asymptotically nonlinear LAOS. A nonlinear contribution is always present in a rheological output signal, but when the strain amplitude is sufficiently small (determined by $Wi = \dot{\gamma}_0 \kappa_D / \kappa_A$) they become comparatively negligible. This is represented by the 'LVE response' region of the Pipkin space shown in Figure 2(b). As the strain amplitude increases (moving upward in the Pipkin space), each of the higher order contributions initially scales as a constant times a power of the strain amplitude [43]. At higher amplitudes this trend does not

hold, but in the amplitude-intrinsic regime these constant values can be computed (or measured), and provide a characterization of a nonlinear response that is a function of frequency, but not of amplitude. These material functions also carry physical interpretations that lend insight into the model behavior [43].

Many constitutive models (e.g. those based on a memory integral expansion) predict a linear shear stress response at $\sigma \sim \mathcal{O}\left(\gamma_0\right)$, no shear stress contributions at order $\sigma \sim \mathcal{O}\left(\gamma_0^2\right)$, and leading order shear nonlinearities occurring at order $\sigma \sim \mathcal{O}\left(\gamma_0^3\right)$ [44]. That is, shear stresses occur at odd orders of strain amplitude (normal stress differences occur at even orders). The stress harmonics can be expressed as

$$\sigma = -\sigma_1' \cos(\omega t) + \sigma_1'' \sin(\omega t) - \sigma_3' \cos(3\omega t) + \sigma_3'' \sin(3\omega t) + \ldots \tag{25}$$

for an input of $\dot{\gamma} = \dot{\gamma}_0 \sin(\omega t)$. Figure 4 shows a plot of the elastic first and third stress harmonics computed by numerical simulation for the Thixoelastic Jeffreys model.

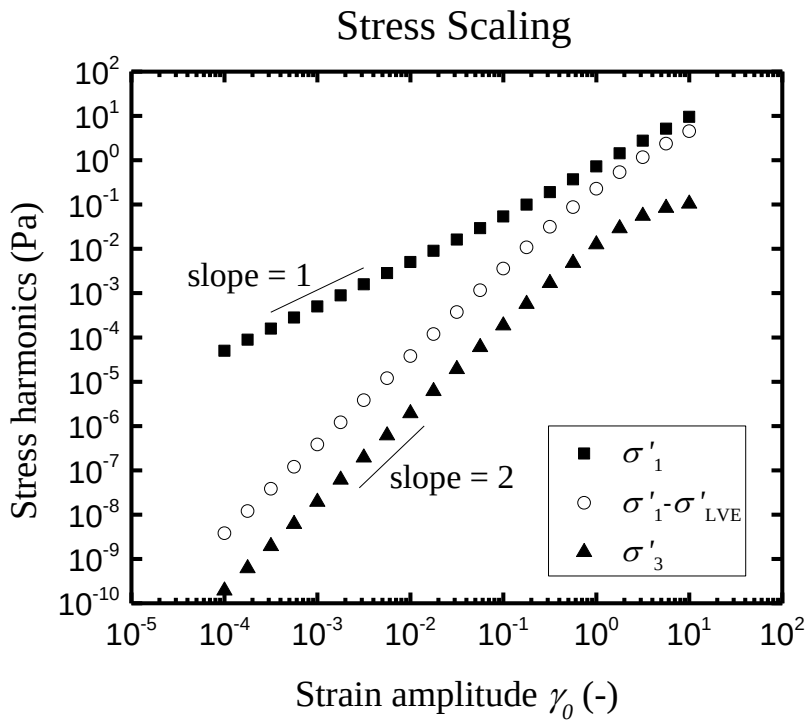

Figure 4 Low amplitude slopes of elastic stress harmonics (viscous harmonics show the same scaling behavior, not shown to avoid clutter). Computed by numerical simulation with $\kappa_D = 1,\ \kappa_A = \omega = 1\text{s}^{-1},\ G_0 = 1\text{Pa},\ \eta_A = 1\ \text{Pa}\cdot\text{s},\ \eta_\infty = 0.01\ \text{Pa}\cdot\text{s}$

The first harmonic shows the expected $\sim \gamma_0^{\ 1}$ scaling that is characteristic of the linear regime. While most constitutive models (and all other known analytical solutions) show $\sim \gamma_0^{\ 3}$ scaling in the third harmonic, this model shows scaling $\sim \gamma_0^{\ 2}$. The viscous harmonics show the same power law behavior with respect to strain amplitude. This scaling is determined by the order of reaction in the kinetic equation (Eq. (1)), and if the structure breakdown term $\kappa_D \xi |\dot{\gamma}_0|$ were raised to an exponent *n*, then the asymptotic nonlinear contributions would scale $\sim \gamma_0^{\ 1+n}$. This is potentially a unique signature that could be used to identify thixotropic effects.

This unusual scaling affects how we must define our material functions as we explore the LAOS response of our model. The measures we explore in detail are the asymptotic Chebyshev

coefficients. Full Chebyshev coefficients (which we will discuss in more detail in 4.4 and 4.5) are defined by the equations

$$\sigma = \gamma_0 \sum_{n\ odd} e_n(\omega,\gamma_0)T_n(x) + \gamma_0\omega \sum_{n\ odd} v_n(\omega,\gamma_0)T_n(y) \tag{26}$$

$$x = \frac{\gamma(t)}{\gamma_0}, y = \frac{\dot{\gamma}(t)}{\dot{\gamma}_0} \tag{27}$$

These conversion between these material functions and the stress harmonics defined in Eq. (25) is given by the expressions

$$e_1 = \frac{\sigma_1'}{\gamma_0},\ e_3 = \frac{\sigma_3'}{\gamma_0},\ v_1 = \frac{\sigma_1''}{\gamma_0},\ v_3 = \frac{-\sigma_3''}{\gamma_0} \tag{28}$$

for an input of $\dot{\gamma} = \dot{\gamma}_0 \sin(\omega t)$. The signs of the third harmonics are dependent upon the choice of input signal (sine or cosine) [43].

For most models (when the leading order nonlinearities occur at $\sigma \sim \mathcal{O}\left(\gamma_0^3\right)$) the intrinsic nonlinearities are defined as

$$\begin{aligned}\sigma(t;\gamma_0,\omega) = \gamma_0 &\left\{G'(\omega)\sin\omega t + G''(\omega)\cos\omega t\right\} + \\ &\gamma_0{}^3\left\{\left[e_1\right](\omega)\sin\omega t + \omega\left[v_1\right](\omega)\cos\omega t\right\} + \\ &\gamma_0{}^3\left\{-\left[e_3\right](\omega)\sin 3\omega t + \omega\left[v_3\right](\omega)\cos 3\omega t\right\} + \mathcal{O}\left(\gamma_0{}^5\right)\end{aligned} \tag{29}$$

where the input signal is $\gamma = \gamma_0 \sin\omega t$. The choice of representing the input as a sine or cosine must be specified to properly define LAOS material functions [45].

With the thixotropic viscoelastic model described in Eq. (1) and Eq. (2) (which predicts leading order nonlinear shear stress contributions of order $\sigma \sim \mathcal{O}\left(\gamma_0^2\right)$ as shown in Figure 4) we must modify the definition of asymptotic shear nonlinearities, employing the expressions

$$\sigma(t;\gamma_0,\omega) = \gamma_0\{G'(\omega)\sin\omega t + G''(\omega)\cos\omega t\} + \gamma_0^{\,2}\{[e_1](\omega)\sin\omega t + \omega[v_1](\omega)\cos\omega t\} + \gamma_0^{\,2}\{-[e_3](\omega)\sin 3\omega t + \omega[v_3](\omega)\cos 3\omega t\} + \mathcal{O}\left(\gamma_0^{\,3}\right) \quad . \tag{30}$$

Plots of the asymptotic Chebyshev coefficients for this model are shown in Figure 5.

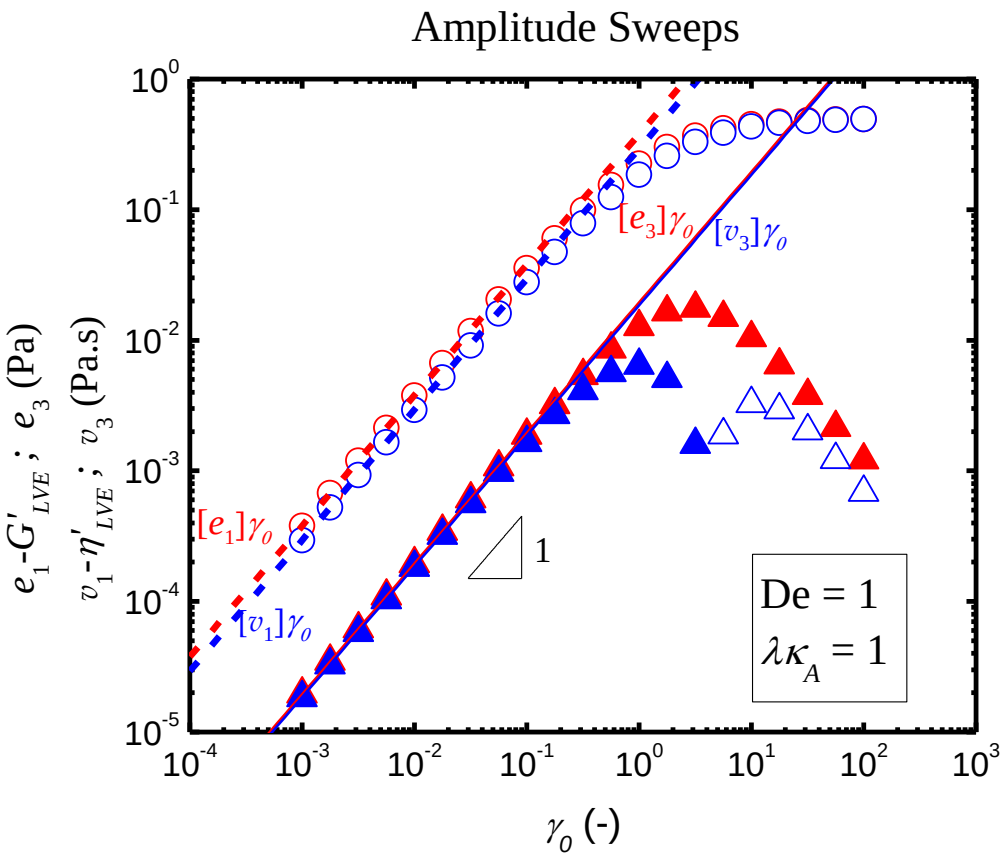

Figure 5 Plot of Chebyshev coefficients vs strain amplitude, showing power law scaling in the terminal regime. Simulation shown is for $\lambda\kappa_A = 1, \mathrm{De} = 1, \kappa_D = 1, \eta^*_\infty = 1$. Open symbols denote negative values.

A limited number of analytical solutions for other constitutive models in LAOS are available in the literature. Examples include the first two harmonics of the Lodge rubber-like liquid [46], nonlinear generalized Jeffreys and corotational Jeffreys [47], 3-constant Oldroyd [48], Bird-Carreau and Oldroyd-Walters-Fredrickson-Spriggs [49], Kelvin-Meyer-Voigt [50], and Goddard integral expansion [51]; the first three harmonics of Giesekus [52], rigid-dumbell shish-kebab

[53,54], reputation [55–57], Curtiss-Bird [58], and simple emulsion [59]; and the first five harmonics of the corotational Maxwell model [60]. A nice summary of the existing solutions is provided by Giacomin [60].

As we are now exploring a test that is both transient and nonlinear, the parameters κ_A and κ_D can be identified independently rather than just their ratio. Figure 6 shows the trends of individually varying these two parameters.

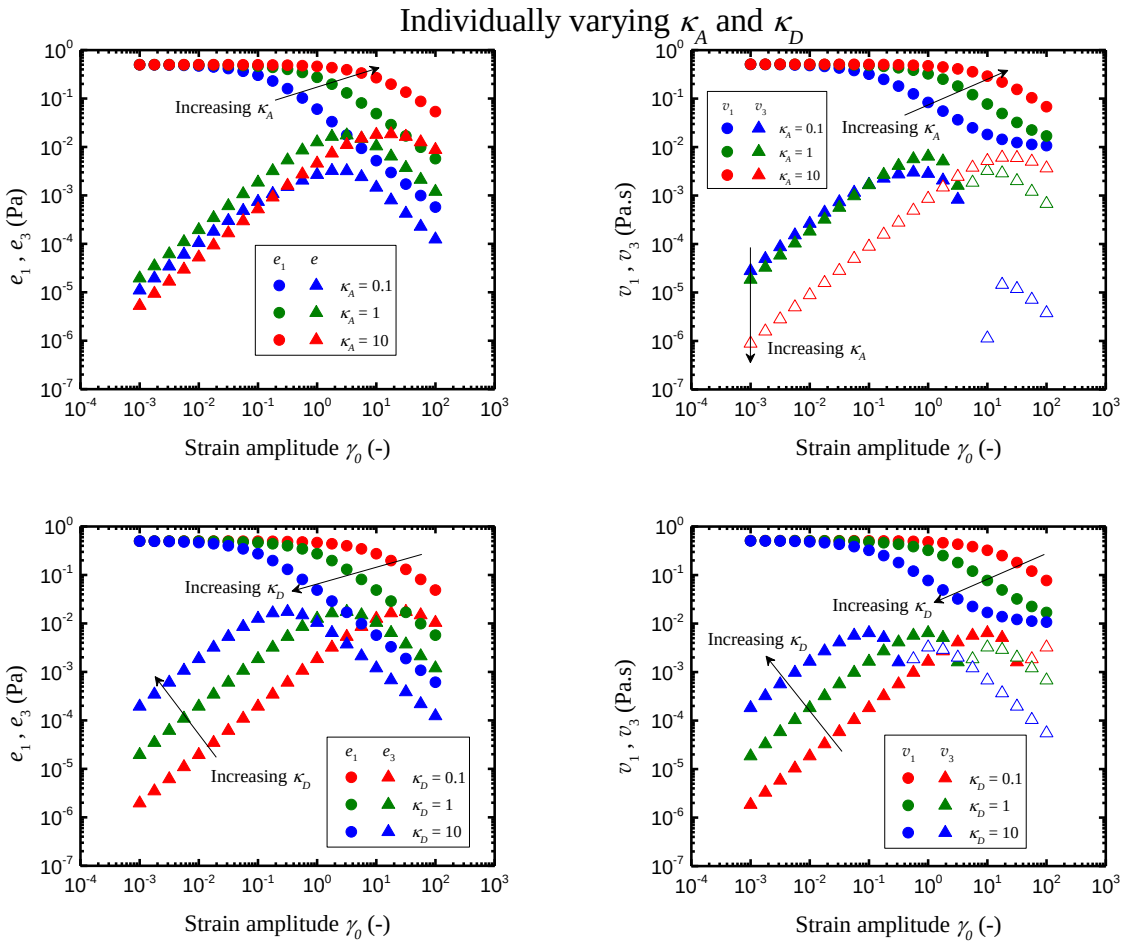

Figure 6 Changing values of the Chebyshev coefficients for varying values of κA and κD (from numerical simulation), with $\omega = 1\,\mathrm{s}^{-1}$, $G_0 = 1\,\mathrm{Pa}$, $\eta_A = 1\,\mathrm{Pa\cdot s}$, $\eta_\infty = 0.01\,\mathrm{Pa\cdot s}$. $\kappa_D = 1$ for all data in the plots where κ_A is varied, and $\kappa_A = 1$ for all data in the plots where κ_D is varied. Open symbols denote negative values.

When examining the first harmonics, κ_A and κ_D shift the curves in opposite directions, hence their ratio is all that can be discerned from an output curve. However, the third harmonics show distinct behavior in response to changing values of each of the two parameters. κ_D simply scales these measures linearly (as can be easily seen from the analytical expressions shown below in Eq. (31)-(34)), while e_3 shows a non-monotonic trend with respect to κ_A at low strain amplitudes, and v_3 shows a sign change with changing κ_A in the asymptotic regime.

For a sinusoidal strain input, Eq. (1) and (2) can be solved analytically in the small Wi limit (an exact solution for $\sigma(t)$ at any γ_0 is attainable, but it is too complex to be of use in this work). We first solve Eq. (1) for $\xi\left(t;\gamma_0,\omega\right)$ subject to input $\dot{\gamma}=\dot{\gamma}_0\sin(\omega t)$. We truncate $\xi\left(t;\gamma_0,\omega\right)$ at $\mathcal{O}\left(\gamma_0^2\right)$, and impose a long-time condition (time sufficient for decaying transients to become negligible) to obtain an expression for steady-state $\xi\left(t;\gamma_0,\omega\right)$ to $\mathcal{O}\left(\gamma_0^2\right)$. We then substitute this expression for $\xi(t;\gamma_0,\omega)$ into Eq. (2) and solve the resulting ODE for $\sigma(t;\gamma_0,\omega)$, again taking the long time solution to obtain the steady-state expression. We likewise truncate the shear stress expression at $\mathcal{O}\left(\gamma_0^2\right)$. After employing various trigonometric identities, Fourier series representations, and much tedious algebra (see Appendix A), we obtain analytical expressions for the intrinsic first and third harmonics, defined in Eq. (30), which appear at order $\sigma\sim\mathcal{O}\left(\gamma_0{}^2\right)$

$$[e_1]=\frac{-4}{3\pi}G_0\kappa_D\frac{\left(1+2L\right)D^3+\frac{6}{L}D^5}{\left(1+D^2\right)\left(L^2+4D^2\right)} \tag{31}$$

$$\omega[v_1]=\frac{-4}{3\pi}G_0\kappa_D\frac{2LD^2+\left(\frac{6}{L}-1\right)D^4}{\left(1+D^2\right)\left(L^2+4D^2\right)} \tag{32}$$

$$[e_3] = \frac{4}{5\pi} G_0 \kappa_D \frac{\left(L^2 + 2L^3\right) D^3 + \left(24 + 38L\right) D^5}{\left(1 + 9D^2\right)\left(L^2 + 4D^2\right)\left(L^2 + 16D^2\right)} \tag{33}$$

$$\omega[v_3] = \frac{-4}{15\pi} G_0 \kappa_D \frac{2L^3 D^2 + \left(38L - 9L^2\right) D^4 - 216D^6}{\left(1 + 9D^2\right)\left(L^2 + 4D^2\right)\left(L^2 + 16D^2\right)} \tag{34}$$

where shorthand notations $D = \mathrm{De}$ and $L = \lambda\kappa_A$ are used for compact representation. The derivation of these expressions can be found in the Appendix. Analytical expressions for the full harmonics at any strain amplitude are attainable, but are of high complexity and limited value. The amplitude-intrinsic material functions in Eq. (31)-(34) are all at $\mathcal{O}\left(\gamma_0^2\right)$ in stress, unlike all prior analytical solutions for asymptotic LAOStrain. This itself may be a unique signature of thixotropic nonlinearities governed by a first-order rate equation as in Eq. (1).

The asymptotic material functions in Eq. (31)-(34) represent the intrinsic strength of different shear nonlinearities for this model. Each nonlinearity scales with the product $G_0\kappa_D$, and includes both viscoelastic (De) and thixotropic ($\lambda\kappa_A$) timescale effects. Plots of the four intrinsic harmonics as a function of frequency for varying values of $\lambda\kappa_A$ are shown in Figure 7.

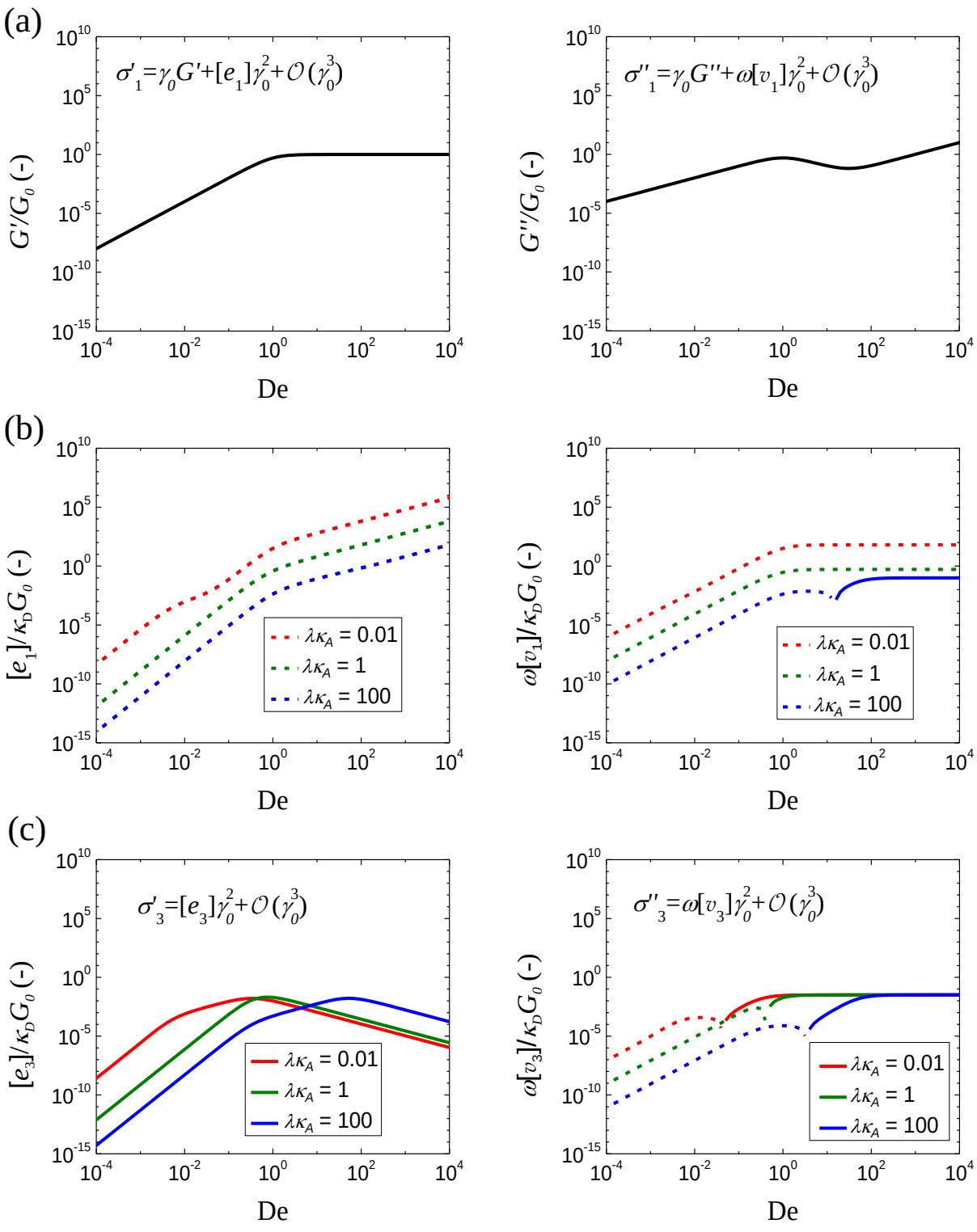

Figure 7 Plots of intrinsic nonlinearities as a function of Deborah number for varying values of model timescale ratio $\lambda\kappa_A$. Dashed lines denote negative values. When $\lambda\kappa_A = 0.01$ the thixotropic timescale is much longer than the viscoelastic timescale; the reverse is true when $\lambda\kappa_A = 100$, and the two timescales are equal when $\lambda\kappa_A \approx 1$.

These low-dimensional model fingerprints serve as the simplest way to characterize the nonlinear and transient response of the model. While the linear measures $G'(\mathrm{De})$ and $G''(\mathrm{De})$ show the same response for all values of $\lambda\kappa_A$ (Figure 2(c) and Figure 7(a)) the asymptotic nonlinearities (Figure 7(b) and Figure 7(c)) clearly show distinct signatures. The parameter κ_D scales the magnitude of these fingerprints, whereas the value of $\lambda\kappa_A$ determines the critical De at which the model nonlinearities transition from their low frequency behavior to their high frequency behavior. This represents a separation of viscoelastic timescale from thixotropic timescales. Given that we can fit λ from the linear viscoelastic data, this means that we can now fit all five of the model parameters. Moreover, the canonical thixotropic-viscoelastic model predicts that the thixotropic rates κ_A and κ_D influence the nonlinear signature over the entire range of De, and could possibly be measured at any accessible frequency timescale.

The intrinsic first elastic harmonic (which is the asymptotic change to G_1') is always negative for all values of $\lambda\kappa_A$. This indicates that the average elasticity of the model response is strain softening (because $[e_1] < 0$) for all De and all $\lambda\kappa_A$. The intrinsic first viscous harmonic (which is the asymptotic change to η_1') changes sign only for large values of $\lambda\kappa_A$. This indicates that the average viscosity of the model response is shear thinning for all De and all $\lambda\kappa_A$, except for when both De and $\lambda\kappa_A$ are both very large. Both the strain softening and the shear thinning are the expected consequence of structure breakdown; the harder we push on the material, the more the structure breaks down, hence we see a decrease in both the viscous and the elastic responses. These average trends, however, are distinct from the intracycle trends shown by the third harmonics.

Examining the intrinsic third elastic harmonic, we see that the model exhibits intracycle strain stiffening ($[e_3] > 0$) for all $\lambda\kappa_A$ and all De. We see this effect because at the maximum strain, the strain rate is zero and structure is building up, increasing the elasticity $G_0\xi$. Similarly, the intrinsic third viscous harmonic shows intracycle shear thinning at high De ($[v_3] < 0$ for all $\lambda\kappa_A$), while at low De the sign of v_1 changes, indicating intracycle shear thickening.

It is also of note that these measures allow κ_A to be fit at any frequency. For step tests such as startup of steady shear, very short time measurements (which are experimentally difficult to obtain) are required to probe large values of κ_A (i.e. very short thixotropic restructuring time). LAOS does not experience this difficulty, allowing for the possibility of measurement for a wider range of thixotropic timescales.

4.4 Lissajous Curves

While the asymptotic nonlinearities provide distinctive information, [LAOS] is only the first step into the vast nonlinear regime. Many materials exhibit multiple modes of deformation, and not all deformation mechanisms are activated by small strains, hence there may be information about a given material that the amplitude-intrinsic material functions cannot access. Furthermore, the amount of detail available from [LAOS] is finite, and some problems may require more than small strain measures alone can offer. Therefore we delve further into the nonlinear response.

As we continue to increase the Weissenberg number, the dimensionalities of both our independent and dependent parameter spaces rise. There is a major challenge of visualizing a rheological response in a high-dimensional space. The two deformation parameters (De, Wi) are organized as a Pipkin space. Additionally, we must consider two dimensionless model

parameters, the viscosity ratio $\eta_\infty^* = \eta_\infty / \eta_A$ and the ratio of viscoelastic to thixotropic timescales $\lambda\kappa_A$. This defines a four-dimensional space of independent dimensionless parameters (De, Wi, $\eta_\infty^*, \lambda\kappa_A$). The output of LAOS is also high-dimensional, and can be represented as Lissajous curves or as quantitative material functions.

Here we address the challenge of visualizing high-dimensional rheological signatures, by (i) defining a visual representation for the independent parameters, (ii) considering Lissajous curve outputs in this 4-D space, and (iii) considering quantitative LAOS material functions. The outputs of (ii) and (iii) serve as the fully nonlinear and transient rheological fingerprints of the canonical thixotropic-viscoelastic constitutive model considered here.

We wish to visualize these curves as a function of changing values of all four of the independent dimensionless model parameters: De, Wi, $\lambda\kappa_A$, and η_∞^*. There are several ways to group parameters as we represent their variation, and we will use the representation in Figure 8. We choose to begin by looking at the Pipkin space, examining the model response over a range of values of the two deformation input parameters (De, Wi) at constant values of the material parameters ($\lambda\kappa_A, \eta_\infty^*$). We do so because this yields 'isomaterial' model responses, meaning the signatures that would be seen if LAOS experiments were performed on a fixed sample. We then arrange these representations of the model response in a two-dimensional layout, with each direction representing variation in a dimensionless material parameter. In this setup, moving within one of the inner plots represents changing how a given material is deformed, while moving from plot to plot in the outer space represents changing the material that is examined (i.e. changing the constitutive model parameters). We like to use the analogy of decks of cards (shown in Figure 8) to visualize the parameter space: each card represents the plot for a given

material, while different cards in a deck and different decks represent the two material parameters.

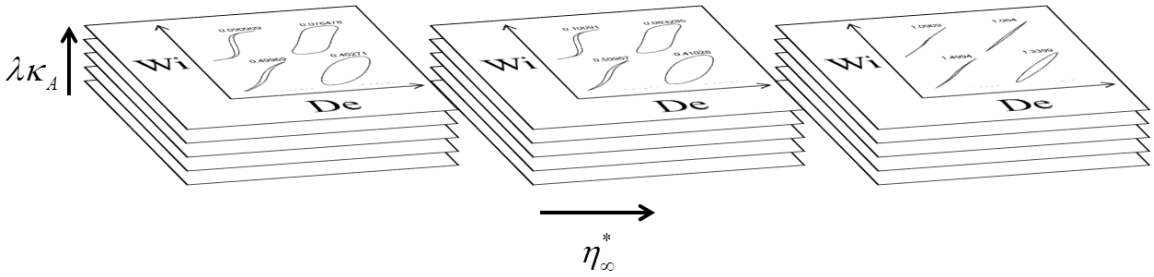

Figure 8 Decks of cards visual analogy of the four dimensional parameter space

An example of an isomaterial plot of Lissajous curves across the Pipkin space can be found in Figure 9, with both elastic (contours of stress $\sigma(t)$ against strain $\gamma(t)$) and viscous (contours of stress $\sigma(t)$ against strain rate $\dot{\gamma}(t)$) Lissajous curves shown.

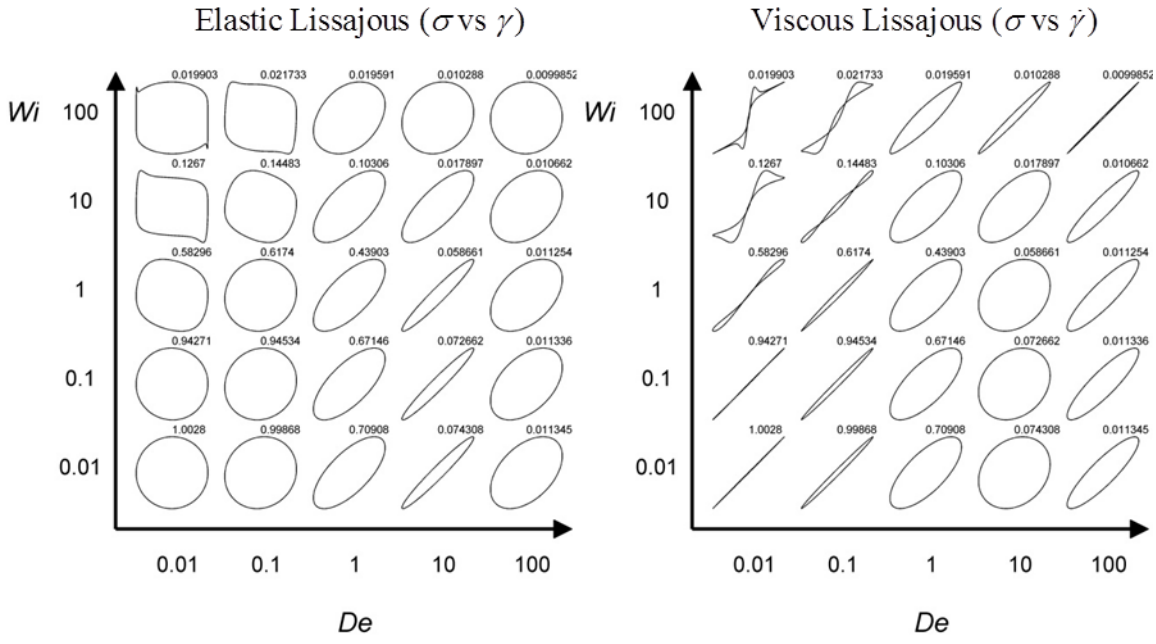

Figure 9 Plot of elastic (left) and viscous (right) Lissajous curves across the Pipkin space for $\lambda\kappa_A = 0.01$, $\eta_\infty^* = 0.01$ (from the lower left deck in Figure 8). The asymptotic nonlinear behavior (analytical solutions, Eqs. (31)-(34)) applies at low Wi.

In general both the elastic and viscous curves are required to fully characterize the model response, but in the case of this model we do not observe any cases where one shows distinctions that the other does not. Therefore to simplify we choose to examine only the viscous representation moving forward (viscous over elastic being an arbitrary aesthetic choice). Viscous Lissajous curves across the Pipkin space for a few demonstrative values of $\lambda\kappa_A$ and η_∞^* are shown in Figure 10. Similar plots for more values of the material parameters can be found in the Appendix.

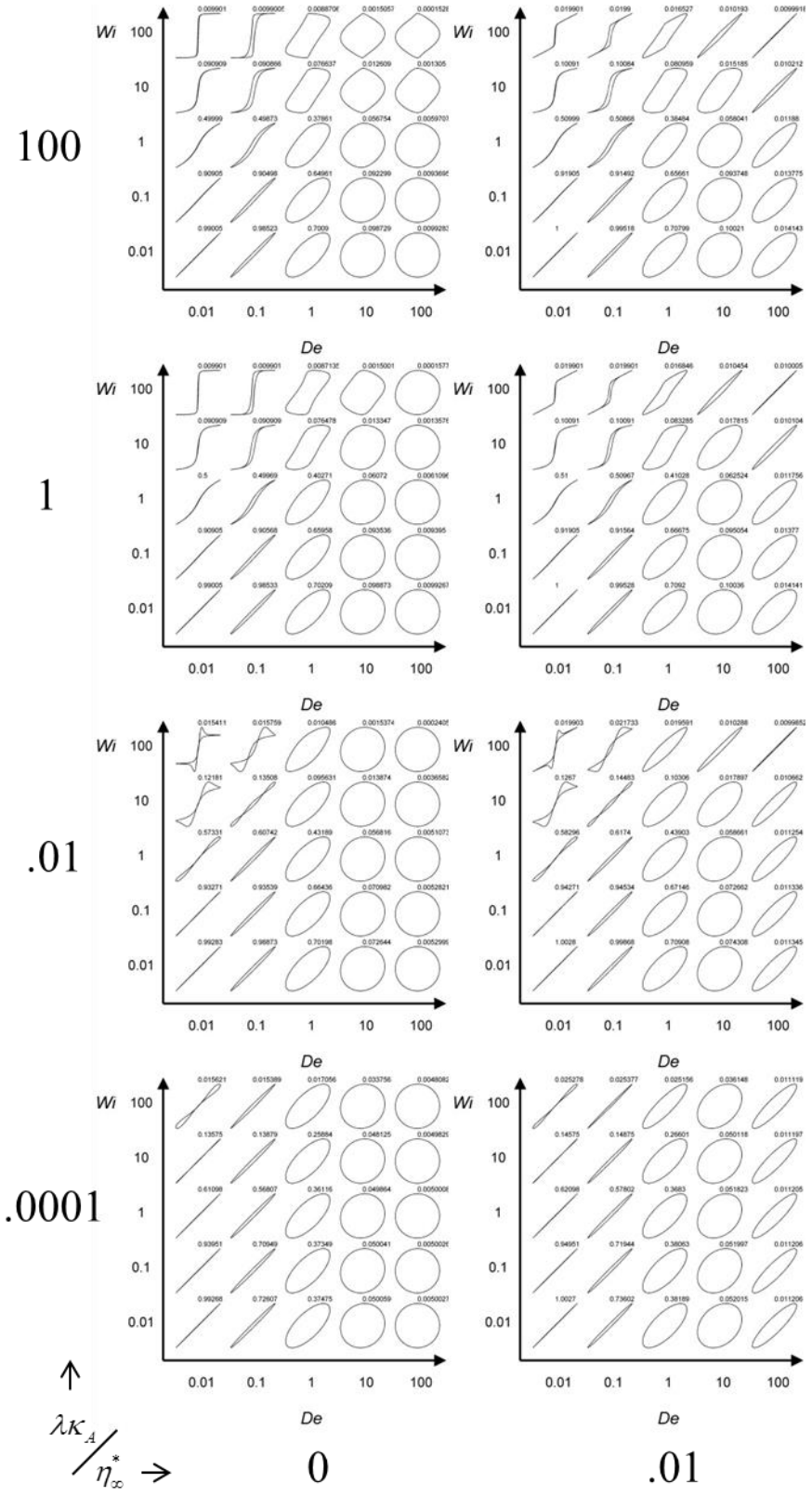

Figure 10 Viscous Lissajous curves across the Pipkin space for varying values of material parameters

One interesting feature of these Lissajous curves is the presence of stress overshoots (when strain rate is quadruple valued at some stresses). These result from ξ achieving a high value as the strain rate goes to zero during the oscillation, causing a spike in stress as the strain rate ramps up before the high rate breaks down the structure. These peaks occur only at low values of De (viscous), high values of Wi (nonlinear), i.e. the top left of Pipkin space, and at moderate values of $\lambda\kappa_A$ (comparable thixotropic and viscoelastic timescales). A low Deborah number is required for the structure to have the necessary time at low strain rate to build up, and a high Wiessenberg number is required for the structure to break down at high strain rate. As explained while examining startup of steady shear (Eq. (23)), $\lambda\kappa_A$ dictates how quickly the structure responds to the strain rate input, with a higher value indicating that ξ very rapidly approaches its steady state value. At very low $\lambda\kappa_A$ the structure does not build up quickly enough to reach a sufficiently high value to generate an overshoot before the strain rate ramps up. At very high $\lambda\kappa_A$ the structure builds up quickly as strain rate passes through zero, but also breaks down quickly (recall that the thixotropic rate is $\kappa_A(1+Wi)$ for both buildup and breakdown, hence higher $\lambda\kappa_A$ results in quicker thixotropic response in either direction) at only slightly elevated strain rates before an overshoot can occur. This is why overshoots are only seen at moderate $\lambda\kappa_A$, with the stress maximum occurring closer to a strain rate of zero for larger $\lambda\kappa_A$. For $\lambda\kappa_A \ll 1$ or $\lambda\kappa_A \gg 1$, there is a separation of the thixotropic aggregation and viscoelastic relaxation timescales, and stress overshoots do not appear.

For viscous Lissajous curves, a purely viscous response is represented by a straight line, while a purely elastic response is represented by a circle. If we examine the curves at varying values of De, we see the expected effect: at lower De the response is primarily viscous, and at

high De the response is primarily elastic. Comparing curves at the same values of De, Wi, and $\lambda\kappa_A$ we see that increasing $\eta_\infty^* = \eta_\infty / \eta_A$ serves to make the curves 'more viscous,' in many cases transforming circles to ellipses. This is also an expected result, as η_∞^* contributes only a linear viscous component to the stress response (Figure 1). We also see that the effect of changing η_∞^* is more pronounced at higher values of Wi. This trend appears because at higher Wi the mean value of ξ is lower, hence the stress contribution from the elastic element $G_0\xi$ and the structure viscosity $\eta_A\xi$ is smaller relative to the unchanging value of the solvent viscosity η_∞.

Finally, we observe that while changing the value of $\lambda\kappa_A$ distinctly changes the curves at high Wi (nonlinear regime), it has no effect at low Wi (linear regime). At very low Wi the value of ξ never deviates significantly from 1 (see Figure 3), and how quickly or slowly ξ achieves its steady state value is of no consequence when that steady state value shows little variation.

4.5 Chebyshev Coefficients

A more quantitative approach to analyzing LAOS data is to use a harmonic decomposition of the output signal. Traditionally this is done using a Fourier series representation of the output signal, with the series coefficients being the material functions of interest [61]. Alternatively, if the signal is examined in the deformation domain rather than the time domain, it can be equivalently represented as a series of Chebyshev polynomials, again with the coefficients of the polynomials of increasing order serving as the material functions of interest [62]. Here we examine the Chebyshev coefficients to represent a periodic stress as shown in Eq. (26)-(27).

In this representation e_n represent the elastic response, and v_n represent the viscous response. These measures more easily lend themselves to physical interpretation than their time-domain counterparts. These interpretations are most robust in the asymptotic nonlinear regime.

As with the Lissajous curves, these measures are functions of both input parameters (amplitude and frequency), hence we wish to examine them for varying values of four parameters in total (the input parameters as well as two material parameters in η_∞^* and $\lambda\kappa_A$). For a visual representation we take the same approach, employing a two-dimensional assembly of two-dimensional 'isomaterial' plots (Figure 7), this time with quantitative output rather than Lissajous curves. In Figure 11, the color of the data points representing the magnitude of the value. These plots of nondimensionalized values of four Chebyshev coefficients (the first and third of the elastic and viscous harmonics) are shown in Figure 11. Measures are shown in the elastic nondimensionalization to highlight the trend in e_1. (Stress is simulated as $\sigma^* = \sigma / \eta_A \dot{\gamma}_{char}$, then converted to the elastic scaling using Eq. (17), and the resulting nondimensional stress is decomposed into the Chebyshev coefficients.) The values of e_1 and v_1 represent average elastic modulus and dynamic viscosity, respectively [43,62]. The functions e_3 and v_3 are the coefficients of the third-harmonics, and represent intracycle deviations about the average values of e_1 and v_1 [43].

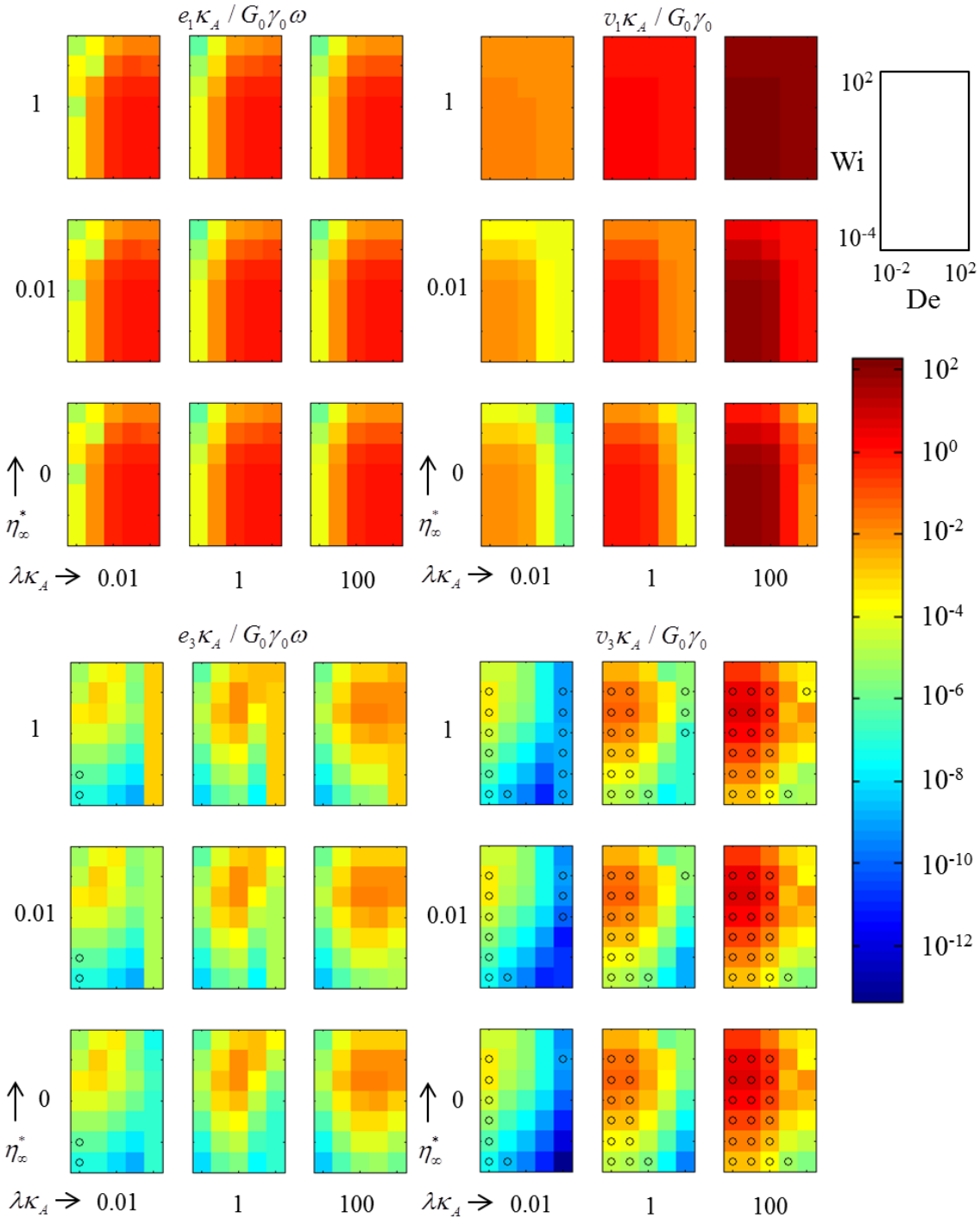

Figure 11 Fully nonlinear LAOStrain fingerprints of the nondimensionalized first and third Chebyshev coefficients e_1, v_1, e_3, v_3 (numerical simulation). Two dimensionless model parameters are varied ($\lambda\kappa_A$ and η_∞^*). Each fingerprint is in the space of (De = $\lambda\omega$; Wi = $\kappa_D\dot{\gamma}_0/\kappa_A$), inset. Circles denote negative values.

We begin by looking at e_1 and v_1. Each measure shows a clear plateau at low Wi (in the linear regime). The same frequency dependence as shown in Figure 2(c) is also apparent in the linear regime: e_1 increases with increasing De at low De, and plateaus at high De; v_1 plateaus at low De and decreases with increasing De. As Wi increases, e_1 decreases for all values of De and all values of $\lambda\kappa_A$ (which is consistent with the sign of $[e_1]$ being negative as shown in Figure 7) representing strain softening. Similarly v1 decreases with increasing Wi, except at high De and high $\lambda\kappa_A$ (again consistent with the signs of $[v_1]$ in Figure 7) representing shear thinning. Each of the third harmonics also displays the expected asymptotic behavior at low Wi: the magnitude increases with a slope of one in the double-logarithmic representation as Wi increases.

In nearly all cases for the third harmonics a local maximum as a function of Wi is observed at $\mathrm{Wi} \approx 1$. Each of the elastic coefficients exhibit a maximum at exactly $\mathrm{Wi} = 1$, while the viscous measures sometimes show a maximum at slightly higher Wi. An explanation can be found in examining the dimensional components of this dimensionless quantity. Increasing $\mathrm{Wi} = \gamma_0 \omega \kappa_D / \kappa_A$ can be thought of as increasing strain amplitude while holding all other factors constant. We generally expect increasing the strain amplitude to increase the stress output, which is the effect we see at low Wi. Recall that $\xi \approx 1$when Wi is very small, so increasing the amplitude is simply pushing harder on the same model elements. However, as the amplitude continues to increase, structure breakdown begins to outweigh structure buildup, and the value of ξ drops (to nearly zero at very high Wi), which is why the stress begins to increase sublinearly, and eventually decreases with increasing Wi.

Exploring the variation of the material parameters, the solvent viscosity η_∞ affects only v_1 with varying values having no effect on either third harmonic or the linear elastic response. This is expected, as all of the nonlinearities in this model arise from variations in the structure parameter, the influence of which is entirely separate from the influence of the solvent viscosity in this model. Therefore η_∞ does not affect e_3 or v_3 because they are entirely nonlinear (while e_1 and v_1 each has a linear and a nonlinear component). The solvent is also a purely viscous element, and therefore does not affect the elastic measures at all.

Changing the value of $\lambda\kappa_A$ alters the values of v_1, e_3, and v_3 while having no effect on e_1. We see this effect because e_1 is a measure of average elasticity, and as the elastic element scales linearly with structure ($G_0\xi$), hence e_1 scales with the average value of ξ throughout the cycle. As shown in Figure 3, the average value of ξ does not change with changing κ_A on its own. Examining the measures that are affected, we see that increasing values of $\lambda\kappa_A$ result in increasing values of the viscous coefficients. This can also be explained by examining the dimensional components of $\lambda\kappa_A$: since $\lambda = \eta_A / G_0$, a higher $\lambda\kappa_A$ is indicative of a larger value of η_A relative to κ_A/G_0, hence the expected effect is the viscous measures comprising a larger portion of the stress response. Here we see this as unchanging elastic components and increasing viscous components due to our choice of nondimensionalization. Recall that these results originated from the nondimensional definition $\sigma^* = \sigma / G_0$; had we nondimesionalized stress by η_A rather than by G_0 we would expect to see constant values of the viscous measures and decreasing values of the elastic measures with increasing $\lambda\kappa_A$. It is also of note that varying the

value of $\lambda\kappa_A$ has very little effect on the trends of Chebyshev coefficients with respect to changing deformation parameters.

Overall the Chebyshev coefficients provide a valuable, detailed fingerprint of the model response. However, at large Wi the first and third harmonics that we have examined do not fully characterize the stress response. While higher harmonics are always present, as Wi grows, the number of nonnegligible harmonics grows without bound. In this case, it is often better to use other measures of nonlinearity defined locally within cyclic deformation, including local moduli and viscosities $G_M', G_L', \eta_M', \eta_L'$ [62,63] or $R'(\omega t), R''(\omega t)$ [64]. For circumstances when the complexity of full LAOS proves cumbersome, the asymptotic nonlinear signatures (Eqs. (31)-(34), Figure 7) may be sufficient.

Chapter 5

Common Modifications of the Simple Model

The minimalist form of the kinetic equation that we have explored so far is typically written as

$$\dot{\xi} = \kappa_A(1-\xi) - \kappa_D \xi \,|\, \dot{\gamma} \,|\,. \tag{35}$$

We choose to write the equation this way because conceptually an aggregation parameter and a destruction parameter is simple and intuitive. As we begin to expand the equation and consider simple common variations on this basic form, it will be helpful to rewrite the equation. Rather than an aggregation parameter and a destruction parameter, it can be reframed as a rate parameter and a critical driving parameter (either a critical stress or a critical strain). This can be convenient when considering stress-driven kinetics and strain-driven kinetics, as it provides a single equation that describes both models. The expression

$$\dot{\xi} = k\left[1-\xi\left(1+\Gamma\right)\right] \tag{36}$$

is equivalent to (35) using the correspondence

$$\kappa_A = k;\ \kappa_D = \frac{k}{\dot{\gamma}_c} \tag{37}$$

where Γ is the forcing parameter defined as

$$\Gamma = \frac{\dot{\gamma}}{\dot{\gamma}_c} \quad \text{or} \quad \Gamma = \frac{\sigma}{\sigma_c}\,. \tag{38}$$

This form is also advantageous when changing the order of reaction of the equation, as the driving parameter Γ is dimensionless, which avoids strange dimensionalities of model parameters when raising the driving term to an exponent. Many models that introduce an exponent simply raise the strain rate to a power *n*, which means that the units of $\left[\kappa_D\right] \doteq s^{n-1}$ where *n* is not necessarily an integer. Raising the dimensionless parameter Γ to the *n* achieves the same phenomenological effect on the model, without the dimensionality of a model parameter being dependent upon the value of another parameter. Therefore for a generalized form of the kinetic equation, incorporating a choice between stress-driven and strain-driven kinetics as well as an extra parameter to govern the order of reaction we choose to write

$$\frac{d\xi}{dt} = k\left[1-\xi\left(1+\Gamma^n\right)\right]. \tag{39}$$

In this form, the definition of the Wiessenberg number is

$$\mathrm{Wi} = \Gamma_0, \text{ hence either } \mathrm{Wi} = \frac{\dot{\gamma}_0}{\dot{\gamma}_c} \quad \text{or} \quad \mathrm{Wi} = \frac{\sigma_0}{\sigma_c}, \tag{40}$$

depending on the parameter that drives destruction. In either framework, it is possible to write a model such that breakdown of structure is driven by stress (stress-kinetic) or by strain rate (strain-kinetic). Strain-kinetic is more prevalent in the literature [1,14], but stress-kinetic also exists [65,66].

In addition to varying whether stress or strain rate dictates kinetic breakdown, the choice of whether to employ rheological characterization with a controlled stress signal or a controlled strain signal as an input affects the model response. While linear responses give equivalent information regardless of choice of input, nonlinear rheological characterization with stress controlled inputs and strain controlled inputs are not interchangeable [67]. So far we have dealt

only with strain controlled LAOS (LAOStrain). This response and the model response in stress controlled LAOS (LAOStress) can have distinct features; therefore we employ both in order to more fully explore the behavior of our constitutive model. In order to do this we require more material functions, as the LAOStrain material functions (e_n and v_n) are well-defined only for a controlled strain input. Using similar Fourier transform methodology, the equivalent material functions can be written for a controlled stress input. The Chebyshev coefficients for LAOStress are defined as

$$\gamma = \sigma_0 \sum_{n\ odd} \left(\frac{f_n(\omega,\sigma_0)}{n\omega} T_n(z) + c_n(\omega,\sigma_0) T_n(z) \right) \tag{41}$$

where the controlled input defines *z*,

$$z = \sigma(\mathrm{t}) / \sigma_0 . \tag{42}$$

Again with identical methodology to LAOStrain, the LAOStress Chebyshev functions scale as additive powers of σ_0 at low amplitude, hence we can define the amplitude-intrinsic measures by the expression [43]

$$\begin{aligned} \gamma\left(t;\sigma_0,\omega\right) = \sigma_0 \left\{ J'(\omega)\sin\omega t - J''(\omega)\cos\omega t \right\} + \\ {\sigma_0}^2 \left\{ \left[c_1\right](\omega)\sin\omega t - \frac{\left[f_1\right](\omega)}{\omega}\cos\omega t \right\} + \\ {\sigma_0}^2 \left\{ \left[f_3\right](\omega)\sin 3\omega t - \frac{\left[f_3\right](\omega)}{3\omega}\cos 3\omega t \right\} + \mathcal{O}\left({\sigma_0}^3\right) \end{aligned} \tag{43}$$

Similarly to the LAOStrain measures shown in Chapter 4, the power of the amplitude at which the leading order nonlinearities arise is dependent upon the model. All existing solutions predict the leading order nonlinearities at $\mathcal{O}\left({\sigma_0}^3\right)$, while the Thixoelastic Jeffreys model predicts $\mathcal{O}\left({\sigma_0}^2\right)$ when *n* = 1. In Chapter 7 we will show that this low amplitude scaling is a function of

the parameter *n*, which will require further modification of the material function definitions. In Chapter 6 we will employ the material functions defined in Eq. (43), as well as the LAOStrain measures defined in Eq. (30), to characterize the constitutive model response.

An important variation in the model response when varying the kinetic breakdown parameter and the controlled input parameter between stress and strain is the functional dependence of the structure parameter, which is summarized in Table 1.

	$\dot{\gamma}$-kinetic	σ-kinetic
LAOStrain	$\xi = \xi\left(\omega t;\gamma_0,k,\dot{\gamma}_c\right)$ Analytical solution attainable	$\xi = \xi\left(\omega t;\gamma_0,k,\dot{\gamma}_c,G_0,\eta_A,\eta_\infty\right)$
LAOStress	$\xi = \xi\left(\omega t;\sigma_0,k,\sigma_c,G_0,\eta_A,\eta_\infty\right)$	$\xi = \xi\left(\omega t;\sigma_0,k,\sigma_c\right)$ Analytical solution attainable

Table 1 Functional dependence of structure as a function of kinetic driving parameter and controlled input parameter

When kinetic breakdown is dictated by the controlled input parameter the structure is only dependent upon the model parameters in the kinetic equation (See Appendix A for the instance of LAOStrain of the strain-kinetic equation). If the kinetic breakdown is not dictated by the same parameter as the controlled input (LAOStrain of the stress-kinetic model or LAOStress of the strain-kinetic model) then the parameters in the constitutive equation also affect the structure (e.g. in LAOStrain the stress is dependent upon the constitutive equation, hence in the stress-kinetic model the structure depends on all of the model parameters rather than just those in the kinetic equation). One additional option that arises when writing the model with stress driving kinetic breakdown is whether to make the structure breakdown a function of the total stress, or the stress in the Maxwell element of the mechanical analog. Here we choose to employ the total stress for simplicity.

Another common feature present in many thixotropic constitutive models is variation in the order of reaction in the kinetic equation [42]. This modification be incorporated in a number of ways. Some models insert $\dot{\gamma}$ as the argument of an exponential [68,69], others add an additional destruction term with $\dot{\gamma}$ raised to a different power (often 0.5) [27], while others simply raise existing terms to an exponent, adding power law dependence to the aggregation term [70], destruction term [28,29], or to both [24]. As a first step in exploring the phenomena we choose to examine a kinetic equation of the form already shown in Eq. (39), as modification to only the destruction term is the most common of these changes, adding an exponent is the simplest mathematical form that such a modification can take. We will explore the consequences of varying *n* in Chapter 7; first we move on to the results of the choice between stress and strain, both in kinetic structure breakdown and in input signal control.

Chapter 6

Stress vs. Strain

6.1 LAOStress of Stress-kinetic Model

We begin exploring the variations of the model with the other form for which we have obtained an analytical solution in asymptotic LAOS. As shown in Table 1, that form is LAOStress of the stress-kinetic model with n = 1: the kinetic equation

$$\frac{d\xi}{dt} = k\left[1 - \xi\left(1 + \frac{\sigma}{\sigma_c}\right)\right] \tag{44}$$

coupled to the constitutive equation shown in Eq. (2), with an input signal

$$\sigma = \sigma_0 \sin(\omega t). \tag{45}$$

The solution we present here is the first analytical solution for any constitutive model in asymptotic LAOStress (all other existing solutions in asymptotic LAOS are in controlled strain).

We begin by looking at the low stress amplitude scaling of the strain harmonics, shown in Figure 12, where the measures being plotted are defined by the equation

$$\gamma(t) = \gamma_1' \sin(\omega t) - \gamma_1'' \cos(\omega t) + \gamma_3' \sin(3\omega t) - \gamma_3'' \cos(3\omega t) + \ldots \tag{46}$$

for an input of $\sigma = \sigma_0 \sin(\omega t)$. We see the same scaling here as we saw in the low strain amplitude behavior of the stress harmonics in Figure 4. At low amplitude the first harmonic scales linearly with σ_0, and the nonlinear contributions scale as $\sim \sigma_0^{\,2}$.

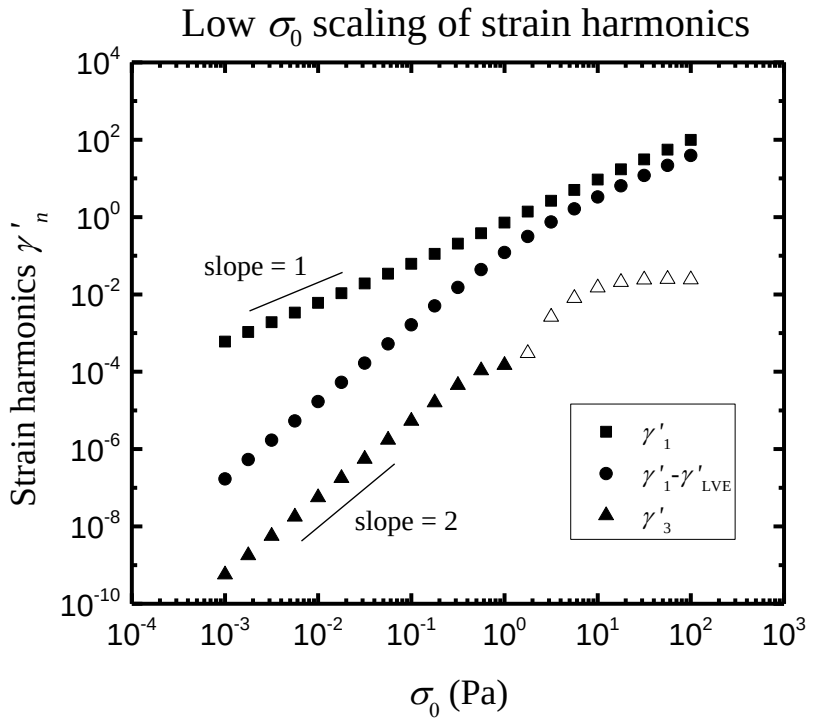

Figure 12 Low stress amplitude scaling of the strain harmonics for $\mathrm{De} = 1,\ \lambda k = 1,\ H = 0.5$. Open symbols denote negative values.

As we transition from the strain harmonics to the material functions defined in Eq. (41)-(43), we again see a similar result to that shown in LAOStrain of the strain-kinetic model. The nonlinear contributions to the LAOStress material functions are shown in Figure 13, and they scale linearly with the amplitude of the driving parameter, exactly as the LAOStrain measures shown in Figure 5 do. (The dimensionless material parameter λk in this framing of the kinetic equation is equivalent to the parameter $\lambda\kappa_A$ from Chapter 1 due to the conversion shown in Eq. (37).) As noted in Chapter 4, this is a unique result; therefore it is worth noting that the unusual scaling seen here is present regardless of whether the model is probed with LAOStrain or LAOStress.

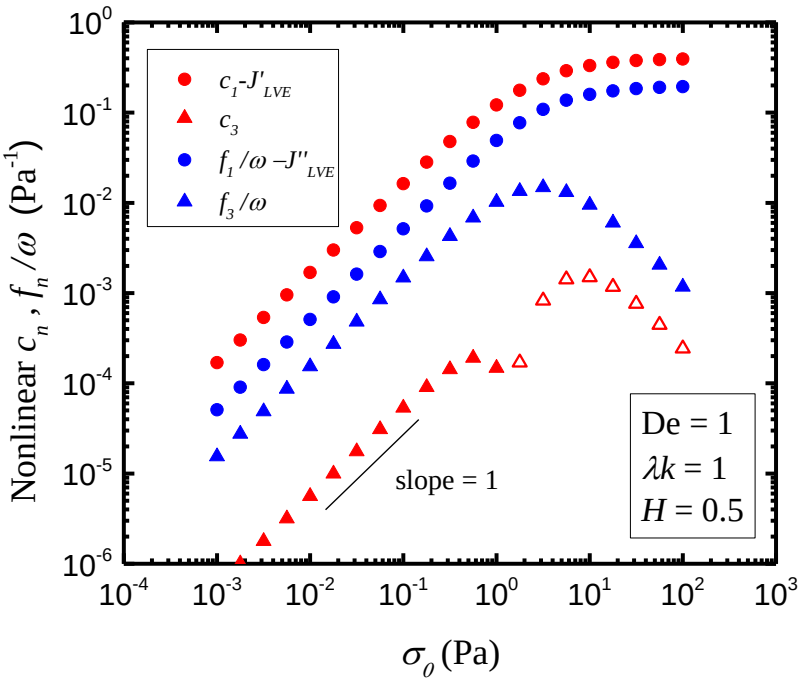

Figure 13 Low stress amplitude scaling of the nonlinear Chebyshev coefficients for $\mathrm{De}=1$, $\lambda k=1$, $H=0.5$. Open symbols denote negative values.

As with the LAOStrain response of the strain-kinetic model, a full analytical solution to the stress-kinetic model in LAOStress is achievable, but too complex to be of use in the current work. Therefore proceeding with parallel methodology, we solve for the asymptotic nonlinearities, truncating at $\mathcal{O}\left(\sigma_0^{\,2}\right)$. With the equivalence between Wi defined in either LAOStrain or LAOStress ($\mathrm{Wi}=\Gamma_0=\dot{\gamma}_0/\dot{\gamma}_c$ or σ_0/σ_c), the solution for $\xi(t)$ is the same in each case. The solution to the constitutive equation proceeds with the same procedure as discussed in Chapter 4 and Appendix A. The full solution is detailed in Appendix B. The resulting expressions for the asymptotic nonlinearities defined in Eq. (43) (defining front factors K_1 and K_3 for compact notation) are

$$K_1=\frac{1}{G_0\sigma_c}\frac{1}{\eta_\infty^*}\frac{H^2}{D\left(1+H^2D^2\right)^2\left(L^2+4D^2\right)} \tag{47}$$

$$K_3 = \frac{1}{G_0\sigma_c}\frac{1}{\eta_\infty^*}\frac{H^2L}{D\left(1+H^2D^2\right)\left(1+9H^2D^2\right)\left(L^2+4D^2\right)\left(L^2+16D^2\right)} \tag{48}$$

$$\left[c_1\right] = \frac{4}{3\pi}K_1\left[2L^2+\left(6-L+3HL^2+H^2L^2\right)D^2+\left(12H-6H^2-H^2L\right)D^4\right] \tag{49}$$

$$\left[f_1\right]/\omega = \frac{4}{3\pi}K_1\left[\left(L+2L^2-3HL^2\right)D+\left(-6+12H+H^2L+H^2L^2\right)D^3+6H^2D^5\right] \tag{50}$$

$$\left[c_3\right] = \frac{-4}{5\pi}K_3\left[\begin{array}{l}2L^3+\left(38L+7L^2-16HL^2+11HL^3-9H^2L^3\right)D^2\ldots\\+\left(88-304H-126H^2L+164HL-9H^2L^2\right)D^4-216H^2D^6\end{array}\right] \tag{51}$$

$$\left[f_3\right]/\omega = \frac{4}{5\pi}K_3\left[\begin{array}{l}\left(-L^2+L^3-3HL^3\right)D\ldots\\+\left(-24+14L-52HL-8HL^2+7H^2L^2-2H^2L^3\right)\mathrm{D}^3\ldots\\+\left(-112H+88H^2-38H^2L\right)D^5\end{array}\right] \tag{52}$$

where $D = \mathrm{De}$, $L = \lambda k$, $H = \eta_\infty^*/\left(1+\eta_\infty^*\right)$. The parameter H is the ratio of the retardation time to the relaxation time. While the intrinsic LAOStrain Chebyshev coefficients are a function only of Deborah number and λk (as shown in Eq. (31)-(34)), the intrinsic LAOStress coefficients are dependent upon the viscoelastic timescale ratio H in addition to De and λk. The reason for this is explained by the mechanical analog of the constitutive model shown in Figure 1. The Maxwell element (from which all of the nonlinearities in the response arise) is in parallel with the solvent viscosity, hence when the strain is prescribed it feels no effect of η_∞, and the nonlinear measures show no dependence on the retardation time. In contrast, when stress is prescribed the parallel element, though linear, does affect the strain that develops in the Maxwell element, hence the nonlinear measures are dependent upon both viscoelastic timescales. This is one way in which LAOStrain and LAOStress are not equivalent, showing that the choice between the two is important both analytically and experimentally.

These measures also do more than simple provide a signature of a constitutive model. They do provide a frequency-dependent fingerprint that is unique to a given model or material, which is of great value, but they also carry physical interpretations that lend insight into the model behavior. The signs of $[c_1]$, $[f_1]$, $[c_3]$, and $[f_3]$ describe the type of nonlinearity that the model exhibits (e.g. whether model is stress stiffening or stress softening), while the magnitudes describe the strength of that nonlinearity.

Plots of the four frequency-dependent intrinsic Chebyshev coefficients (Eq. (47)-(52)) are shown in Figure 14.

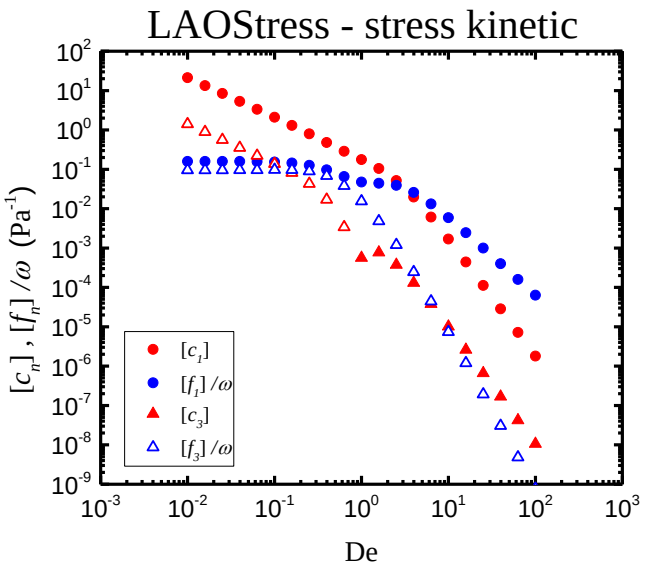

Figure 14 Intrinsic Chebyshev coefficients for the stress-kinetic model (Eq. (44) coupled with Eq. (2)) in LAOStress. Data shown are from analytical solution, $\lambda k = 1$ and $H = 0.5$. Open symbols denote negative values.

As with the LAOStrain material functions, the signs of the LAOStress measures are indicative of physical interpretations of the model response, though the meaning of the signs is reversed from that of $[e_1]$, $[v_1]$, $[e_3]$, and $[v_3]$. Positive sign indicates softening/thinning and negative sign indicates stiffening/thickening, as positive signs represent higher strains/strain rates

for a given stress. From Figure 14, the signs of $[c_1]$ and $[f_1]$ are always positive, indicating that the average response is stress softening and stress thinning, as expected (higher stress always causing greater structure breakdown). This is identical to the effect seen in the LAOStrain response of the strain-kinetic model. While the average trends (from the first harmonics) are the same, the third harmonics are qualitatively different for the stress-kinetic model in LAOStress and the strain-kinetic model in LAOStrain. In the LAOStress response, for all De viscous thinning is driven by large instantaneous stresses ($[f_1]>0$ and $[f_3]<0$ in Figure 14). In contrast, in the LAOStrain response the shear thinning is driven by large rates at low De and by large strains at high De (i.e. the driving mechanism of viscous nonlinearities is frequency dependent for LAOStrain of the strain-kinetic model). Also in the LAOStrain response the elastic softening is driven by large rates at all De ($[e_1]<0$ and $[e_3]>0$ at all De in Figure 7), whereas in the LAOStress response it is driven by large rates at low De and by large stresses at high De.

In summary, we see distinct signatures from stress control and strain control when kinetic structure breakdown is driven by the controlled input parameter. As shown in Table 1, in these two cases the structure depends only upon the kinetic equation. We now proceed to examine the model signatures when the kinetic breakdown parameter is different from the controlled input parameter, and the structure is dependent upon the constitutive equation.

6.2 Stress-kinetic and Strain-kinetic in LAOStress

Comparison between two different models subjected to the same input is somewhat more direct than the comparison between LAOStress and LAOStrain, as the material functions used to express the model response are the same in both cases. First, we compare the stress-kinetic

model and the strain-kinetic model in LAOStress, and we see that the signatures are qualitatively similar. Figure 15 shows the LAOStress responses of the stress-kinetic and strain-kinetic models.

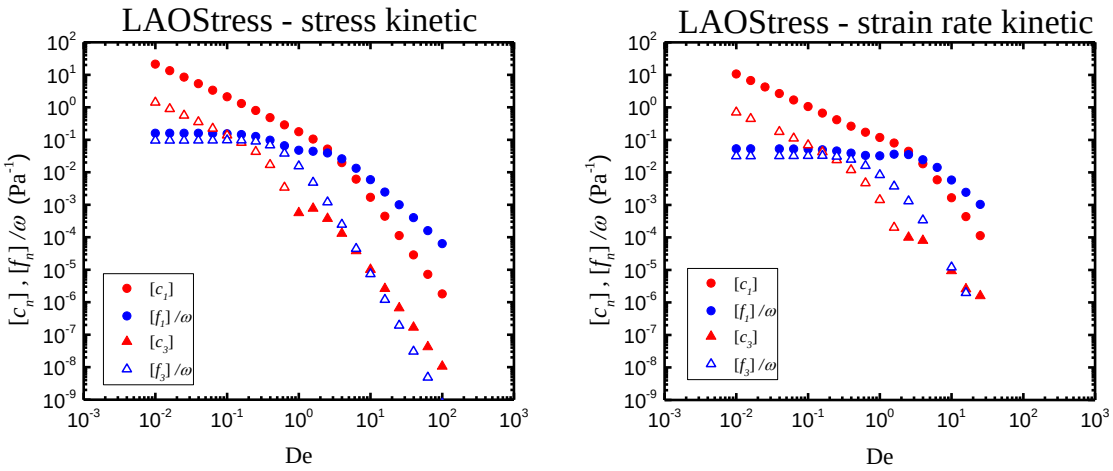

Figure 15 Comparison of intrinsic nonlinear signatures in LAOStress between stress dictated kinetics and strain rate dictated kinetics. Data are from simulation with $\lambda\kappa_A = 1, H = 0.5$. Open symbols denote negative values.

The signs of all four harmonics are the same at high and low De, with the only difference being a small shift in the De at which the third elastic harmonic transitions from negative to positive. At high De the magnitudes of the Chebyshev coefficients are the same, but at low De all four nonlinearities show a larger magnitude in the stress-kinetic model than they do in the strain-kinetic model. Physically, this means that the critical stress required to see the effects of these nonlinearities is smaller (i.e. the model nonlinearities are more sensitive to the applied stress). This disparity is caused by the fact that in the stress-kinetic model the structure is dependent only upon the kinetic equation, whereas in the strain-kinetic model the structure feeds through the constitutive equation, which can dampen the variations in ξ, and hence decrease the magnitude of the nonlinearities (as all nonlinearities arise from structure variation).

6.3 Stress-kinetic and Strain-kinetic in LAOStrain

Figure 16 shows the comparison of the same two models in LAOStrain, in which we see a difference in the sign of $[e_3]$ as a function of frequency.

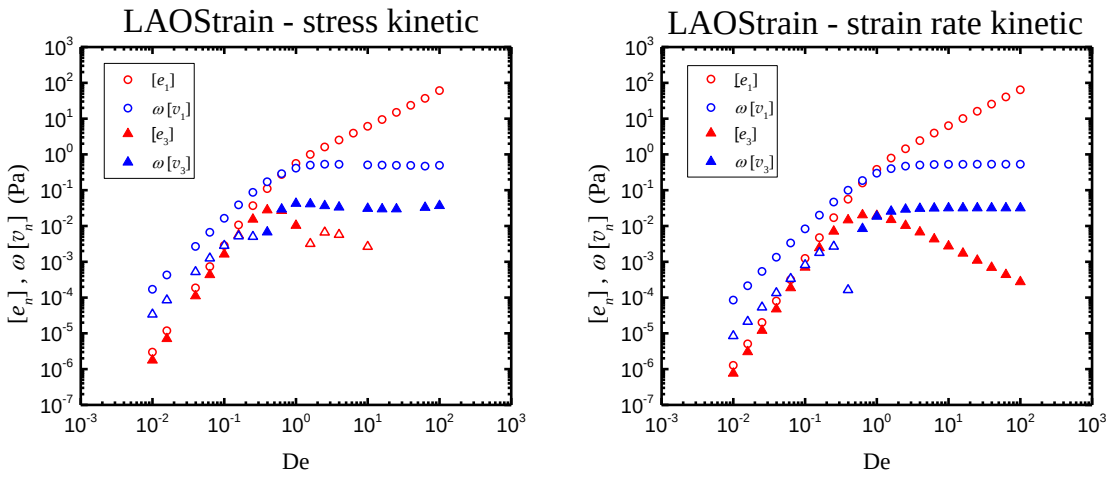

Figure 16 Comparison of intrinsic nonlinear signatures in LAOStrain between stress dictated kinetics and strain rate dictated kinetics. Data for stress-kinetic are from simulation, data for strain-kinetic are from the analytical solution, both with $\lambda\kappa_A = 1$. Open symbols denote negative values.

The LAOStrain material functions do not show the same magnitude difference that the LAOStress, but the viscous third harmonic does show a small shift in transitional De, similar to that of the elastic third harmonic in LAOStress. The larger difference that is observed is the sign change in the elastic third harmonic of the stress-kinetic model that is not present in the strain-kinetic model. These signs indicate that in the strain-kinetic equation the strain softening is driven by large rates at all De, whereas in the stress-kinetic equation large rates drive the nonlinearity at low De and large strains drive the nonlinearity at high De. This transition is seen because the response is primarily viscous (stress arising from strain rate) at low De, and primarily elastic (stress arising from strain) at high De. The same effect is not seen in the strain-kinetic model because in LAOStrain the strain rate is prescribed, hence the structure depends

only on the controlled input and not the developed stress in the constitutive equation (see Table 1). In contrast, in the stress-kinetic model the structure is coupled to the constitutive equation allowing the viscoelastic response of the model to affect the nonlinearities.

To summarize, as we vary the controlled input parameter and the kinetic breakdown parameter between stress and strain, one important feature of the model response that does not change is the power-function scaling of the nonlinearities at low amplitudes. In all cases the leading order nonlinearities arise at $\mathcal{O}\left(\gamma_0^{\,2}\right)$ or $\mathcal{O}\left(\sigma_0^{\,2}\right)$, which is a response unique to this model; all other known solutions predict a leading order of $\mathcal{O}\left(\gamma_0^{\,3}\right)$ or $\mathcal{O}\left(\sigma_0^{\,3}\right)$ [60]. After modifying the definition of our intrinsic material functions to accommodate this feature, we present a new analytical solution for LAOStress of our stress-kinetic model. We then show that varying the stress and strain does produce some key differences in the frequency-dependent signatures exhibited by the LAOS material functions. We now move on from the discussion of stress and strain, and focus on LAOStress of the stress-kinetic model as we explore the effects of the additional model parameter *n*.

Chapter 7

LAOStrain of Strain-kinetic at Varying *n*

7.1 Temporal Structure Variation

In Chapter 4 we established the power-function scaling of the simple strain-kinetc TEJ model in LAOStrain: linearities at $\mathcal{O}\left(\gamma_0^{\,1}\right)$, shear nonlinearities at $\mathcal{O}\left(\gamma_0^{\,2}\right)$. The $\mathcal{O}\left(\gamma_0^{\,2}\right)$ scaling is unique, as all other models with known analytical solutions predict that nonlinearities arise at $\mathcal{O}\left(\gamma_0^{\,3}\right)$. This includes the very general model known as the memory integral expansion (or Boltzmann superposition expansion) [44]. As we examine the effect of the parameter *n* as defined in Chapter 5 (Eq. (39)), we will show that the order of reaction *n* changes the scaling of the shear nonlinearities to be $\mathcal{O}\left(\gamma_0^{\,n+1}\right)$.

Recall that the general form of the kinetic equation incorporating the order of reaction parameter is

$$\frac{d\xi}{dt} = k\left[1-\xi\left(1+\Gamma^n\right)\right] \tag{53}$$

Because all nonlinearities arise from variation in structure over time, as a first step to understanding the effect of the power law exponent on the nonlinearities in the model response we explore the temporal changes to the structure at varying values of *n*. First, it is important to note that the behavior with changing *n* is fundamentally dependent on the values of Γ relative to 1. For a fixed value of strain rate (or stress) the steady-state value of ξ is

$$\xi_{SS} = \left(1+\Gamma^n\right)^{-1}. \tag{54}$$

The differential equation governing the evolution of structure is first order, hence at any point during an oscillation ξ is tending toward its steady-state value. Therefore it is the function Γ^n in Eq. (54) that expresses the tendency of ξ in response to a dynamic input. Figure 17 shows Γ^n as a function of Γ for three different values of n (0.5, 1, and 2).

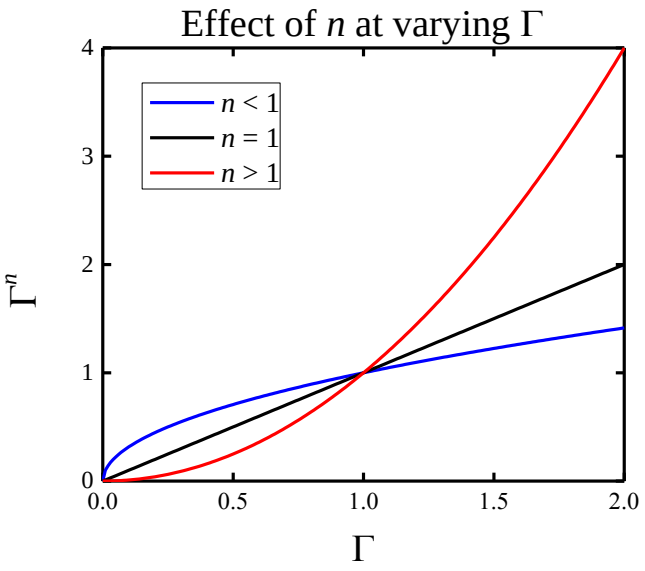

Figure 17 Plot of Γ^n vs Γ at several values of n, showing that the direction of the trend is dependent upon whether each of n and Γ are less than, equal to, or greater than zero

When $\Gamma < 1$, increasing n decreases Γ^n, whereas when $\Gamma > 1$ increasing n increases Γ^n. This observation will inform the trends that we will see in structure variations at changing n.

Figure 18 shows structure as a function of time (from simulation) with $k = 1$ and $\dot{\gamma}_c = 1$ at varying values of n.

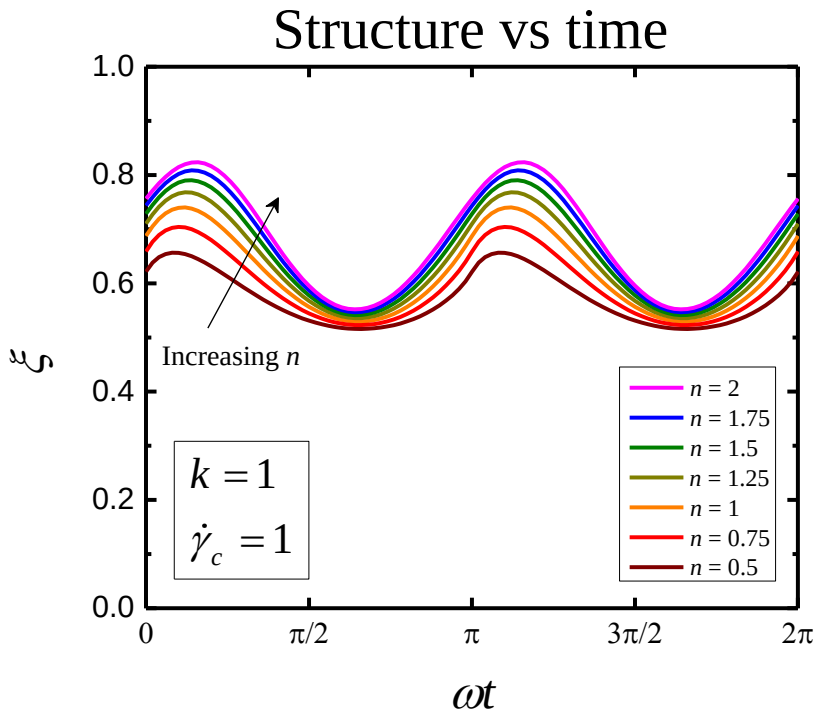

Figure 18 Structure as a function of time at varying values of n for $k = 1$, $\dot{\gamma}_c = 1$ (equivalent to $\kappa_A = 1$, $\kappa_D = 1$), and an input signal of $\dot{\gamma} = \sin(\omega t)$

In this case changing the value of n has a slight effect on the shape of the curve, but a significant effect on the average value of ξ, with larger n causing the structure to oscillate about a larger value. This is because the data in Figure 18 are simulated with parameter values $\dot{\gamma}_0 = 1$ and $\dot{\gamma}_c = 1$, so $\Gamma = \sin(\omega t)$, and $\Gamma \leq 1$ throughout the cycle. As illustrated in Figure 17, this means that larger n produces smaller Γ^n, and hence larger ξ_{SS} according to Eq. (54). Therefore an increasing value of n produces a higher average value of ξ. Note also that the intracycle variation (peak-to-valley difference) is greater for greater value of n.

These trends in structure, which determine the model nonlinearities, are dependent upon the values of the model parameters, as shown in Figure 19. Values of k and $\dot{\gamma}_c$ are chosen because they correspond to the values of κ_A and κ_D displayed in Figure 3.

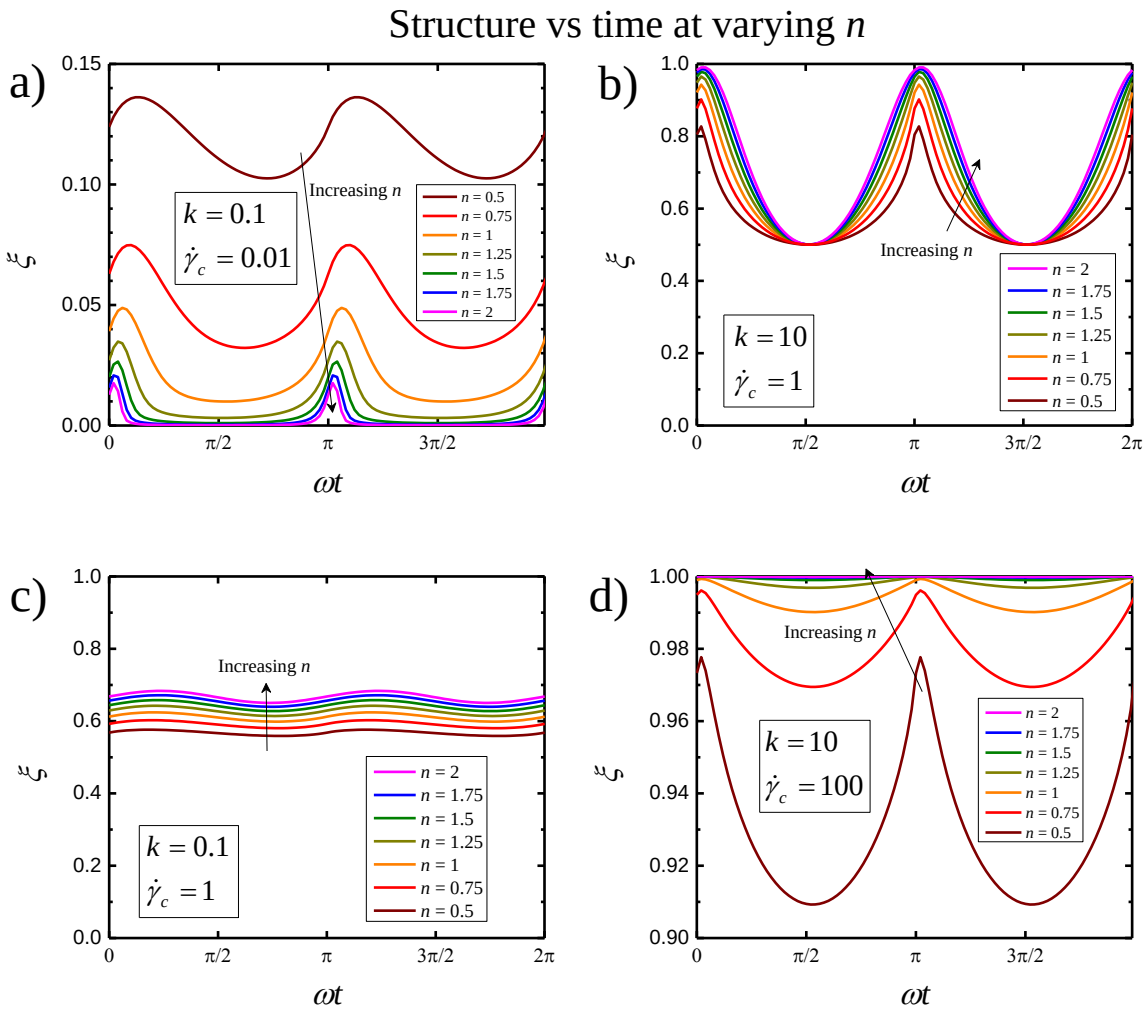

Figure 19 Structure as a function of time at varying values of n for a) $\kappa_A = 0.1$, $\kappa_D = 10$, b) $\kappa_A = 10$, $\kappa_D = 10$, c) $\kappa_A = 0.1$, $\kappa_D = 0.1$, d) $\kappa_A = 10$, $\kappa_D = 0.1$. All data are for an input signal of $\dot{\gamma} = \sin(\omega t)$.

For values of $\dot{\gamma}_c \geq 1$ (and hence $\Gamma \leq 1$ as $\dot{\gamma}_0 = 1$) as seen in Figure 19 b), c), and d) the same trend of average structure is seen as in Figure 18; a greater value of n causes ξ to oscillate about a greater mean value. As expected from the same analysis that predicted this correlation (Eq. (54)), when $\dot{\gamma}_c < 1$ as seen in Figure 19 a), the reverse is true and higher n leads to lower average ξ (recall that by Eq. (38) smaller $\dot{\gamma}_c$ means higher Γ). Figure 19 b) and c) show the same trend in intracycle variation as Figure 18 (all three of which have a value of $\dot{\gamma}_c = 1$), with larger n resulting in greater peak-to-valley variation, while Figure 19 a) and d) (which have a smaller and

larger value of $\dot{\gamma}_c$, respectively) shows the opposite. Similarly to the average values of ξ, this is also governed entirely by the trends illustrated in Figure 17 and Eq. (54).

7.2 Intrinsic Nonlinearities

As we have done before, we begin by looking at the stress harmonics (as defined in Eq. (25)). The low amplitude scaling for the strain-kinetic model in LAOStrain with n = 1 has already been shown in Figure 4; to compare with this result, Figure 20 shows the same measures for two n = 0.5 and n = 2.

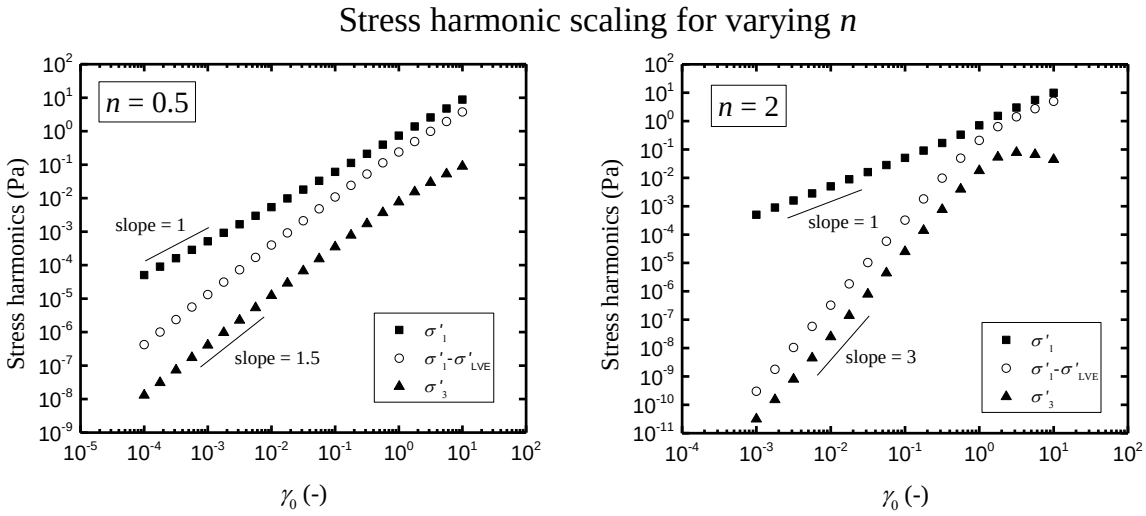

Figure 20 Low amplitude stress harmonic scaling for two values of n with $\mathrm{De} = 1$, $\lambda\kappa_A = 1$. Open symbols denote negative values.

For all values of n the scaling of the first harmonic is the expected linear response. The nonlinear harmonics, however, shows a slope of 1+n at low amplitude. As mentioned in prior sections, all know model solutions predict a slope of 2, so the fact that the power law scaling in this model not only deviates from this result, but is also dependent upon the value of a model parameter, is noteworthy.

As we move to the level of material functions, we begin with the low strain amplitude scaling of the nonlinear Chebyshev coefficients (as defined in Eq.(26)-(27)), which is shown in Figure 21.

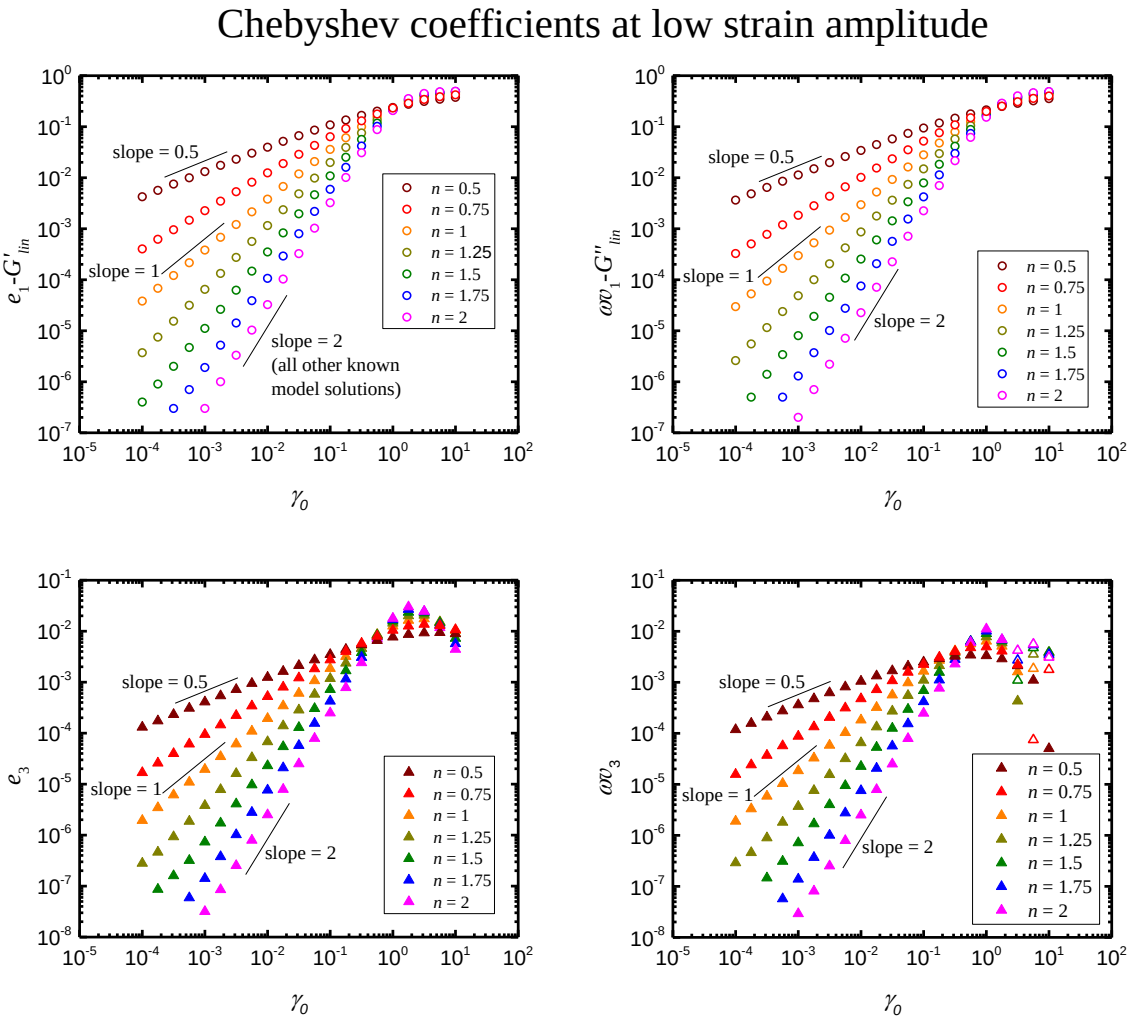

Figure 21 Chebyshev coefficients as a function of strain amplitude for varying values of reaction order n as defined in Eq. (39). Data are from simulation with $\mathrm{De}=1$, $\lambda\kappa_A=1$. Open symbols denote negative values.

As already established in Figure 5, when $n=1$ the third harmonics and the deviations of the first harmonics from their linear values scale as $\sim\gamma_0^{\,1}$ at low strain amplitudes. Figure 21 shows that in the more generalized case, the nonlinear harmonics scale as $\sim\gamma_o^{\,n}$. This variable scaling with changing value of a material parameter has not seen in any existing analysis of any

constitutive model. Because of this result we must once again modify the definition of the intrinsic Chebyshev coefficients to reflect the different scaling. The expression

$$\begin{aligned}\sigma(t;\gamma_0,\omega) = {} & \gamma_0\left\{G'(\omega)\sin\omega t + G''(\omega)\cos\omega t\right\} + \\ & {\gamma_0}^n\left\{\left[e_1\right](\omega)\sin\omega t + \omega\left[v_1\right](\omega)\cos\omega t\right\} + \\ & {\gamma_0}^n\left\{-\left[e_3\right](\omega)\sin 3\omega t + \omega\left[v_3\right](\omega)\cos 3\omega t\right\} + \mathcal{O}\left({\gamma_0}^{2+n}\right)\end{aligned} \tag{55}$$

accounts for the new slopes, allowing us to continue our analysis and compare the asymptotic material coefficients across varying order of reaction.

Figure 22 shows the amplitude-intrinsic Chebyshev coefficients as a function of frequency for varying values of *n*. Data are from simulation with $\lambda\kappa_A = 1$. Changing the order of reaction does not change the sign of any of the four material functions for any value of Deborah number (the data for *n* = 1 in Figure 22 are identical to the data for $\lambda\kappa_A = 1$ in Figure 7).

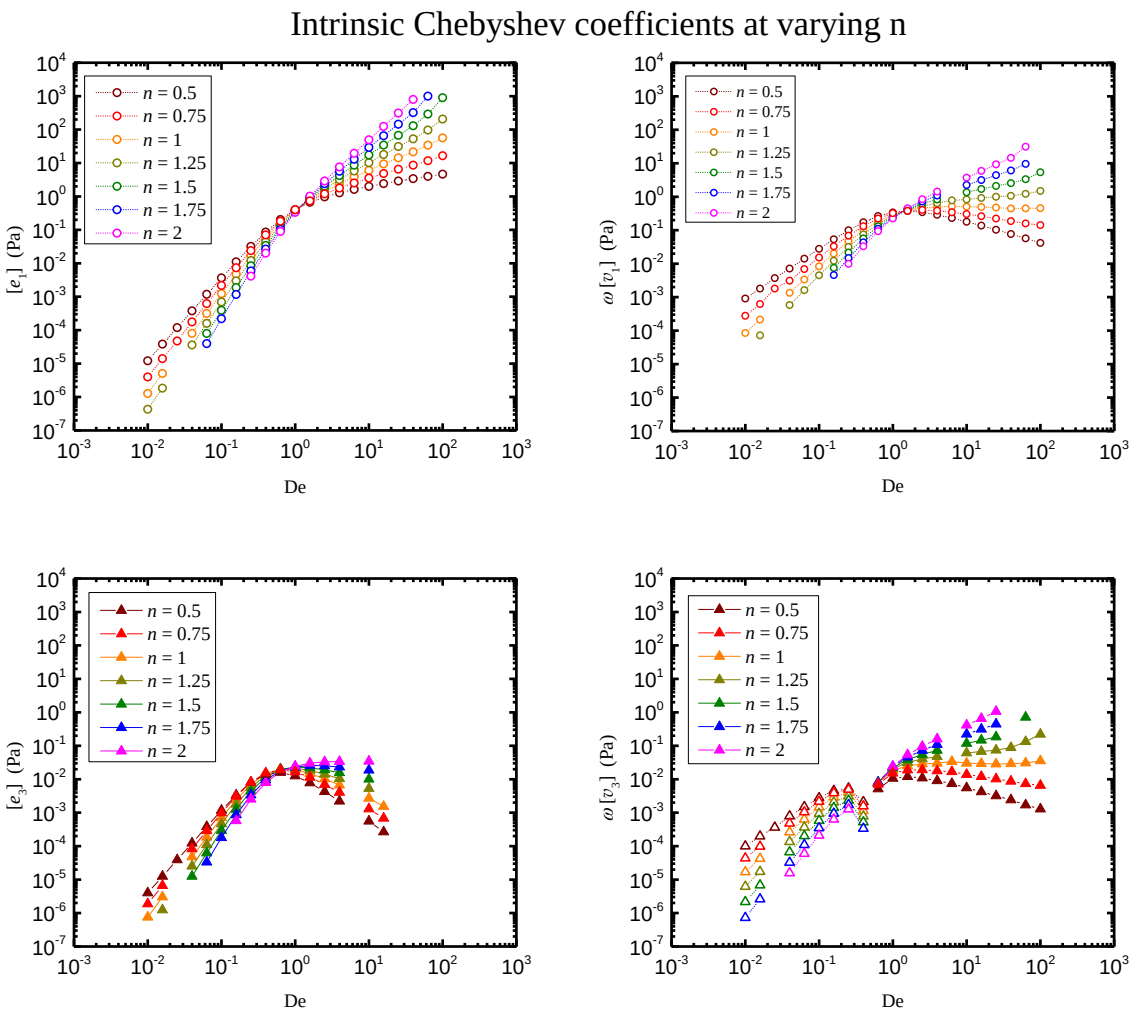

Figure 22 Intrinsic Chebyshev coefficients as defined in Eq. (55) as a function of frequency for varying values of the order of reaction exponent *n*. All plots shown are for $\lambda\kappa_A = 1$. Open symbols denote negative values.

This indicates that *n* does not affect whether the material response is shear thickening/thinning or strain stiffening/softening with respect to either intercycle or intracycle changes. It does, however, affect the magnitude of all four intrinsic Chebyshev coefficients. Increasing *n* increases the slope of each material function with respect to De, decreasing the magnitude at low De and increasing the magnitude at high De. The contour of each material function has one point (near De = 1) where the magnitude is the same for all values of *n* that are shown. The terminal regime slopes are also changed (decreased at low De and increased at high

De) by *n*—for example the plateaus that are seen at high De in $[v_1]$ and $[v_3]$ when $n = 1$ show a positive terminal slope for the greater values and a negative terminal slope for lesser values, always equal to n-1.

In summary, the addition of the sixth model parameter n to govern the order of reaction brings about a fundamental change in the model response when the value of $n \neq 1$. The unique power-function scaling of the nonlinear harmonics at low amplitude established in Chapter 4 is shown to be a function of n, which makes this model quite different in that aspect from any other model that has been analyzed in LAOS. This also requires a flexible definition of the amplitude-intrinsic material functions to accommodate the dependence of this scaling on the value of a model parameter. Furthermore varying the value of n is shown to affect the frequency-dependent asymptotic nonlinear fingerprint of the model. The form of modifying the order of reaction that we have explored here is one of many that exist in the literature; given the broad and fundamental effect of this modification, changing the order of reaction in other manners stands as an interesting subject for further exploration. Here we conclude our examination of the LAOS signatures of the Thixoelastic Jeffreys model, and take a step back to give context as to where this model fits into the bigger picture.

Chapter 8

Broader Context – Yield-stress Fluid Constitutive Modeling

A wide variety of constitutive models are used in the literature to predict the behavior of yield-stress fluids. There are a number of features that are present in some models but not in others that are important factors in the process of selecting a model to use for a given material in a given flow. In Table 2 we show a representative sample of these models, categorized by the subset of these features that they exhibit. The different model traits that we use to characterize these models are: viscoelastic time dependency, elasticity below yield, elasticity during flow, thixotropy, analytical solutions, and number of parameters.

The simplest yield-stress fluid models are written as a single equation for stress or viscosity as a function of shear rate, resulting in an expression that does not incorporate any elasticity (category 1 in the chart). The addition of elasticity can be accomplished in a number of ways, hence we have three separate model traits to characterize the elastic properties. The first is "viscoelastic time dependency," which refers to the presence of a model timescale (e.g. a relaxation time) that gives rise to behavioral dependence on flow timescale. We also differentiate "elasticity below yield," which refers to the ability to accumulate elastic strain without flow. The third distinct elastic trait is "elasticity during flow," which denotes the ability to track and evolve elastic strain at finite shear rates.

Some models exhibit thixotropy (such as the models explored in Chapters 2-7) while others do not, therefore we include this trait as another category in the summary chart. The ability to

achieve an analytical solution for a flow problem can also be an important consideration when selecting a model to use, so we also include columns to denote whether each model is generally solvable in controlled stress flows and controlled strain flows (obviously the ability to obtain a solution is dependent upon the precise problem or flow and the full designation is more complex than a "yes" or "no," but here for compact representation we choose the short designation that is most representative of the more complex truth). Finally we include a column in the chart to display the total number of parameters present in each model. As discussed in Chapter 2, the number of parameters in a model is a delicate balance between flexibility to fit data and capture a wide variety of phenomena (with more parameters) and manageability of analysis and understanding (with fewer parameters).

It is also important to note that in the process of model selection the optimal model is a function of both the fluid and the flow being examined. For example, if the circumstance in which a fluid is being modeled is exclusively steady flow, then models that incorporate transients may add unnecessary complexity, even if the fluid being modeled shows transient effects in other flows. Therefore our recommended procedure of model down-selection is to establish what features have an impact on the problem in question (examining the properties of both the material and the flow), then consult the chart in Table 2 to determine the model that best captures those features.

MODEL		FEATURES									
Name	Equation(s)	Viscoelastic time-dependent?	Elasticity below yield?	Elasticity during flow?	Thixotropy?	Control $\sigma(t)$, solve for γ?	Control $\gamma(t)$, solve for σ?	Number of parameters	Microstructural origin?	General comments
Category 1: Purely viscous										
Bingham (1916)	$\sigma = \sigma_y + \eta_p \dot{\gamma}$	No	No	No	No	Yes	Yes	2	No	
Casson (1957)	$\sqrt{\sigma} = \sqrt{\sigma_y} + \sqrt{\eta_p \dot{\gamma}}$	No	No	No	No	Yes	Yes	2	No	
Herschel-Bulkley (1926)	$\sigma = \sigma_y + k\dot{\gamma}^n$	No	No	No	No	Yes	Yes	3	No	
Genralized Casson (1975)	$\sqrt{\sigma} = \sqrt{\sigma_y} + K\dot{\gamma}^m$	No	No	No	No	Yes	Yes	3	No	Hybrid of Casson and Herschel-Bulkley
Shul'man (1970)	$\sigma^{1/n} = {\sigma_y}^{1/n} + (\eta_p \dot{\gamma})^{1/n}$	No	No	No	No	Yes	Yes	3	No	Same as Casson when n=2
Papanastasiou (1987)	$\eta - \eta_\infty = \frac{\sigma_y(1-\exp(-a\dot{\gamma}))}{\dot{\gamma}}$	No	No	No	No	Yes	Yes	3	No	
Carreau-Yasuda	$\frac{\eta-\eta_\infty}{\eta_0-\eta_\infty} = \frac{1}{[1+(\lambda\dot{\gamma})^a](1-n)/a}$	No	No	No	No	some cases	Yes	5	No	
Cross (1965)	$\frac{\eta-\eta_\infty}{\eta_0-\eta_\infty} = \frac{1}{1+(\lambda\dot{\gamma})^m}$	No	No	No	No	some cases	Yes	4	No	
Powell-Eyring	$\frac{\eta-\eta_\infty}{\eta_0-\eta_\infty} = \frac{\sinh^{-1}(\lambda\dot{\gamma})}{\lambda\dot{\gamma}}$	No	No	No	No	some cases	Yes	3	No	
Ellis	$\frac{\eta}{\eta_0} = \frac{1}{1+(\sigma/\sigma_2)^{a-1}}$	No	No	No	No	Yes	Yes	3	No	
Coussot (2010)	$\sigma = \mu\dot{\gamma} + \frac{\sigma_c}{1+\dot{\gamma}\theta/\gamma_c}$	No	No	No	No*	Yes	Yes	4	Yes	Can exhibit shear-banding

Table 2 Yield-stress fluid model summary chart.

Table 2 (cont.)

MODEL		FEATURES								
Name	Equation(s)	Viscoelastic time-dependent?	Elasticity below yield?	Elasticity during flow?	Thixotropy?	Control $\sigma(t)$, solve for $\dot{\gamma}$?	Control $\dot{\gamma}(t)$, solve for σ?	Number of parameters	Microstructural origin?	General comments
Category 2: Viscoelastic addition to purely viscous										
Elastic Bingham	$\sigma = G\gamma_E \quad (\lvert\gamma_E\rvert < \gamma_y)$ $\sigma = G\gamma_E + \eta_p\dot{\gamma} \quad (\lvert\gamma_E\rvert \geq \gamma_y)$	No	Yes	Yes	No	Yes	Yes	3	No	Same adjustment can be made to any of the above models
Schwedoff (1890)	$\sigma + \lambda_0\frac{\partial\sigma}{\partial t} = \sigma_0 + \mu\dot{\gamma}$	Yes	No	No	No	Yes	Yes	3	No	Same as Bingham if $\lambda_0 = 0$
Category 3: Structure Parameter										
Moller (2006)	$\sigma = \eta_0(1+\beta\lambda^n)\dot{\gamma}; \quad \frac{d\lambda}{dt} = \frac{1}{\tau} - \alpha\lambda\dot{\gamma}$	No	No	No	Yes	some cases	Yes	5	No	Simplest structure parameter model
Thixo-elastic Maxwell (1999)	$\frac{1}{G(S)}\dot{\sigma} + \frac{\sigma}{\eta(S)} = \dot{\gamma}(t)$ $\frac{dS}{dt} = \kappa_A(S_0 - S) - \kappa_D(S - S_\infty)$ $\eta(S) = \eta_\infty + (\eta_0 - \eta_\infty)S(\Gamma)$ $G(S) = G_0 S$	Yes	Yes	Yes	Yes	Yes	Yes	5	No	
Thixo-elastic Maxwell-Jeffreys	$\frac{\dot{\sigma}}{G(S)} + \frac{\sigma}{\eta(S)} = \dot{\gamma}(t) + t_R\ddot{\gamma}(t)$ S, η, G defined as in Thixoelastic Maxwell	Yes	Yes	Yes	Yes	Yes	Yes	6	No	
Thixo-elastic Burgers	$\dot{\gamma}(t) + t_R\ddot{\gamma}(t) = t_R\frac{\ddot{\sigma}}{G_i} + \frac{\dot{\sigma}}{G(S)} + \frac{\sigma}{\eta(S)}$ S, η, G defined as in Thixoelastic Maxwell	Yes	Yes	Yes	Yes	Yes	No	7	No	

Table 2 (cont.)

MODEL		FEATURES								
Name	Equation(s)	Viscoelastic time-dependent?	Elasticity below yield?	Elasticity during flow?	Thixotropy?	Control $\sigma(t)$, solve for $\dot{\gamma}$?	Control $\dot{\gamma}(t)$, solve for σ?	Number of parameters	Microstructural origin?	General comments
Category 3: Structure Parameter (cont.)										
de Souza Mendes (2009)	$\sigma + \dot{\sigma}\frac{\eta_v(\lambda)}{G(\lambda)} = \eta_v(\lambda)\dot{\gamma}$ $G = \frac{G_0}{\lambda^m}$; $\eta_v(\lambda) = \left(\frac{\eta_0}{\eta_\infty}\right)^\lambda \eta_\infty$ $\frac{d\lambda}{dt} = \frac{1}{t_{eq}}[(1-\lambda)^a - D]$ $D = (1-\lambda_{ss})^a \left(\frac{\lambda}{\lambda_{ss}}\right)^b \left(\frac{\sigma}{\eta_v(\lambda_{ss})\dot{\gamma}}\right)^c$ $\lambda_{ss}(\dot{\gamma}) = \left(\frac{\ln\eta_{ss}(\dot{\gamma}) - \ln\eta_\infty}{\ln\eta_0 - \ln\eta_\infty}\right)$ $\eta_{ss}(\dot{\gamma}) = \left[1 - \exp\left(-\frac{\eta_0\dot{\gamma}}{\sigma_0}\right)\right]$ $\times\left\{\frac{\sigma_0 - \sigma_{0d}}{\dot{\gamma}} e^{-\dot{\gamma}/\dot{\gamma}_{0d}} + \frac{\sigma_{0d}}{\dot{\gamma}} + K\dot{\gamma}^{n-1}\right\} + \eta_\infty$	Yes	Yes	Yes	Yes	Yes	No	12	Yes	Equivalent to Thixoelastic Maxwell, but with more complex relation for the evolution of the structure parameter
de Souza Mendes (2011)	$\sigma + \dot{\sigma}\theta_1 = \eta_v(\dot{\gamma} + \theta_2\ddot{\gamma})$ $\theta_1 = \left(1 - \frac{\eta_\infty}{\eta_v(\lambda)}\right)\frac{\eta_v(\lambda)}{G_s(\lambda)}$; $\theta_2 = \left(1 - \frac{\eta_\infty}{\eta_v(\lambda)}\right)\frac{\eta_\infty}{G_s(\lambda)}$ $G_s, \eta_v(\lambda)$, $\frac{d\lambda}{dt}, \lambda_{ss}(\dot{\gamma}), \eta_{ss}(\dot{\gamma})$ as def. in dSM 2009	Yes	Yes	Yes	Yes	Yes	No	12	Yes	TEMJ with more complex structure equation
Putz (2009)	$\Phi\frac{d\sigma}{dt} = \frac{G}{\sigma\eta} + \frac{G}{\sigma}\frac{d\dot{\gamma}}{dt}$ $\frac{d\Phi}{dt} = -K_d\Gamma\Phi + K_r\left[1 - \tanh\left(\frac{\Gamma - 1}{w}\right)\right]\Phi(1-\Phi) + \delta$	Yes	Yes	Yes	Yes	Yes	Yes	6	Yes	
Mujumdar (2002)	$\sigma = \lambda G\gamma_e + (1-\lambda)K\dot{\gamma}^n$ $\frac{d\gamma_e}{dt} = \dot{\gamma}$ if $\lvert\gamma_e\rvert < \gamma_c(\lambda)$; else $\lvert\gamma_e\rvert = \gamma_c(\lambda)$ $\gamma_c = \gamma_{c0}\lambda^m$ $\frac{d\lambda}{dt} = -k_1\dot{\gamma}_+\lambda + k_2(1-\lambda)$ $\dot{\gamma}_+ = 0$ if $\dot{\gamma}\gamma_e \leq 0$; $\dot{\gamma}_+ = \lvert\dot{\gamma}\rvert$ if $\dot{\gamma}\gamma_e > 0$	Yes	Yes	Yes	Yes	some cases	Yes	7	No	

Table 2 (cont.)

MODEL		FEATURES								
Name	Equation(s)	Viscoelastic time-dependent?	Elasticity below yield?	Elasticity during flow?	Thixotropy?	Control $\sigma(t)$, solve for $\dot{\gamma}$?	Control $\dot{\gamma}(t)$, solve for σ?	Number of parameters	Microstructural origin?	General comments
Dullaert (2006)	$\sigma = G_0\lambda\gamma_e + (\eta_{st0}\lambda + \eta_\infty)\dot{\gamma}$ $\frac{d\lambda}{dt} = \left(\frac{1}{t}\right)^\beta [-k_1\dot{\gamma}\lambda + k_2\dot{\gamma}^{0.5}(1-\lambda) + k_3(1-\lambda)]$ $\frac{d\gamma_e}{dt} = \left(\frac{k_4}{t}\right)^\beta [\sigma\gamma_c - \sigma_{ss}(\dot{\gamma})\gamma_e]$ $\sigma_{ss} = \lambda_{ss}(\dot{\gamma})G_0\gamma_c + \lambda_{ss}(\dot{\gamma})\eta_{st0}\dot{\gamma} + \eta_\infty\dot{\gamma}$	Yes	Yes	Yes	Yes	No	Yes	9	No	
Moore (1959)	$\sigma = (\eta_\infty + c\lambda)\dot{\gamma}$ $\frac{d\lambda}{dt} = a(1-\lambda) - b\lambda\dot{\gamma}$	No	No	No	Yes	Yes	Yes	4	No	First structure parameter model
Cross – Transient (1965)	$\eta = \eta_\infty + BL$ $\frac{dL}{dt} = k_2P - (k_0 + (k_1\dot{\gamma})^m)L$	No	No	No	Yes	No	Yes	6	No	
Ardakani (2011)	$\sigma = \sigma_y(1 - \exp(-m\dot{\gamma})) + (1+\xi)\eta_\infty\dot{\gamma}$ $\frac{d\xi}{dt} = -k_1\dot{\gamma}\xi + k_2(1-\xi)$	No	No	No	Yes	some cases	Yes	5	No	
Category 4: Glassy rheology										
Soft Glassy Rheology (1998)	$\sigma(t) = \gamma(t)G_0(Z(t,0)) + \int_0^t \dot{\gamma}(t')G_p(Z(t,t'))dt'$ $Z(t,t') = \int_{t'}^t \exp([\gamma(t'') - \gamma(t')]^2/2x)dt''$ $G_p(Z) = \int_0^\infty \rho(E)\exp(-Ze^{-E/x})\,dE$	Yes	Yes	Yes	Yes	No	Yes	4	Yes	

Chapter 9

Conclusions

Here we anchor future exploration of thixotropic viscoelastic constitutive models by characterizing the simplest model that captures both phenomena. A transient and nonlinear test is required in order to fully characterize this model, and we demonstrate that large-amplitude oscillatory shear serves this purpose effectively. The fully nonlinear response provides a highly detailed signature of the model that is dense with information, but at the cost of high dimensionality. The asymptotic nonlinearities provide a rheological fingerprint with lower dimensionality, which is more easily manageable, and maintains the ability to separate and identify thixotropic and viscoelastic timescales. These signatures impart a basic understanding of the interplay of thixotropy and viscoelasticity, and serve as a basis for studying more complex constitutive models. Analysis here is limited to only the alternant state of the oscillatory response, which provides the output with the least complexity, and it is worth noting that more information on the interplay of thixotropic and viscoelastic timescales may lie in the transient startup of these oscillatory waves.

These intrinsic nonlinearities provide a useful model fingerprint that can aid and improve constitutive model selection to match experimental data, especially for cases with "unobservable" thixotropy below the transient step resolution of experiments, since this model predicts the ability to identify short thixotropic timescales across the range of oscillatory frequency using amplitude-intrinsic LAOStrain material functions derived in Eq. (31)-(34). This motivates future experimental measurements of thixotropy using amplitude-intrinsic LAOS.

Observations of short thixotropic (aging and rejuvenation) timescales would bring deeper insight into categorizing yield-stress fluids based on quantifiable thixotropy, rather than the absence of observable thixotropy [17], a definition currently limited by the experimental equipment and protocol being used.

Having established the amplitude-intrinsic fingerprint of our simplest-case model, we proceed to observe the changes to this fingerprint that arise in response to two modifications that are common in thixotropic constitutive modeling. The kinetic structure breakdown can be driven either by stress or by strain rate, and the model can be subjected to either a controlled stress input or a controlled strain input. We compare and contrast all four model permutations that arise from these two choices. The distinction between the stress-kinetic model and the strain-kinetic model is most distinctly seen in LAOStrain, while the stress-kinetic model showed a sharper contrast between LAOStress and LAOStrain. Overall, these variations show unique signatures, highlighting the importance of the choice between stress control and strain control both in the kinetic structure breakdown and in the controlled input. We also introduce a sixth model parameter 'n' to govern the order of reaction of the kinetic equation. The most remarkable result shown here is the low amplitude power-function scaling of the model nonlinearities, which is unique among known model solutions in LAOS. The parameter n further modifies this unique feature, and we show that the power-function slope of the nonlinearities is a function of n.

Overall, this exploration provides a foundation and starting point for further exploration of the broad and diverse space of thixotropic constitutive models. We establish a detailed signature of the simplest representative model, and observe the changes to this signature in response to two common modifications, providing the framework to compare and contrast more complicated variants.

References

[1] H.A. Barnes, Thixotropy - a review, Journal of Non-Newtonian Fluid Mechanics. 70 (1997) 1–33.

[2] A.L. Copley, The phenomenon of thixotropy in hemophilic and heparinized blood, Science (New York, N.Y.). 94 (1941) 543–4.

[3] Y.S. Pek, A.C.A. Wan, A. Shekaran, L. Zhuo, J.Y. Ying, A thixotropic nanocomposite gel for three-dimensional cell culture., Nature Nanotechnology. 3 (2008) 671–5.

[4] P.N. Zawaneh, S.P. Singh, R.F. Padera, P.W. Henderson, J.A. Spector, D. Putnam, Design of an injectable synthetic and biodegradable surgical biomaterial., Proceedings of the National Academy of Sciences of the United States of America. 107 (2010) 11014–9.

[5] P. Kollmannsberger, B. Fabry, Linear and Nonlinear Rheology of Living Cells, Annual Review of Materials Research. 41 (2011) 75–97.

[6] G. Well, Thixotropy, and the Mechanics of Burrowing in the Lugworm (Arenicola marina L.), Nature. 162 (1948) 652–653.

[7] A. Kerst, C. Chmielewski, C. Livesay, R.E. Buxbaum, S.R. Heidemann, Liquid crystal domains and thixotropy of filamentous actin suspensions., Proceedings of the National Academy of Sciences. 87 (1990) 4241–4245.

[8] J. Eliassaf, A. Silberberg, A. Katchalsky, Negative Thixotropy of Aqueous Solutions of Polymethacrylic Acid, Nature. 176 (1955) 1119–1119.

[9] P. Coussot, Q.D. Nguyen, H.T. Huynh, D. Bonn, Viscosity bifurcation in thixotropic, yielding fluids, Journal of Rheology. 46 (2002) 573.

[10] F. Pignon, Thixotropic colloidal suspensions and flow curves with minimum: Identification of flow regimes and rheometric consequences, Journal of Rheology. 40 (1996) 573.

[11] K. Masschaele, J. Fransaer, J. Vermant, Direct visualization of yielding in model two-dimensional colloidal gels subjected to shear flow, Journal of Rheology. 53 (2009) 1437.

[12] X. Cheng, J.H. McCoy, J.N. Israelachvili, I. Cohen, Imaging the microscopic structure of shear thinning and thickening colloidal suspensions., Science (New York, N.Y.). 333 (2011) 1276–9.

[13] D. Bonn, M.M. Denn, Yield stress fluids slowly yield to analysis, Science. 324 (2009) 1401–1402.

[14] J. Mewis, N.J. Wagner, Thixotropy., Advances in Colloid and Interface Science. 147-148 (2009) 214–27.

[15] C. Goodeve, G. Whitfield, The measurement of thixotropy in absolute units, Transactions of the Faraday Society. 34 (1938) 511–520.

[16] F. Moore, The rheology of ceramic slips and bodies, Transactions of the British Ceramic Society. 58 (1959) 470–494.

[17] P. Moller, A. Fall, V. Chikkadi, D. Derks, D. Bonn, An attempt to categorize yield stress fluid behaviour., Philosophical Transactions. Series A, Mathematical, Physical, and Engineering Sciences. 367 (2009) 5139–55.

[18] T. Divoux, D. Tamarii, C. Barentin, S. Manneville, Transient Shear Banding in a Simple Yield Stress Fluid, Physical Review Letters. 104 (2010) 208301.

[19] P. Coussot, G. Ovarlez, Physical origin of shear-banding in jammed systems., The European Physical Journal. E, Soft Matter. 33 (2010) 183–8.

[20] J. Paredes, N. Shahidzadeh-Bonn, D. Bonn, Shear banding in thixotropic and normal emulsions., Journal of Physics. Condensed Matter : an Institute of Physics Journal. 23 (2011) 284116.

[21] A. Malkin, S. Ilyin, A. Semakov, V. Kulichikhin, Viscoplasticity and stratified flow of colloid suspensions, Soft Matter. 8 (2012) 2607.

[22] P. Chaudhuri, L. Berthier, L. Bocquet, Inhomogeneous shear flows in soft jammed materials with tunable attractive forces, Physical Review E. 85 (2012) 021503.

[23] M. Aytouna, J. Paredes, N. Shahidzadeh-Bonn, S. Moulinet, C. Wagner, Y. Amarouchene, et al., Drop Formation in Non-Newtonian Fluids, Physical Review Letters. 110 (2013) 034501.

[24] M.M. Denn, D. Bonn, Issues in the flow of yield-stress liquids, Rheologica Acta. 50 (2010) 307–315.

[25] J. Mewis, N.J. Wagner, Colloidal Suspension Rheology (Cambridge Series in Chemical Engineering), Cambridge University Press, 2012.

[26] P.C.F. Møller, J. Mewis, D. Bonn, Yield stress and thixotropy: on the difficulty of measuring yield stresses in practice, Soft Matter. 2 (2006) 274.

[27] K. Dullaert, J. Mewis, A structural kinetics model for thixotropy, Journal of Non-Newtonian Fluid Mechanics. 139 (2006) 21–30.

[28] M.M. Cross, Rheology of Non-Newtonian fluids: A new flow equation for pseudoplastic systems, Journal of Colloid Science. 20 (1964) 417–437.

[29] A.M. Grillet, R.R. Rao, D.B. Adolf, S. Kawaguchi, L. a. Mondy, Practical application of thixotropic suspension models, Journal of Rheology. 53 (2009) 169.

[30] A. Mujumdar, A.N. Beris, A.B. Metzner, Transient phenomena in thixotropic systems, Journal of Non-Newtonian Fluid Mechanics. 102 (2002) 157–178.

[31] D. Quemada, Rheological modelling of complex fluids:AV: Thixotropic and "thixoelastic" behaviour. Start-up and stress relaxation, creep tests, and hysteresis cycles, The European Physical Journal - Applied Physics. 5 (1999) 191–207.

[32] P.R. de Souza Mendes, Thixotropic elasto-viscoplastic model for structured fluids, Soft Matter. 7 (2011) 2471.

[33] A.G. Fredrickson, A model for the thixotropy of suspensions, AIChE Journal. 16 (1970) 436–441.

[34] H.A. Ardakani, E. Mitsoulis, S.G. Hatzikiriakos, Thixotropic flow of toothpaste through extrusion dies, Journal of Non-Newtonian Fluid Mechanics. 166 (2011) 1262–1271.

[35] F. Bautista, J.M. de Santos, J.E. Puig, O. Manero, Understanding thixotropic and antithixotropic behavior of viscoelastic micellar solutions and liquid crystalline dispersions. I. The model, Journal of Non-Newtonian Fluid Mechanics. 80 (1999) 93–113.

[36] R.S. Jeyaseelan, A.J. Giacomin, Network theory for polymer solutions in large amplitude oscillatory shear, Journal of Non-Newtonian Fluid Mechanics. 148 (2008) 24–32.

[37] J.J. Stickel, R.J. Phillips, R.L. Powell, A constitutive model for microstructure and total stress in particulate suspensions, Journal of Rheology. 50 (2006) 379.

[38] J.D. Goddard, A dissipative anisotropic fluid model for non-colloidal particle dispersions, Journal of Fluid Mechanics. 568 (2006) 1.

[39] A.N. Beris, E. Stiakakis, D. Vlassopoulos, A thermodynamically consistent model for the thixotropic behavior of concentrated star polymer suspensions, Journal of Non-Newtonian Fluid Mechanics. 152 (2008) 76–85.

[40] B.R. Munson, A.P. Rothmayer, T.H. Okiishi, W.W. Huebsch, Fundamentals of Fluid Mechanics, Wiley, 2012.

[41] A. Pipkin, Lectures on Viscoelasticity Theory, Springer, New York, 1972.

[42] J. Mewis, N.J. Wagner, Colloidal Suspension Rheology (Cambridge Series in Chemical Engineering), Cambridge University Press, 2012.

[43] R.H. Ewoldt, N.A. Bharadwaj, Low-dimensional intrinsic material functions for nonlinear viscoelasticity, Rheologica Acta. 52 (2013) 201–219.

[44] W.M. Davis, C.W. Macosko, Nonlinear Dynamic Mechanical Moduli for Polycarbonate and PMMA, Journal of Rheology. 22 (1978) 53.

[45] R.H. Ewoldt, Defining nonlinear rheological material functions for oscillatory shear, Journal of Rheology. 57 (2013) 177.

[46] A. Lodge, Elastic Liquids, Springer, London, 1964.

[47] T. Spriggs, Constitutive equations for viscoelasic fluids, University of Wisconsin, Madison, 1966.

[48] M.C. Williams, R.B. Bird, Oscillatory behavior, Ind. Eng. Chem. Fundam. (1964) 42–49.

[49] I.A.N.F. Macdonaldt, B.D. Marsh, E. Ashare, Rheological behavior for large amplitude oscillatory motion, Chemical Engineering Science. 24 (1969) 1615–1625.

[50] N. Phan-thien, M. Newberry, R.I. Tanner, Non-linear oscillatory flow of a soft solid-like viscoelastic material, Journal of Non-Newtonian Fluid Mechanics. 92 (2006) 67–80.

[51] R.B. Bird, O. Hassager, S.I. Abdel-Khalik, Co-rotational rheological models and the Goddard expansion, AIChE Journal. 20 (1974) 1041–1066.

[52] A.K. Gurnon, N.J. Wagner, Large amplitude oscillatory shear (LAOS) measurements to obtain constitutive equation model parameters: Giesekus model of banding and nonbanding wormlike micelles, Journal of Rheology. 56 (2012) 333.

[53] J.G. Kirkwood, R.J. Plock, Non-Newtonian Viscoelastic Properties of Rod-Like Macromolecules in Solution, The Journal of Chemical Physics. 24 (1956) 665.

[54] E. Paul, Non-Newtonian Viscoelastic Properties of Rodlike Molecules in Solution: Comment on a Paper by Kirkwood and Plock, The Journal of Chemical Physics. 51 (1969) 1271.

[55] D.S. Pearson, W.E. Rochefort, Behavior of Concentrated Polystyrene Solutions in Large-Amplitude Oscillating Shear Fields, Journal of Polymer Science: Polymer Physics Edition. 20 (1982) 83–98.

[56] O.S. Fields, E. Helfand, D.S. Pearson, B. Laboratories, Calculation of the Nonlinear Stress of Polymers in Oscillatory Shear Fields, Journal of Polymer Science: Polymer Physics Edition. 20 (1982) 1249–1258.

[57] M.H. Wagner, V.H. Rolón-Garrido, K. Hyun, M. Wilhelm, Analysis of medium amplitude oscillatory shear data of entangled linear and model comb polymers, Journal of Rheology. 55 (2011) 495.

[58] X.-J. Fan, R. Byron Bird, A kinetic theory for polymer melts VI. calculation of additional material functions, Journal of Non-Newtonian Fluid Mechanics. 15 (1984) 341–373.

[59] W. Yu, M. Bousmina, M. Grmela, C. Zhou, Modeling of oscillatory shear flow of emulsions under small and large deformation fields, Journal of Rheology. 46 (2002) 1401.

[60] A.J. Giacomin, R.B. Bird, L.M. Johnson, A.W. Mix, Large-amplitude oscillatory shear flow from the corotational Maxwell model, Journal of Non-Newtonian Fluid Mechanics. 166 (2011) 1081–1099.

[61] M. Wilhelm, Fourier-Transform Rheology, Macromolecular Materials and Engineering. 287 (2002) 83–105.

[62] R.H. Ewoldt, A.E. Hosoi, G.H. McKinley, New measures for characterizing nonlinear viscoelasticity in large amplitude oscillatory shear, Journal of Rheology. 52 (2008) 1427.

[63] C.J. Dimitriou, R.H. Ewoldt, G.H. McKinley, Describing and prescribing the constitutive response of yield stress fluids using large amplitude oscillatory shear stress (LAOStress), Journal of Rheology. 57 (2013) 27.

[64] S.A. Rogers, A sequence of physical processes determined and quantified in LAOS: An instantaneous local 2D/3D approach, Journal of Rheology. 56 (2012) 1129.

[65] D. Quemada, Rheological modelling of complex fluids. I. The concept of effective volume fraction revisited, The European Physical Journal Applied Physics. 1 (1998) 119–127.

[66] P.R. de Souza Mendes, Modeling the thixotropic behavior of structured fluids, Journal of Non-Newtonian Fluid Mechanics. 164 (2009) 66–75.

[67] J.D. Ferry, Viscoelastic Properties of Polymers, Wiley, 1980.

[68] S.J. Hahn, T. Ree, H. Eyring, Thixotropic Substances, Industrial and Engineering Chemistry. 51 (1959) 856–857.

[69] G.R. Burgos, A.N. Alexandrou, V. Entov, Thixotropic rheology of semisolid metal suspensions, Journal of Materials Processing Technology. 110 (2001) 164–176.

[70] J. Vicente, C.L. a. Berli, Aging, rejuvenation, and thixotropy in yielding magnetorheological fluids, Rheologica Acta. (2013) 467–483.

Appendix A: Analytical Solution of Strain-kinetic in LAOStrain

Given:

Model

$$\frac{\dot{\sigma}}{G_0}+\frac{\sigma}{\eta_A}=\left(\xi+\frac{\eta_\infty}{\eta_A}\right)\dot{\gamma}+\frac{\eta_\infty}{G_0}\ddot{\gamma} \tag{56}$$

$$\dot{\xi}=(1-\xi)\kappa_A-\kappa_D\xi\,|\dot{\gamma}| \tag{57}$$

With input

$$\dot{\gamma}=\gamma_0\omega\sin(\omega t) \tag{58}$$

Find: Time periodic stress response to $\mathcal{O}\left(\gamma_0{}^2\right)$

Solution:

Solve for $\xi(t;\gamma_0,\omega)$

Begin by solving the kinetic equation, substituting Eq. (58) into Eq. (57):

$$\dot{\xi}=(1-\xi)\kappa_A-\kappa_D\xi\gamma_0\omega\,|\sin(\omega t)| \tag{59}$$

Group terms:

$$\begin{aligned}\dot{\xi}+\left(\kappa_A+\kappa_D\gamma_0\omega\,|\sin(\omega t)|\right)\xi&=\kappa_A\\ \dot{\xi}+A(t)\xi&=\kappa_A\end{aligned} \tag{60}$$

$$A(t)=\kappa_A+\kappa_D\gamma_0\omega\,|\sin(\omega t)| \tag{61}$$

Solution for a first order linear non-homogeneous ODE using an integrating factor:

$$\xi(t;\gamma_0,\omega) = e^{-\int A(t)dt}\left[\int \kappa_A e^{\int A(t)dt}dt + C\right] \tag{62}$$

The absolute value in (61) is cumbersome. As our end goal is a harmonic representation, it is convenient to substitute a Fourier series representation of $|\sin(\omega t)|$.

Fourier series (see (112)-(124) for derivation):

$$|\sin(\omega t)| = \frac{2}{\pi} - \sum_{n\ even}^{\infty} \frac{4}{\pi\left(n^2-1\right)}\cos(n\omega t) \tag{63}$$

Coefficients scale $\sim 1/n^2$ as expected due to discontinuous first derivative. Substitute Eq. (63) into Eq. (61) and integrate:

$$\int A(t)dt = \kappa_A t + \kappa_D\gamma_0\left(\frac{2\omega}{\pi}t - \sum_{n\ \text{even}}^{\infty}\frac{4}{n\pi(n^2-1)}\sin(n\omega t)\right) \tag{64}$$

Substitute Eq. (64) into Eq. (62):

$$\int \kappa_A e^{\int A(t)dt}dt = \int \kappa_A e^{\kappa_A t} e^{\kappa_D\gamma_0\left(\frac{2\omega}{\pi}t - \sum_{n\ even}^{\infty}\frac{4}{n\pi(n^2-1)}\sin(n\omega t)\right)}dt \tag{65}$$

We cannot directly integrate $e^{\sin(\omega t)}$. A full solution can be achieved by substituting a Fourier series, but the resulting expression is very complex. Here we seek only a solution to $\mathcal{O}\left(\gamma_0{}^2\right)$, hence we employ a MacLaurin series for the exponential: $e^x = 1 + x + \mathcal{O}(x^2)$

$$e^{\kappa_D\gamma_0\omega\left(\frac{2}{\pi}t - \sum_{n\ even}^{\infty}\frac{4}{n\pi\omega(n^2-1)}\sin(n\omega t)\right)} = 1 + \kappa_D\gamma_0\omega\left(\frac{2}{\pi}t - \sum_{n\ even}^{\infty}\frac{4}{n\pi\omega(n^2-1)}\sin(n\omega t)\right) + \mathcal{O}\left(\kappa_D{}^2\gamma_0{}^2\right) \tag{66}$$

Substitute Eq. (66) into Eq. (65):

$$\int \kappa_A e^{\int A(t)dt}dt = \int \kappa_A e^{\kappa_A t}\left[1 + \kappa_D\gamma_0\omega\left(\frac{2}{\pi}t - \sum_{n\ even}^{\infty}\frac{4}{n\pi\omega(n^2-1)}\sin(n\omega t)\right) + \mathcal{O}\left(\kappa_D{}^2\gamma_0{}^2\right)\right]dt \tag{67}$$

Integrate. $\int e^{\kappa_A t}\sin(n\omega t)dt$ is done by integrating by parts twice (which recovers the original integral plus two summative terms) then solving for the original term:

$$\begin{aligned}\int \kappa_A e^{\int A(t)dt}dt &= e^{\kappa_A t} + \frac{2}{\pi}\kappa_A\kappa_D\gamma_0\omega\int te^{\kappa_A t}dt... \\ &-\frac{4}{\pi}\kappa_A\kappa_D\gamma_0\sum_{n\ \text{even}}^{\infty}\frac{1}{n(n^2-1)}\int e^{\kappa_A t}\sin(n\omega t)dt + e^{\kappa_A t}\mathcal{O}\left(\kappa_D{}^2\gamma_0{}^2\right)\end{aligned} \tag{68}$$

$$\begin{aligned}\int \kappa_A e^{\int A(t)dt}dt &= e^{\kappa_A t} + \frac{2}{\pi}\kappa_D\gamma_0\omega e^{\kappa_A t}\left(t-\frac{1}{\kappa_A}\right)-... \\ &\frac{4}{\pi}\kappa_A\kappa_D\gamma_0\sum_{n\ \text{even}}^{\infty}\frac{1}{n(n^2-1)}\left[\frac{e^{\kappa_A t}}{\kappa_A{}^2+n^2\omega^2}\left(\kappa_A\sin(n\omega t)-n\omega\cos(n\omega t)\right)\right]+e^{\kappa_A t}\mathcal{O}\left(\kappa_D{}^2\gamma_0{}^2\right)\end{aligned} \tag{69}$$

Substitute Eq. (69) and (66) into Eq. (62) (again expanding the exponential to $\mathcal{O}\left(\kappa_D{}^2\gamma_0{}^2\right)$):

$$\begin{aligned}\xi(t;\gamma_0,\omega) &= e^{-\kappa_A t}\left[1-\kappa_D\gamma_0\omega\left(\frac{2}{\pi}t-\sum_{n\ even}^{\infty}\frac{4}{n\pi\omega(n^2-1)}\sin(n\omega t)\right)+\mathcal{O}\left(\kappa_D\gamma_0{}^2\right)\right]\times \\ &\left\{\begin{aligned}&e^{\kappa_A t}+\frac{2}{\pi}\kappa_D\gamma_0\omega e^{\kappa_A t}\left(t-\frac{1}{\kappa_A}\right)... \\ &-\frac{4}{\pi}\kappa_A\kappa_D\gamma_0\sum_{n\ even}^{\infty}\frac{1}{n(n^2-1)}\left[\frac{e^{\kappa_A t}}{\kappa_A{}^2+n^2\omega^2}\begin{pmatrix}\kappa_A\sin(n\omega t)-\\ n\omega\cos(n\omega t)\end{pmatrix}\right]+C+e^{\kappa_A t}\mathcal{O}\left(\kappa_D\gamma_0{}^2\right)\end{aligned}\right\}\end{aligned} \tag{70}$$

Multiply terms, while neglecting $\mathcal{O}\left(\kappa_D{}^2\gamma_0{}^2\right)$

$$\begin{aligned}\xi(t;\gamma_0,\omega) &= 1+\frac{2}{\pi}\kappa_D\gamma_0\omega\left(t-\frac{1}{\kappa_A}\right)... \\ &-\frac{4}{\pi}\kappa_A\kappa_D\gamma_0\sum_{n\ \text{even}}^{\infty}\frac{1}{n(n^2-1)}\frac{1}{\kappa_A{}^2+n^2\omega^2}\left(\kappa_A\sin(n\omega t)-n\omega\cos(n\omega t)\right)... \\ &-\frac{2}{\pi}\kappa_D\gamma_0\omega t+\kappa_D\gamma_0\sum_{n\ \text{even}}^{\infty}\frac{4}{n\pi(n^2-1)}\sin(n\omega t)+Ce^{-\kappa_A t}+\mathcal{O}\left(\kappa_D{}^2\gamma_0{}^2\right)\end{aligned} \tag{71}$$

Group terms:

$$\xi(t;\gamma_0,\omega) = 1 - \frac{2}{\pi}\kappa_D\gamma_0\frac{\omega}{\kappa_A}... + \frac{4}{\pi}\kappa_D\gamma_0\sum_{n\ \text{even}}^{\infty}\frac{1}{n(n^2-1)}\frac{1}{1+n^2\frac{\omega^2}{\kappa_A{}^2}}\left(\left(n^2\frac{\omega^2}{\kappa_A{}^2}\right)\sin(n\omega t) + n\frac{\omega}{\kappa_A}\cos(n\omega t)\right)... + Ce^{-\kappa_A t} + \mathcal{O}\left(\kappa_D{}^2\gamma_0{}^2\right) \quad (72)$$

Define:

$$W = \frac{\omega}{\kappa_A} \quad (73)$$

Take t to be large (long time $\rightarrow$ steady-state), hence $Ce^{-\kappa_A t} \approx 0$

$$\boxed{\xi(t;\gamma_0,\omega) = 1 - \frac{2}{\pi}\kappa_D\gamma_0 W\left[1 - 2\sum_{n\ even}^{\infty}\frac{nW\sin(n\omega t)+\cos(n\omega t)}{\left(n^2-1\right)\left(1+n^2W^2\right)}\right] + \mathcal{O}\left(\kappa_D{}^2\gamma_0{}^2\right)} \quad (74)$$

Comments:

- This expression is valid for all $\kappa_A t >> 1$
- The average value of structure over the cycle is $\xi_{avg} = 1 - \frac{2}{\pi}\kappa_D\gamma_0 W = 1 - \frac{2}{\pi}\text{Wi}$

(recall that this disregards higher order terms, and is only accurate at low amplitude and hence low Wi)

- As shown in Figure 23, the asymptotic solution is near perfect at Wi = 0.01, shows very slight deviation from numerical simulation at Wi = 0.1, and greatly underestimates ξ at Wi = 1.

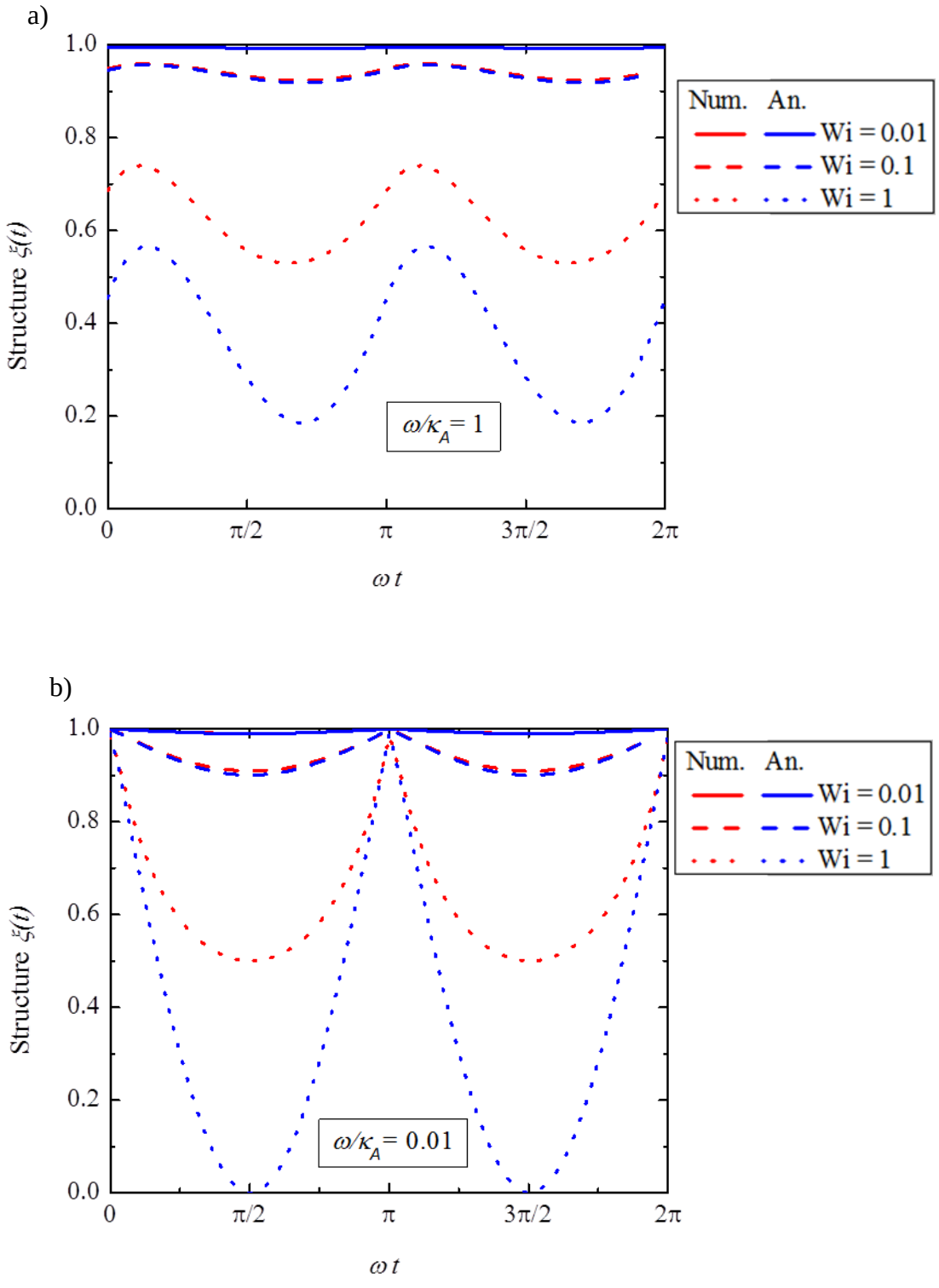

Figure 23 Comparison of asymptotic analytical solution to numerical solution for structure as a function of time at varying Weissenberg number, shown for two values of ω/κ_A, a) $\omega/\kappa_A = 1$, b) $\omega/\kappa_A = 0.01$.

Solve for $\sigma(t;\gamma_0,\omega)$

Moving on to the constitutive equation:

$$\begin{aligned}\dot{\sigma}+\frac{1}{\lambda}\sigma &= G_0\left(\xi+\frac{\eta_\infty}{\eta_A}\right)\gamma_0\omega\sin(\omega t)+\eta_\infty\gamma_0\omega^2\cos(\omega t)\\ \dot{\sigma}+\frac{1}{\lambda}\sigma &= B(t)\end{aligned} \tag{75}$$

$$B(t)=G_0\left(\xi+\frac{\eta_\infty}{\eta_A}\right)\gamma_0\omega\sin(\omega t)+\eta_\infty\gamma_0\omega^2\cos(\omega t) \tag{76}$$

Using the same ODE solution as in (62)

$$\sigma=e^{-t/\lambda}\left(\int e^{t/\lambda}B(t)dt+C_1\right) \tag{77}$$

Substitute (74) for $\xi(t)$

$$\begin{aligned}B(t)=G_0\left[1-\kappa_D\gamma_0\left(\frac{2W}{\pi}-\frac{4}{\pi}\sum_{n\ even}^{\infty}\frac{nW^2\sin(n\omega t)+W\cos(n\omega t)}{\left(n^2-1\right)\left(1+n^2W^2\right)}\right)+\frac{\eta_\infty}{\eta_A}\right]\gamma_0\omega\sin(\omega t)...\\ +\eta_\infty\gamma_0\omega^2\cos(\omega t)\end{aligned} \tag{78}$$

Distribute factors and separate the integral into its summative terms to deal with each individually:

$$\int e^{t/\lambda} B(t)dt = \alpha^* + \beta^* + \gamma^* + \delta^* + \varepsilon^* + \zeta^*$$

$$\alpha^* = \int e^{t/\lambda} G_0 \gamma_0 \omega \sin(\omega t)dt$$

$$\beta^* = -\int e^{t/\lambda} \frac{2G_0 \kappa_D {\gamma_0}^2 \omega W}{\pi} \sin(\omega t)dt$$

$$\gamma^* = \int e^{t/\lambda} \frac{4G_0 \kappa_D {\gamma_0}^2 \omega}{\pi} \sum_{n\ even}^{\infty} \frac{nW^2}{\left(n^2-1\right)\left(1+n^2W^2\right)} \sin(n\omega t)\sin(\omega t)dt \tag{79}$$

$$\delta^* = \int e^{t/\lambda} \frac{4G_0 \kappa_D {\gamma_0}^2 \omega}{\pi} \sum_{n\ even}^{\infty} \frac{W}{\left(n^2-1\right)\left(1+n^2W^2\right)} \cos(n\omega t)\sin(\omega t)dt$$

$$\varepsilon^* = \int e^{t/\lambda} G_0 \gamma_0 \omega \frac{\eta_\infty}{\eta_A} \sin(\omega t)dt$$

$$\zeta^* = \int e^{t/\lambda} \eta_\infty \gamma_0 \omega^2 \cos(\omega t)dt$$

Substitute using product-to-sum identities

$$\sin(u)\sin(v) = \frac{\cos(u-v) - \cos(u+v)}{2} \tag{80}$$

$$\cos(u)\sin(v) = \frac{\sin(u+v) - \sin(u-v)}{2} \tag{81}$$

and using the formulae

$$\int e^{ax} \cos(bx)dx = \frac{e^{ax}}{a^2+b^2}\left(b\sin(bx) + a\cos(bx)\right) \tag{82}$$

$$\int e^{ax} \sin(bx)dx = \frac{e^{ax}}{a^2+b^2}\left(a\sin(bx) - b\cos(bx)\right) \tag{83}$$

integrate each term individually, using the short-hand notation $c(n) \equiv \cos(n\omega t),\ \ s(n) \equiv \sin(n\omega t)$:

$$\alpha^* = G_0 \gamma_0 \omega \frac{e^{t/\lambda}}{\lambda^{-2}+\omega^2}\left(\lambda^{-1}\sin(\omega t) - \omega\cos(\omega t)\right) \tag{84}$$

$$\beta^* = \frac{-2G_0 \kappa_D {\gamma_0}^2 \omega W}{\pi} \frac{e^{t/\lambda}}{\lambda^{-2}+\omega^2}\left(\lambda^{-1}\sin(\omega t) - \omega\cos(\omega t)\right) \tag{85}$$

$$\gamma^* = \frac{2G_0\kappa_D{\gamma_0}^2\omega}{\pi}\sum_{n\ even}^{\infty}\frac{nW^2}{\left(n^2-1\right)\left(1+n^2W^2\right)}\int e^{t/\lambda}\left(c(n-1)-c(n+1)\right)dt \tag{86}$$

$$\gamma^* = \frac{2G_0\kappa_D{\gamma_0}^2\omega}{\pi}\times\ldots$$
$$\sum_{n\ even}^{\infty}\frac{nW^2}{\left(n^2-1\right)\left(1+n^2W^2\right)}\left[\begin{array}{l}\dfrac{e^{t/\lambda}}{\lambda^{-2}+\left(n-1\right)^2\omega^2}\left((n-1)\omega s(n-1)+\lambda^{-1}c(n-1)\right)\ldots\\ -\dfrac{e^{t/\lambda}}{\lambda^{-2}+\left(n+1\right)^2\omega^2}\left((n+1)\omega s(n+1)+\lambda^{-1}c(n+1)\right)\end{array}\right] \tag{87}$$

$$\delta^* = \frac{2G_0\kappa_D{\gamma_0}^2\omega}{\pi}\sum_{n\ even}^{\infty}\frac{W}{\left(n^2-1\right)\left(1+n^2W^2\right)}\int e^{t/\lambda}\left(s(n+1)-s(n-1)\right)dt \tag{88}$$

$$\delta^* = \frac{2G_0\kappa_D{\gamma_0}^2\omega}{\pi}\times\ldots$$
$$\sum_{n\ even}^{\infty}\frac{W}{\left(n^2-1\right)\left(1+n^2W^2\right)}\left[\begin{array}{l}\dfrac{e^{t/\lambda}}{\lambda^{-2}+\left(n+1\right)^2\omega^2}\left(\lambda^{-1}s(n+1)-(n+1)\omega c(n+1)\right)-\ldots\\ \dfrac{e^{t/\lambda}}{\lambda^{-2}+\left(n-1\right)^2\omega^2}\left(\lambda^{-1}s(n-1)-(n-1)\omega c(n-1)\right)\end{array}\right] \tag{89}$$

$$\varepsilon^* = \frac{\gamma_0\omega\eta_\infty}{\lambda}\frac{e^{t/\lambda}}{\lambda^{-2}+\omega^2}\left(\lambda^{-1}\sin(\omega t)-\omega\cos(\omega t)\right) \tag{90}$$

$$\zeta^* = \gamma_0\omega^2\eta_\infty\frac{e^{t/\lambda}}{\lambda^{-2}+\omega^2}\left(\omega\sin(\omega t)+\lambda^{-1}\cos(\omega t)\right) \tag{91}$$

Substitute these into the full expression for stress:

$$\sigma = e^{-t/\lambda}\left(\alpha^*+\beta^*+\gamma^*+\delta^*+\varepsilon^*+\zeta^*+C_1\right) \tag{92}$$

Define $D=\lambda\omega$, as well as $\alpha = e^{-t/\lambda}\alpha^*$, $\beta = e^{-t/\lambda}\beta^*$, etc.

$$\sigma = \alpha + \beta + \gamma + \delta + \varepsilon + \zeta + C_1 e^{-t/\lambda}$$

$$\alpha = \frac{G_0 \gamma_0 D}{1+D^2}\left(\sin(\omega t) - D\cos(\omega t)\right)$$

$$\beta = \frac{-2G_0 \kappa_D {\gamma_0}^2 DW}{\pi\left(1+D^2\right)}\left(\sin(\omega t) - D\cos(\omega t)\right)$$

$$\gamma = \frac{2G_0 \kappa_D {\gamma_0}^2 D}{\pi} \sum_{n\ even}^{\infty} \frac{nW^2}{\left(n^2-1\right)\left(1+n^2W^2\right)} \left[\begin{array}{l} \frac{1}{1+\left(n-1\right)^2 D^2}\left((n-1)Ds(n-1) + c(n-1)\right) - \ldots \\ \frac{1}{1+\left(n+1\right)^2 D^2}\left((n+1)Ds(n+1) + c(n+1)\right) \end{array} \right]$$

$$\delta = \frac{2G_0 \kappa_D {\gamma_0}^2 D}{\pi} \sum_{n\ even}^{\infty} \frac{W}{\left(n^2-1\right)\left(1+n^2W^2\right)} \left[\begin{array}{l} \frac{1}{1+\left(n+1\right)^2 D^2}\left(s(n+1) - (n+1)Dc(n+1)\right) - \ldots \\ \frac{1}{1+\left(n-1\right)^2 D^2}\left(s(n-1) - (n-1)Dc(n-1)\right) \end{array} \right]$$

$$\varepsilon = \frac{\gamma_0 \omega \eta_\infty}{1+D^2}\left(\sin(\omega t) - D\cos(\omega t)\right)$$

$$\zeta = \frac{\gamma_0 D \omega \eta_\infty}{1+D^2}\left(D\sin(\omega t) + \cos(\omega t)\right)$$

(93)

Solve for the stress harmonics

- $C_1 e^{-t/\lambda}$ is a decaying transient, $\rightarrow 0$ at steady-state
- $\alpha, \varepsilon, \zeta$ contribute only n=1 harmonics, $\mathcal{O}(\gamma_0)$
- β, γ, δ contribute odd harmonics, $\mathcal{O}({\gamma_0}^2)$

Group the $\mathcal{O}\left(\gamma_0\right)$ terms and reduce:

$$\alpha + \varepsilon + \zeta = \frac{1}{\lambda^{-2} + \omega^2} \left[\begin{array}{l} \left(\frac{G_0 \gamma_0 \omega}{\lambda} + \frac{\gamma_0 \omega \eta_\infty}{\lambda^2} + \eta_\infty \gamma_0 \omega^3 \right) \sin(\omega t) \ldots \\ + \left(-G_0 \gamma_0 \omega^2 - \frac{\gamma_0 \omega^2 \eta_\infty}{\lambda} + \frac{\eta_\infty \gamma_0 \omega^2}{\lambda} \right) \cos(\omega t) \end{array} \right] \qquad (94)$$

$$\alpha+\varepsilon+\zeta=\frac{1}{1+\left(\lambda\omega\right)^2}\left[\left(G_0\gamma_0\omega\lambda+\gamma_0\omega\eta_\infty\left(1+\left(\lambda\omega\right)^2\right)\right)\sin(\omega t)+\left(-G_0\gamma_0\left(\lambda\omega\right)^2\right)\cos(\omega t)\right] \quad (95)$$

$$\alpha+\varepsilon+\zeta=G_0\gamma_0\left[\left(\frac{D}{1+D^2}+\frac{\eta_\infty}{\eta_A}D\right)\sin(\omega t)-\frac{D^2}{1+D^2}\cos(\omega t)\right] \quad (96)$$

Group the $\mathcal{O}\left({\gamma_0}^2\right)$ terms and reduce. Define harmonics E_1, V_1, E_3, V_3 such that

$$\beta+\gamma+\delta=E_1c(1)+V_1s(1)+E_3c(3)+V_3s(3)+.... \quad (97)$$

For the sums in γ and δ, n = 2 contributes to both the first and third harmonics, n = 4 contributes only to the third harmonics (also to the fifth, for which we do not solve here)

Gather the coefficients of $\cos(\omega t)$ in β, γ, and δ and reduce (coefficient of $c(1)$ in β, coefficients of $c(n-1)$ for the n = 2 terms in γ and δ):

$$E_1=\frac{2G_0\kappa_D{\gamma_0}^2DW}{\pi\left(1+D^2\right)}(D)+\frac{2G_0\kappa_D{\gamma_0}^2D}{\pi}\frac{1}{3\left(1+4W^2\right)}\frac{1}{\left(1+D^2\right)}\left[2W^2(1)+W(D)\right] \quad (98)$$

$$E_1=\frac{2G_0\kappa_D{\gamma_0}^2}{\pi}\frac{DW}{\left(1+D^2\right)}\left(D+\frac{2W+D}{3\left(1+4W^2\right)}\right) \quad (99)$$

$$E_1=\frac{4}{3\pi}G_0\kappa_D{\gamma_0}^2\frac{DW\left(2D+W+6DW^2\right)}{\left(1+D^2\right)\left(1+4W^2\right)} \quad (100)$$

Gather the coefficients of $\sin(\omega t)$ in β, γ, and δ and reduce (coefficient of $s(1)$ in β, coefficients of $s(n-1)$ for the n = 2 terms in γ and δ):

$$V_1=\frac{2G_0\kappa_D{\gamma_0}^2DW}{\pi\left(1+D^2\right)}(-1)+\frac{2G_0\kappa_D{\gamma_0}^2}{\pi}\frac{1}{3\left(1+4W^2\right)}\frac{1}{\left(1+D^2\right)}\left[2W^2(D)+W(-1)\right] \quad (101)$$

$$V_1=\frac{2G_0\kappa_D{\gamma_0}^2DW}{\pi\left(1+D^2\right)}\left(-1+\frac{2DW-1}{3\left(1+4W^2\right)}\right) \quad (102)$$

$$V_1 = \frac{4}{3\pi} G_0 \kappa_D {\gamma_0}^2 \frac{DW\left(-2 + DW - 6W^2\right)}{\left(1+D^2\right)\left(1+4W^2\right)} \tag{103}$$

Gather the coefficients of $\cos(3\omega t)$ in γ and δ and reduce (coefficients of $c(n+1)$ for the n = 2 terms and $c(n-1)$ for the n = 4 terms):

$$E_3 = \frac{2G_0 \kappa_D {\gamma_0}^2 D}{\pi\left(1+9D^2\right)} \left\{ \begin{array}{l} \frac{1}{3\left(1+4W^2\right)}\left[2W^2(-1) + W(-3D)\right]... \\ + \frac{1}{15\left(1+16W^2\right)}\left[4W^2(1) + W(3D)\right] \end{array} \right\} \tag{104}$$

$$E_3 = \frac{-4}{5\pi} G_0 \kappa_D {\gamma_0}^2 \frac{DW\left(W + 2D + 24W^3 + 38W^2 D\right)}{\left(1+9D^2\right)\left(1+4W^2\right)\left(1+16W^2\right)} \tag{105}$$

Gather the coefficients of $\sin(3\omega t)$ in γ and δ and reduce (coefficients of $s(n+1)$ for the n = 2 terms and $s(n-1)$ for the n = 4 terms):

$$V_3 = \frac{2G_0 \kappa_D {\gamma_0}^2 D}{\pi\left(1+9D^2\right)} \left\{ \begin{array}{l} \frac{1}{3\left(1+4W^2\right)}\left[2W^2(-3D) + W(1)\right]... \\ + \frac{1}{15\left(1+16W^2\right)}\left[4W^2(3D) + W(-1)\right] \end{array} \right\} \tag{106}$$

$$V_3 = \frac{4}{15\pi} G_0 \kappa_D {\gamma_0}^2 \frac{DW\left(2 - 9DW + 38W^2 - 216DW^3\right)}{\left(1+9D^2\right)\left(1+4W^2\right)\left(1+16W^2\right)} \tag{107}$$

In summary, at steady-state:

(Recall $\dot{\gamma} = \gamma_0 \omega \sin(\omega t)$, $\gamma = -\gamma_0 \cos(\omega t)$)

$$\begin{array}{l} \sigma = G_0 \gamma_0 \left[\left(\frac{D}{1+D^2} + \frac{\eta_\infty}{\eta_A} D \right) \sin(\omega t) - \frac{D^2}{1+D^2} \cos(\omega t) \right]... \\ + V_1 \sin(\omega t) + E_1 \cos(\omega t) + V_3 \sin(3\omega t) + E_3 \cos(3\omega t) + \mathcal{O}\left({\gamma_0}^3\right) \end{array}$$

$$
\begin{aligned}
E_1 &= \frac{4}{3\pi} G_0 \kappa_D {\gamma_0}^2 \frac{DW\left(2D + W + 6DW^2\right)}{\left(1+D^2\right)\left(1+4W^2\right)} \\
V_1 &= \frac{4}{3\pi} G_0 \kappa_D {\gamma_0}^2 \frac{DW\left(-2 + DW - 6W^2\right)}{\left(1+D^2\right)\left(1+4W^2\right)} \\
E_3 &= \frac{-4}{5\pi} G_0 \kappa_D {\gamma_0}^2 \frac{DW\left(W + 2D + 24W^3 + 38W^2 D\right)}{\left(1+9D^2\right)\left(1+4W^2\right)\left(1+16W^2\right)} \\
V_3 &= \frac{4}{15\pi} G_0 \kappa_D {\gamma_0}^2 \frac{DW\left(2 - 9DW + 38W^2 - 216DW^3\right)}{\left(1+9D^2\right)\left(1+4W^2\right)\left(1+16W^2\right)}
\end{aligned}
\tag{108}
$$

Isolate frequency dependence by defining $L = \lambda \kappa_A$ and substituting $W = \dfrac{\omega}{\kappa_A} = \dfrac{\lambda\omega}{\lambda\kappa_A} = \dfrac{D}{L}$

$$
\begin{aligned}
E_1 &= \frac{4}{3\pi} G_0 \kappa_D {\gamma_0}^2 \frac{\left(1+2L\right)D^3 + \dfrac{6}{L}D^5}{\left(1+D^2\right)\left(L^2+4D^2\right)} \\
V_1 &= \frac{4}{3\pi} G_0 \kappa_D {\gamma_0}^2 \frac{-2LD^2 + \left(1 - \dfrac{6}{L}\right)D^4}{\left(1+D^2\right)\left(L^2+4D^2\right)} \\
E_3 &= \frac{-4}{5\pi} G_0 \kappa_D {\gamma_0}^2 \frac{\left(L^2 + 2L^3\right)D^3 + \left(24 + 38L\right)D^5}{\left(1+9D^2\right)\left(L^2+4D^2\right)\left(L^2+16D^2\right)} \\
V_3 &= \frac{4}{15\pi} G_0 \kappa_D {\gamma_0}^2 \frac{2L^3D^2 + \left(38L - 9L^2\right)D^4 - 216D^6}{\left(1+9D^2\right)\left(L^2+4D^2\right)\left(L^2+16D^2\right)}
\end{aligned}
\tag{109}
$$

To convert the above measures to more familiar material functions:

Recall that our inputs were $\dot{\gamma} = \gamma_0 \omega \sin(\omega t)$, $\gamma = -\gamma_0 \cos(\omega t)$, hence the conversion to the Fourier coefficients is given by

$$
\gamma_0 G_n{}' = -E_n; \;\; \gamma_0 G_n{}'' = V_n \tag{110}
$$

and the conversion to Chebyshev coefficients by

$$
\gamma_0 e_n = -E_n; \;\; \gamma_0 \omega v_n = V_n (-1)^{(n-1)/2} \tag{111}
$$

using Table 1 of [45].

Figure 24 shows the analytical expressions for the intrinsic Chebyshev coefficients of the strain-kinetic model in LAOStrain coplotted with data from numerical simulation of the same model. Data show slight deviation at high De where the simulation is less robust, otherwise agreement is near perfect.

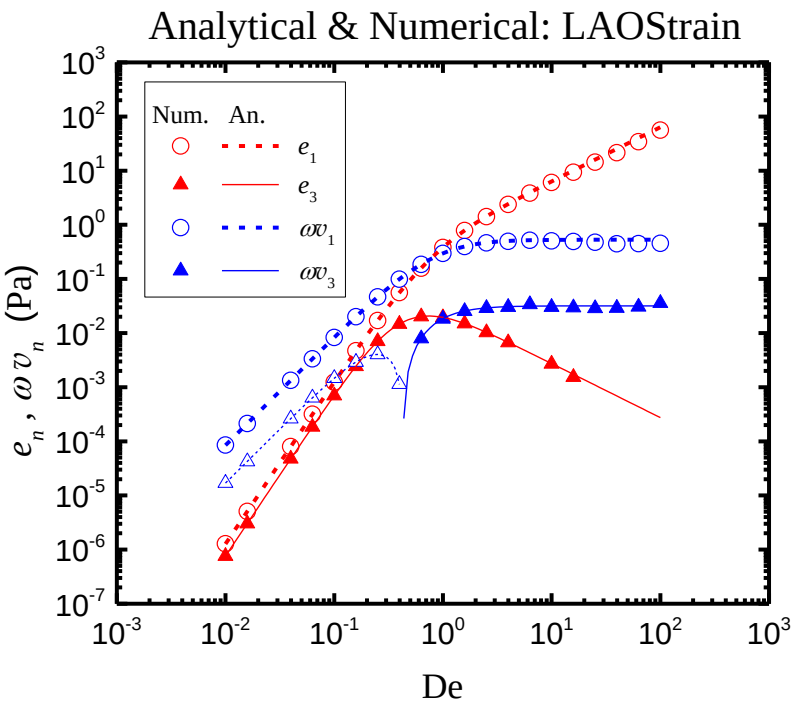

Figure 24 Comparison of analytical solution to data from simulation as verification of the analytical expressions for the strain-kinetic model in LAOStrain. Data shown are for $\lambda\kappa_A = 1$.

Aside: Derivation of Fourier series for $|\sin(\omega t)|$:

Function definition:

$$f(t) = \sin(\omega t); \qquad 0 \le t < \frac{\pi}{\omega} \tag{112}$$

Series Definition:

$$f(t) = a_0 + \sum_{n=1}^{\infty}\left[a_n \cos(n\omega t) + b_n \sin(n\omega t)\right] \tag{113}$$

$f(t)$ is and even function, hence $b_n = 0$ for all n

$$a_0 = \frac{\omega}{\pi}\int_0^{\pi/\omega} f(t)dt = \frac{\omega}{\pi}\int_0^{\pi/\omega} \sin(\omega t)dt \tag{114}$$

$$a_0 = \frac{\omega}{\pi}\left[\frac{-1}{\omega}\cos(\omega t)\right]_0^{\frac{\pi}{\omega}} \tag{115}$$

$$a_0 = \frac{2}{\pi} \tag{116}$$

$$a_n = \frac{2\omega}{\pi}\int_0^{\pi/\omega} f(t)\cos(n\omega t)dt = \frac{2\omega}{\pi}\int_0^{\pi/\omega} \sin(\omega t)\cos(n\omega t)dt \tag{117}$$

$$a_n = \frac{\omega}{\pi}\int_0^{\pi/\omega}\left[\sin\left((n+1)\omega t\right) - \sin\left((n-1)\omega t\right)\right]dt \tag{118}$$

$$a_n = \frac{1}{\pi}\left[\frac{-\cos\left((n+1)\omega t\right)}{n+1} + \frac{\cos\left((n-1)\omega t\right)}{n-1}\right]_0^{\frac{\pi}{\omega}} \tag{119}$$

$$\cos(m\omega t) = (-1)^m \tag{120}$$

$$a_n = \frac{1}{\pi}\left[\frac{-\left((-1)^{n+1} - 1\right)}{n+1} + \frac{\left((-1)^{n-1} - 1\right)}{n-1}\right] \tag{121}$$

$$a_n = \frac{1+(-1)^n}{\pi}\left[\frac{1}{n+1} - \frac{1}{n-1}\right] \tag{122}$$

$$a_n = \frac{-2\left(1+(-1)^n\right)}{\pi(n+1)(n-1)} \tag{123}$$

$\left(1+(-1)^n\right)$ is 0 when n is odd, 2 when n is even.

$$f(t) = \frac{2}{\pi} - \sum_{n\ even}^{\infty} \frac{4}{\pi\left(n^2 - 1\right)} \cos(n\omega t) \tag{124}$$

This is the expression that we employ in (63).

Appendix B: Analytical Solution of Stress-kinetic in LAOStress

For an input of

$$\sigma = \sigma_0 \sin(\omega t) \tag{125}$$

Solve for $\dot{\gamma}(t;\sigma_0,\omega)$

Expression for $\xi(t)$ is the same as (74) (substituting σ_0 for $\gamma_0\omega$)

Substituting (125) into (56) and rearranging yields the expression

$$\ddot{\gamma} + \frac{G_0}{\eta_\infty}\left(\xi + \frac{\eta_\infty}{\eta_A}\right)\dot{\gamma} = \frac{\sigma_0}{\eta_\infty \lambda}\left(\mathrm{D}\cos(\omega t) + \sin(\omega t)\right) \tag{126}$$

$$\ddot{\gamma} + A(t)\dot{\gamma} = B(t)$$

$$A(t) = \frac{G_0}{\eta_\infty}\left(\xi + \frac{\eta_\infty}{\eta_A}\right) \tag{127}$$

$$B(t) = \frac{\sigma_0}{\eta_\infty \lambda}\left(\mathrm{D}\cos(\omega t) + \sin(\omega t)\right) \tag{128}$$

Using the same ODE solution as in (62)

$$\dot{\gamma}(t) = e^{-\int A(t)dt}\left(\int e^{\int A(t)dt} B(t)dt + C_1\right) \tag{129}$$

Substitute (74) into (127) and integrate:

$$A(t) = \frac{G_0}{\eta_\infty}\left[1 - \frac{2}{\pi}\frac{\kappa_D \sigma_0}{\kappa_A}\left(1 - 2\sum_{n\ even}^{\infty}\frac{nW\sin(n\omega t) + \cos(n\omega t)}{\left(n^2 - 1\right)\left(1 + n^2 W^2\right)}\right) + \mathcal{O}\left({\kappa_D}^2 {\sigma_0}^2\right) + \frac{\eta_\infty}{\eta_A}\right] \tag{130}$$

$$\int A(t)dt = \frac{G_0}{\eta_\infty}\left[\begin{array}{l}\int\left(1-\frac{2}{\pi}\frac{\kappa_D\sigma_0}{\kappa_A}+\eta_\infty^*\right)dt... \\ +\frac{4}{\pi}\frac{\kappa_D\sigma_0}{\kappa_A}\sum_{n\ even}^{\infty}\frac{\int\left(nW\sin(n\omega t)+\cos(n\omega t)\right)dt}{\left(n^2-1\right)\left(1+n^2W^2\right)}+\mathcal{O}\left({\kappa_D}^2{\sigma_0}^2\right)\end{array}\right] \tag{131}$$

$$\int A(t)dt = \frac{G_0}{\eta_\infty}\left[\begin{array}{l}\left(1-\frac{2}{\pi}\frac{\kappa_D\sigma_0}{\kappa_A}+\eta_\infty^*\right)t... \\ +\frac{4}{\pi}\frac{\kappa_D\sigma_0}{\kappa_A}\sum_{n\ even}^{\infty}\frac{-\frac{1}{\kappa_A}\cos(n\omega t)+\frac{1}{n\omega}\sin(n\omega t)}{\left(n^2-1\right)\left(1+n^2W^2\right)}+\mathcal{O}\left({\kappa_D}^2{\sigma_0}^2\right)\end{array}\right] \tag{132}$$

$$\int A(t)dt = \frac{G_0}{\eta_\infty}\left[\begin{array}{l}\left(1+\eta_\infty^*\right)t... \\ +\frac{2}{\pi}\frac{\kappa_D\sigma_0}{\kappa_A}\left(-t+\frac{2}{\kappa_A}\sum_{n\ even}^{\infty}\frac{\frac{1}{nW}\sin(n\omega t)-\cos(n\omega t)}{\left(n^2-1\right)\left(1+n^2W^2\right)}\right)+\mathcal{O}\left({\kappa_D}^2{\sigma_0}^2\right)\end{array}\right] \tag{133}$$

Once again employing the MacLaurin series $e^x = 1+x+\mathcal{O}(x^2)$ for the exponential,

$$e^{\int A(t)dt} = e^{\frac{G_0}{\eta_\infty}\left(1+\eta_\infty^*\right)t}e^{\frac{2}{\pi}\frac{G_0}{\eta_\infty}\frac{\kappa_D\sigma_0}{\kappa_A}\left(-t+\frac{2}{\kappa_A}\sum_{n\ even}^{\infty}\frac{\frac{1}{nW}\sin(n\omega t)-\cos(n\omega t)}{\left(n^2-1\right)\left(1+n^2W^2\right)}\right)+\mathcal{O}\left({\kappa_D}^2{\sigma_0}^2\right)} \tag{134}$$

$$e^{\int A(t)dt} = e^{\frac{G_0}{\eta_\infty}\left(1+\eta_\infty^*\right)t}\left[\begin{array}{l}1-\frac{2}{\pi}\frac{G_0}{\eta_\infty}\frac{\kappa_D\sigma_0}{\kappa_A}\left(t+\frac{2}{\kappa_A}\sum_{n\ even}^{\infty}\frac{\cos(n\omega t)-\frac{1}{nW}\sin(n\omega t)}{\left(n^2-1\right)\left(1+n^2W^2\right)}\right)... \\ +\mathcal{O}\left({\kappa_D}^2{\sigma_0}^2\right)\end{array}\right] \tag{135}$$

Combine this expression with (128), and substitute using product-to-sum identities

$$\sin(u)\sin(v) = \frac{\cos(u-v)-\cos(u+v)}{2} \tag{136}$$

$$\cos(u)\sin(v) = \frac{\sin(u+v)-\sin(u-v)}{2} \tag{137}$$

$$\cos(u)\cos(v) = \frac{\cos(u-v)+\cos(u+v)}{2} \tag{138}$$

To achieve an expression for the integrand in (129), introducing the short-hand notation $c(n) = \cos(n\omega t),\ s(n) = \sin(n\omega t)$

$$\begin{aligned} & e^{\int A(t)dt} B(t) = e^{\frac{G_0}{\eta_\infty}\left(1+\eta_\infty^*\right)t} \times \ldots \\ & \left[1 - \frac{2}{\pi}\frac{G_0}{\eta_\infty}\frac{\kappa_D\sigma_0}{\kappa_A}\left(t + \frac{2}{\kappa_A}\sum_{n\ even}^{\infty} \frac{c(n) - \frac{1}{nW}s(n)}{\left(n^2-1\right)\left(1+n^2W^2\right)} \right)\ldots \right] \frac{\sigma_0}{\eta_\infty \lambda}\left(Dc(1) + s(1) \right) \\ & + \mathcal{O}\left({\kappa_D}^2 {\sigma_0}^2 \right) \end{aligned} \tag{139}$$

$$\begin{aligned} & e^{\int A(t)dt} B(t) = e^{\frac{G_0}{\eta_\infty}\left(1+\eta_\infty^*\right)t} \times \ldots \\ & \left\{ \begin{array}{l} Dc(1) + s(1)\ldots \\ -\frac{2}{\pi}\frac{G_0}{\eta_\infty}\frac{\kappa_D\sigma_0}{\kappa_A}\left[\begin{array}{l} tDc(1) + ts(1)\ldots \\ +\sum_{n\ even}^{\infty} \frac{1}{\kappa_A\left(n^2-1\right)\left(1+n^2W^2\right)}\left(\begin{array}{l} D\left(c(n-1)+c(n+1)\right)\ldots \\ -\frac{D}{nW}\left(s(n+1)+s(n-1)\right)\ldots \\ +\left(s(n+1)-s(n-1)\right)\ldots \\ -\frac{1}{nW}\left(c(n-1)-c(n+1)\right) \end{array} \right) \end{array} \right] \end{array} \right\} \end{aligned} \tag{140}$$

To simplify taking the integral of this expression, define

$$\tau = \left(\frac{G_0}{\eta_\infty}\left(1+\eta_\infty^*\right) \right)^{-1}, \tag{141}$$

$$f_n = \frac{1}{\kappa_A\left(n^2-1\right)\left(1+n^2W^2\right)}, \tag{142}$$

and

$$g = \frac{-2}{\pi}\frac{G_0}{\eta_\infty}\frac{\kappa_D\sigma_0}{\kappa_A}, \tag{143}$$

for compact notation, and separate the integral into additive terms

$$\int e^{\int A(t)dt} B(t)dt = \frac{\sigma_0}{\eta_\infty \lambda} \int \left(\alpha + \beta + \gamma + \delta + \varepsilon + \zeta + \eta + \theta\right) dt$$

$$\alpha = e^{t/\tau} Dc(1)$$

$$\beta = e^{t/\tau} s(1)$$

$$\gamma = e^{t/\tau} gtDc(1)$$

$$\delta = e^{t/\tau} gts(1)$$

$$\varepsilon = \sum_{n\ even}^{\infty} e^{t/\tau} gf_n \left(D - \frac{1}{nW}\right) c(n-1)$$

$$\zeta = \sum_{n\ even}^{\infty} e^{t/\tau} gf_n \left(D + \frac{1}{nW}\right) c(n+1)$$

$$\eta = \sum_{n\ even}^{\infty} e^{t/\tau} gf_n \left(-\frac{D}{nW} - 1\right) \mathrm{s}(n-1)$$

$$\theta = \sum_{n\ even}^{\infty} e^{t/\tau} gf_n \left(-\frac{D}{nW} + 1\right) \mathrm{s}(n+1) \tag{144}$$

then employ the formulae

$$\int e^{ax} \cos(bx)dx = \frac{e^{ax}}{a^2 + b^2} \left(b \sin(bx) + a \cos(bx)\right) \tag{145}$$

$$\int e^{ax} \sin(bx)dx = \frac{e^{ax}}{a^2 + b^2} \left(a \sin(bx) - b \cos(bx)\right) \tag{146}$$

$$\int xe^{ax} \sin(bx)dx = \frac{e^{ax}}{a^2 + b^2} \left[\left(ax - \frac{a^2 - b^2}{a^2 + b^2}\right) \sin(bx) - \left(bx - \frac{2ab}{a^2 + b^2}\right) \cos(bx)\right] \tag{147}$$

$$\int xe^{ax} \cos(bx)dx = \frac{e^{ax}}{a^2 + b^2} \left[\left(bx + \frac{2ab}{a^2 + b^2}\right) \sin(bx) + \left(ax + \frac{a^2 - b^2}{a^2 + b^2}\right) \cos(bx)\right] \tag{148}$$

to integrate each term individually.

$$\int \alpha dt = \frac{De^{t/\tau}}{\tau^{-2} + \omega^2} \left(\omega s(1) + \frac{1}{\tau} c(1)\right) \tag{149}$$

$$\int \beta dt = \frac{e^{t/\tau}}{\tau^{-2}+\omega^2}\left(\frac{1}{\tau}s(1)-\omega c(1)\right) \tag{150}$$

$$\int \gamma dt = \frac{gDe^{t/\tau}}{\tau^{-2}+\omega^2}\left[\left(\omega t+\frac{2\omega/\tau}{\tau^{-2}+\omega^2}\right)s(1)+\left(\frac{t}{\tau}+\frac{\tau^{-2}-\omega^2}{\tau^{-2}+\omega^2}\right)c(1)\right] \tag{151}$$

$$\int \delta dt = \frac{ge^{t/\tau}}{\tau^{-2}+\omega^2}\left[\left(\frac{t}{\tau}-\frac{\tau^{-2}-\omega^2}{\tau^{-2}+\omega^2}\right)s(1)-\left(\omega t-\frac{2\omega/\tau}{\tau^{-2}+\omega^2}\right)c(1)\right] \tag{152}$$

$$\int \varepsilon dt = \sum_{n\ even}^{\infty} gf_n\left(D-\frac{1}{nW}\right)\frac{e^{t/\tau}}{\tau^{-2}+\left(n-1\right)^2\omega^2}\left[\left(n-1\right)\omega s(\mathrm{n}-1)+\frac{1}{\tau}c(\mathrm{n}-1)\right] \tag{153}$$

$$\int \zeta dt = \sum_{n\ even}^{\infty} gf_n\left(D+\frac{1}{nW}\right)\frac{e^{t/\tau}}{\tau^{-2}+\left(n+1\right)^2\omega^2}\left[\left(n+1\right)\omega s(\mathrm{n}+1)+\frac{1}{\tau}c(\mathrm{n}+1)\right] \tag{154}$$

$$\int \eta dt = \sum_{n\ even}^{\infty} gf_n\left(-\frac{D}{nW}-1\right)\frac{e^{t/\tau}}{\tau^{-2}+\left(n-1\right)^2\omega^2}\left[\frac{1}{\tau}s(\mathrm{n}-1)-\left(n-1\right)\omega c(\mathrm{n}-1)\right] \tag{155}$$

$$\int \theta dt = \sum_{n\ even}^{\infty} gf_n\left(-\frac{D}{nW}+1\right)\frac{e^{t/\tau}}{\tau^{-2}+\left(n+1\right)^2\omega^2}\left[\frac{1}{\tau}s(\mathrm{n}+1)-\left(n+1\right)\omega c(\mathrm{n}+1)\right] \tag{156}$$

Plugging (144) and (149)-(156) into (129) yields an expression for strain rate:

$$\begin{aligned}\dot{\gamma} = e^{-t/\tau}\left\{1-g\left[t+2\sum_{n\ enen}^{\infty} f_n\left(c(n)-\frac{1}{nW}s(n)\right)\right]+\mathcal{O}\left({\kappa_D}^2{\sigma_0}^2\right)\right\}\times\ldots \\ \left[\frac{\sigma_0}{\eta_\infty\lambda}\int\left(\alpha+\ldots+\theta\right)dt+C+\mathcal{O}\left({\kappa_D}^2{\sigma_0}^2\right)\right]\end{aligned} \tag{157}$$

Foiling and grouping terms by order of σ_0—recalling that g contains a factor of σ_0 (also assume $\tau t \gg 1$ hence $C_1 e^{-t'\tau} \to 0$)

First, the $\mathcal{O}\left(\sigma_0\right)$ terms:

$$\dot{\gamma} = \frac{\sigma_0}{\eta_\infty \lambda}\left[\frac{D}{\tau^{-2}+\omega^2}\left(\omega s(1)+\frac{1}{\tau}c(1)\right)+\frac{1}{\tau^{-2}+\omega^2}\left(\frac{1}{\tau}s(1)-\omega c(1)\right)\right] \tag{158}$$

$$\dot{\gamma} = \frac{\sigma_0}{\eta_\infty \lambda\left(\tau^{-2}+\omega^2\right)}\left[\left(D\omega+\frac{1}{\tau}\right)s(1)+\left(\frac{D}{\tau}-\omega\right)c(1)\right] \tag{159}$$

Defining $H = \frac{\eta_\infty^*}{1+\eta_\infty^*} = \frac{\tau}{\lambda}$ and simplifying

$$\dot{\gamma} = \frac{\sigma_0}{\eta_\infty}\frac{H}{1+H^2D^2}\left[\left(1+HD^2\right)s(1)+\left(1-H\right)Dc(1)\right]+\mathcal{O}\left(\sigma_0{}^2\right) \tag{160}$$

And the $\mathcal{O}\left(\sigma_0{}^2\right)$ terms:

$$\dot{\gamma} = e^{-t/\tau}\left\{\begin{array}{l}\frac{\sigma_0}{\eta_\infty \lambda}\int\left(\gamma+\delta+\varepsilon+\zeta+\eta+\theta\right)dt... \\ -g\left[t+2\sum_{n\ even}^{\infty} f_n\left(c(n)-\frac{1}{nW}s(n)\right)\right]\frac{\sigma_0}{\eta_\infty \lambda}\int\left(\alpha+\beta\right)dt\end{array}\right\} \tag{161}$$

Once again we break the expression into smaller pieces and simplify each individually:

$$\dot{\gamma} = (*)+(**)+(***) \tag{162}$$

$$\begin{array}{l}(*) = e^{-t/\tau}\left\{\frac{\sigma_0}{\eta_\infty \lambda}\int\left(\gamma+\delta\right)dt\right\} = \\ \frac{g\sigma_0}{\eta_\infty \lambda\left(\tau^{-2}+\omega^2\right)}\times \\ \left\{\begin{array}{l}\left(D\omega+\frac{1}{\tau}\right)ts(1)+\left(\frac{D}{\tau}-\omega\right)tc(1)... \\ +\frac{1}{\tau^{-2}+\omega^2}\left[\left(\frac{2D\omega}{\tau}-\tau^{-2}+\omega^2\right)s(1)+\left(D\tau^{-2}-D\omega^2+\frac{2\omega}{\tau}\right)c(1)\right]\end{array}\right\}\end{array} \tag{163}$$

$$(**) = e^{-t/\tau}\left\{\frac{\sigma_0}{\eta_\infty \lambda}\int\left(\varepsilon+\zeta+\eta+\theta\right)dt\right\} =$$

$$\frac{g\sigma_0}{\eta_\infty \lambda}\times$$

$$\left\{\begin{array}{l}\displaystyle\sum_{n\ even}\frac{f_n}{\tau^{-2}+(n-1)^2\omega^2}\left\{\begin{array}{l}\left[\left(D-\frac{1}{nW}\right)(n-1)\omega-\left(\frac{D}{nW}+1\right)\frac{1}{\tau}\right]s(n-1)\ldots\\ +\left[\left(D-\frac{1}{nW}\right)\frac{1}{\tau}+\left(\frac{D}{nW}+1\right)(n-1)\omega\right]\mathrm{c}(n-1)\end{array}\right\}\ldots\\ +\displaystyle\sum_{n\ even}\frac{f_n}{\tau^{-2}+(n+1)^2\omega^2}\left\{\begin{array}{l}\left[\left(D+\frac{1}{nW}\right)(n+1)\omega+\left(-\frac{D}{nW}+1\right)\frac{1}{\tau}\right]s(n+1)\ldots\\ +\left[\left(D+\frac{1}{nW}\right)\frac{1}{\tau}-\left(-\frac{D}{nW}+1\right)(n+1)\omega\right]\mathrm{c}(n+1)\end{array}\right\}\end{array}\right\} \qquad (164)$$

$$(***) = -e^{-t/\tau}g\left[t+2\sum_{n\ even}^{\infty}f_n\left(c(n)-\frac{1}{nW}s(n)\right)\right]\frac{\sigma_0}{\eta_\infty\lambda}\int\left(\alpha+\beta\right)dt =$$

$$\frac{-g\sigma_0}{\eta_\infty\lambda\left(\tau^{-2}+\omega^2\right)}\times$$

$$\left\{\begin{array}{l}\left(D\omega+\frac{1}{\tau}\right)ts(1)+\left(\frac{D}{\tau}-\omega\right)tc(1)\ldots\\ +\displaystyle\sum_{n\ even}f_n\left[\begin{array}{ll}\left(D\omega+\frac{1}{\tau}\right)\left(s(n+1)-s(n-1)\right)+\left(\frac{D}{\tau}-\omega\right)\left(c(n-1)+c(n+1)\right)\ldots\\ -\frac{D\omega+\frac{1}{\tau}}{nW}\left(c(n-1)-c(n+1)\right)-\frac{\frac{D}{\tau}-\omega}{nW}\left(s(\mathrm{n}+1)+\mathrm{s}(\mathrm{n}-1)\right)\end{array}\right]\end{array}\right\} \qquad (165)$$

The term $\frac{g\sigma_0}{\eta_\infty\lambda\left(\tau^{-2}+\omega^2\right)}\left[\left(D\omega+\frac{1}{\tau}\right)ts(1)+\left(\frac{D}{\tau}-\omega\right)tc(1)\right]$ is present in (*) and (***) with opposite signs, hence it cancels. The full expression for strain rate at $\mathcal{O}\left(\sigma_0^{\,2}\right)$ is therefore

$$\dot{\gamma} = \frac{g\sigma_0}{\eta_\infty \lambda} \times$$

$$\left\{ \begin{array}{l} \frac{1}{\left(\tau^{-2}+\omega^2\right)^2}\left[\left(\frac{2D\omega}{\tau}-\tau^{-2}+\omega^2\right)s(1)+\left(D\tau^{-2}-D\omega^2+\frac{2\omega}{\tau}\right)c(1)\right]... \\ +\sum_{n\ even}\frac{f_n}{\tau^{-2}+(n-1)^2\omega^2}\left\{\begin{array}{l}\left[\left(D-\frac{1}{nW}\right)(n-1)\omega-\left(\frac{D}{nW}+1\right)\frac{1}{\tau}\right]s(n-1)... \\ +\left[\left(D-\frac{1}{nW}\right)\frac{1}{\tau}+\left(\frac{D}{nW}+1\right)(n-1)\omega\right]c(n-1)\end{array}\right\}... \\ +\sum_{n\ even}\frac{f_n}{\tau^{-2}+(n+1)^2\omega^2}\left\{\begin{array}{l}\left[\left(D+\frac{1}{nW}\right)(n+1)\omega+\left(-\frac{D}{nW}+1\right)\frac{1}{\tau}\right]s(n+1)... \\ +\left[\left(D+\frac{1}{nW}\right)\frac{1}{\tau}-\left(-\frac{D}{nW}+1\right)(n+1)\omega\right]c(n+1)\end{array}\right\}... \\ +\frac{1}{\tau^{-2}+\omega^2}\sum_{n\ even}f_n\left\{\begin{array}{l}\left[\left(D\omega+\frac{1}{\tau}\right)+\frac{\frac{D}{\tau}-\omega}{nW}\right]s(n-1)... \\ +\left[-\left(\frac{D}{\tau}-\omega\right)+\frac{D\omega+\frac{1}{\tau}}{nW}\right]c(n-1)... \\ +\left[-\left(D\omega+\frac{1}{\tau}\right)+\frac{\frac{D}{\tau}-\omega}{nW}\right]s(n+1)... \\ +\left[-\left(\frac{D}{\tau}-\omega\right)-\frac{D\omega+\frac{1}{\tau}}{nW}\right]c(n+1)\end{array}\right\} \end{array} \right\} \quad (166)$$

Solve for the harmonics:

Define harmonics

$$\dot{\gamma}-\dot{\gamma}_{lin} = C_1 s(1)+F_1 c(1)+C_3 s(3)+F_3 c(3) \quad (167)$$

$$\dot{\gamma} - \dot{\gamma}_{lin} = \frac{g\sigma_0}{\eta_\infty \lambda}\left(C_1^* s(1) + F_1^* c(1) + C_3^* s(3) + F_3^* c(3)\right) \tag{168}$$

Gather terms that contribute to C_1^* (coefficients of $s(1)$, $s(n-1)$ with $n = 2$)

$$C_1^* = \frac{1}{\left(\tau^{-2} + \omega^2\right)^2}\left(\frac{2D\omega}{\tau} - \tau^{-2} + \omega^2\right) + \frac{f_2}{\tau^{-2} + \omega^2}\left[\left(D - \frac{1}{2W}\right)\omega - \left(\frac{D}{2W} + 1\right)\frac{1}{\tau}\right]\ldots$$
$$+ \frac{f_2}{\tau^{-2} + \omega^2}\left[\left(D\omega + \frac{1}{\tau}\right) + \frac{\frac{D}{\tau} - \omega}{2W}\right] \tag{169}$$

$$C_1^* = \frac{1}{\tau^{-2} + \omega^2}\left[\frac{\frac{2D\omega}{\tau} - \tau^{-2} + \omega^2}{\tau^{-2} + \omega^2} + f_2\left(2D\omega - \kappa_A\right)\right] \tag{170}$$

Define $T = \tau\omega$, recall $f_n = \dfrac{1}{\kappa_A\left(n^2 - 1\right)\left(1 + n^2 W^2\right)}$

$$C_1^* = \frac{1}{\tau^{-2} + \omega^2}\left[\frac{\frac{2D\omega}{\tau} - \tau^{-2} + \omega^2}{\tau^{-2} + \omega^2} \times \frac{\tau^2}{\tau^2} + \frac{1}{3\kappa_A\left(1 + 4W^2\right)}\left(2D\omega - \kappa_A\right)\right] \tag{171}$$

$$C_1^* = \frac{1}{\tau^{-2} + \omega^2}\left[\frac{2DT - 1 + T^2}{1 + T^2} + \frac{2DW - 1}{3\left(1 + 4W^2\right)}\right] \tag{172}$$

$$C_1^* = \frac{1}{\tau^{-2} + \omega^2}\left[\frac{-4 + 6DT + 2T^2 - 12W^2 + 2DW + 24DTW^2 + 12T^2W^2 + 2DT^2W}{3\left(1 + 4W^2\right)\left(1 + T^2\right)}\right] \tag{173}$$

Simplifying and substituting $H = \dfrac{\eta_\infty^*}{1 + \eta_\infty^*}$

$$\frac{g\sigma_0}{\eta_\infty \lambda} = \frac{-2}{\pi}\frac{\kappa_D \sigma_0}{\kappa_A}\frac{\sigma_0}{\eta_\infty\left(1 + \eta_\infty^*\right)} H \frac{1}{\tau^2} \tag{174}$$

and adding back in the front factor to achieve an expression for C_1

$$C_1 = \frac{-2}{\pi}\frac{\kappa_D\sigma_0}{\kappa_A}\frac{\sigma_0}{\eta_\infty\left(1+\eta_\infty^*\right)}H\left[\frac{-4+6DT+2T^2-12W^2+2DW+24DTW^2+12T^2W^2+2DT^2W}{3\left(1+4W^2\right)\left(1+T^2\right)^2}\right]$$

(175)

Isolate frequency dependence in Deborah number by substituting $T = HD, W = \frac{D}{L}$ where $L = \lambda\kappa_A$

$$C_1 = \frac{-4}{3\pi}\frac{\kappa_D\sigma_0}{\kappa_A}\frac{\sigma_0}{\eta_\infty\left(1+\eta_\infty^*\right)}H\left[\frac{-2L^2+\left(-6+L+3HL^2+H^2L^2\right)D^2+\left(12H+6H^2+H^2L\right)D^4}{\left(1+H^2D^2\right)^2\left(L^2+4D^2\right)}\right]$$

(176)

Gather terms that contribute to F_1^* (coefficients of $\mathrm{c}(1)$, $\mathrm{c}(n-1)$ with $n = 2$)

$$F_1^* = \frac{1}{\left(\tau^{-2}+\omega^2\right)^2}\left(D\tau^{-2}-D\omega^2+\frac{2\omega}{\tau}\right)+\frac{f_2}{\tau^{-2}+\omega^2}\left[\left(D-\frac{1}{2W}\right)\frac{1}{\tau}+\left(\frac{D}{2W}+1\right)\omega\right]\ldots$$
$$+\frac{f_2}{\tau^{-2}+\omega^2}\left[-\left(\frac{D}{\tau}-\omega\right)+\frac{D\omega+\frac{1}{\tau}}{2W}\right] \quad (177)$$

$$F_1^* = \frac{1}{\tau^{-2}+\omega^2}\left[\frac{D\tau^{-2}-D\omega^2+\frac{2\omega}{\tau}}{\tau^{-2}+\omega^2}+f_2\left(2\omega+D\kappa_A\right)\right] \quad (178)$$

$$F_1^* = \frac{1}{\tau^{-2}+\omega^2}\left[\frac{D-DT^2+2T}{1+T^2}+\frac{2W+D}{3\left(1+4W^2\right)}\right] \quad (179)$$

$$F_1^* = \frac{1}{\tau^{-2}+\omega^2}\left[\frac{4D+6T+2W-2DT^2+12DW^2+24TW^2+2WT^2-12DT^2W^2}{3\left(1+T^2\right)\left(1+4W^2\right)}\right] \quad (180)$$

$$F_1 = \frac{-4}{3\pi}\frac{\kappa_D\sigma_0}{\kappa_A}\frac{\sigma_0}{\eta_\infty\left(1+\eta_\infty^*\right)}H\left[\frac{2D+3T+W-DT^2+6DW^2+12TW^2+WT^2-6DT^2W^2}{\left(1+T^2\right)^2\left(1+4W^2\right)}\right]$$

(181)

$$F_1 = \frac{-4}{3\pi}\frac{\kappa_D\sigma_0}{\kappa_A}\frac{\sigma_0}{\eta_\infty\left(1+\eta_\infty^*\right)}H\left[\frac{\left(L+2L^2+3HL^2\right)D+\left(6+12H+H^2L-H^2L^2\right)D^3-6H^2D^5}{\left(1+H^2D^2\right)^2\left(L^2+4D^2\right)}\right]$$

(182)

Gather terms that contribute to C_3^* (coefficients $s(n+1)$ with $n = 2$, $s(n-1)$ with $n = 4$)

$$C_3^* = \frac{f_2}{\tau^{-2}+9\omega^2}\left[\left(D+\frac{1}{2W}\right)3\omega+\left(-\frac{D}{2W}+1\right)\frac{1}{\tau}\right]+\frac{f_2}{\tau^{-2}+\omega^2}\left[-\left(D\omega+\frac{1}{\tau}\right)+\frac{\frac{D}{\tau}-\omega}{2W}\right]\ldots$$
$$+\frac{f_4}{\tau^{-2}+9\omega^2}\left[\left(D-\frac{1}{4W}\right)3\omega-\left(\frac{D}{4W}+1\right)\frac{1}{\tau}\right]+\frac{f_4}{\tau^{-2}+\omega^2}\left[\left(D\omega+\frac{1}{\tau}\right)+\frac{\frac{D}{\tau}-\omega}{4W}\right] \quad (183)$$

$$C_3^* = f_2\frac{2D\omega\tau^{-2}+\kappa_A\tau^{-2}-6D\omega^3-3\kappa_A\omega^2+4D\kappa_A\omega\tau^{-1}-8\omega^2\tau^{-1}}{\left(\tau^{-2}+9\omega^2\right)\left(\tau^{-2}+\omega^2\right)}\ldots$$
$$+f_4\frac{4D\omega\tau^{-2}-\kappa_A\tau^{-2}+12D\omega^3-3\kappa_A\omega^2+2D\kappa_A\omega\tau^{-1}+8\omega^2\tau^{-1}}{\left(\tau^{-2}+\omega^2\right)\left(\tau^{-2}+9\omega^2\right)} \quad (184)$$

$$C_3^* = \frac{\tau^2}{\left(1+9T^2\right)\left(1+T^2\right)}\left[\frac{2DW+1-6DWT^2-3T^2+4DT-8WT}{3\left(1+4W^2\right)}\ldots\right.$$
$$\left.+\frac{4DW-1+12DWT^2-3T^2+2DT+8WT}{15\left(1+16W^2\right)}\right] \quad (185)$$

$$C_3^* = \frac{\tau^2}{15\left(1+9T^2\right)\left(1+T^2\right)\left(1+4W^2\right)\left(1+16W^2\right)} \times \left[\begin{array}{l} 4+14DW-18T^2+22DT-32WT+76W^2-18DWT^2\ldots \\ +176DW^3-252W^2T^2+328DW^2T-608W^3T-432DW^3T^2 \end{array}\right] \tag{186}$$

$$C_3 = \frac{-4}{15\pi}\frac{\kappa_D\sigma_0}{\kappa_A}\frac{\sigma_0}{\eta_\infty\left(1+\eta_\infty^*\right)}\frac{HL}{\left(1+9H^2D^2\right)\left(1+H^2D^2\right)\left(L^2+4D^2\right)\left(L^2+16D^2\right)} \times \left[\begin{array}{l} 2L^3+\left(38L+7L^2-16HL^2+11HL^3-9H^2L^3\right)D^2\ldots \\ \left(88-304H-126H^2L+164HL-9H^2L^2\right)D^4-216H^2D^6 \end{array}\right] \tag{187}$$

Gather terms that contribute to F_3^* (coefficients $c(n+1)$ with $n = 2$, $c(n-1)$ with $n = 4$)

$$F_3^* = \frac{f_2}{\tau^{-2}+9\omega^2}\left[\left(D+\frac{1}{2W}\right)\frac{1}{\tau}-\left(-\frac{D}{2W}+1\right)3\omega\right]+\frac{f_2}{\tau^{-2}+\omega^2}\left[-\left(\frac{D}{\tau}-\omega\right)-\frac{D\omega+\frac{1}{\tau}}{2W}\right]\ldots$$
$$+\frac{f_4}{\tau^{-2}+9\omega^2}\left[\left(D-\frac{1}{4W}\right)\frac{1}{\tau}+\left(\frac{D}{4W}+1\right)3\omega\right]+\frac{f_4}{\tau^{-2}+\omega^2}\left[-\left(\frac{D}{\tau}-\omega\right)+\frac{D\omega+\frac{1}{\tau}}{4W}\right] \tag{188}$$

$$F_3^* = f_2\frac{D\kappa_A\tau^{-2}-2\omega\tau^{-2}-8D\omega^2\tau^{-1}-4\kappa_A\omega\tau^{-1}-3D\kappa_A\omega^2+6\omega^3}{\left(\tau^{-2}+\omega^2\right)\left(\tau^{-2}+9\omega^2\right)}\ldots$$
$$+f_4\frac{D\kappa_A\tau^{-2}+4\omega\tau^{-2}-8D\omega^2\tau^{-1}+2\kappa_A\omega\tau^{-1}+3D\kappa_A\omega^2+12\omega^3}{\left(\tau^{-2}+\omega^2\right)\left(\tau^{-2}+9\omega^2\right)} \tag{189}$$

$$F_3^* = \frac{\tau^2}{\left(1+T^2\right)\left(1+9T^2\right)}\left[\begin{array}{l} \frac{D-2W-8DWT-4T-3DT^2+6WT^2}{3\left(1+4W^2\right)}\ldots \\ +\frac{D+4W-8DWT+2T+3DT^2+12WT^2}{15\left(1+16W^2\right)} \end{array}\right] \tag{190}$$

$$F_3^* = \frac{\tau^2}{15\left(1+T^2\right)\left(1+9T^2\right)\left(1+4W^2\right)\left(1+16W^2\right)} \times \begin{bmatrix} 6D-6W-18T-48DWT-12DT^2+42WT^2+84DW^2\ldots \\ -144W^3-312W^2T-672DW^3T-228DW^2T^2+528W^3T^2 \end{bmatrix} \tag{191}$$

$$F_3 = \frac{-2}{15\pi}\frac{\kappa_D\sigma_0}{\kappa_A}\frac{\sigma_0}{\eta_\infty\left(1+\eta_\infty^*\right)}\frac{HL}{\left(1+H^2D^2\right)\left(1+9H^2D^2\right)\left(L^2+4D^2\right)\left(L^2+16D^2\right)} \times \begin{bmatrix} \left(-6L^2+6L^3-18HL^3\right)D\ldots \\ +\left(-144+84L-312HL-48HL^2+42H^2L^2-12H^2L^3\right)\mathrm{D}^3\ldots \\ +\left(-672H+528H^2-228H^2L\right)D^5 \end{bmatrix} \tag{192}$$

In summary, at steady-state:

(Recall $\sigma = \sigma_0 s(1)$)

$$\boxed{\dot{\gamma} = \frac{\sigma_0}{\eta_\infty}\frac{H}{1+H^2D^2}\left[\left(1+HD^2\right)s(1)+\left(1-H\right)Dc(1)\right]+C_1s(1)+F_1c(1)+C_3s(3)+F_3c(3)+\mathcal{O}\left({\sigma_0}^3\right)}$$

$$\boxed{\begin{aligned} K_1 &= \frac{\kappa_D\sigma_0}{\kappa_A}\frac{\sigma_0}{\eta_\infty^*\left(\eta_\infty+\eta_A\right)}\frac{H}{\left(1+H^2D^2\right)^2\left(L^2+4D^2\right)} \\ K_3 &= \frac{\kappa_D\sigma_0}{\kappa_A}\frac{\sigma_0}{\eta_\infty^*\left(\eta_\infty+\eta_A\right)}\frac{HL}{\left(1+H^2D^2\right)\left(1+9H^2D^2\right)\left(L^2+4D^2\right)\left(L^2+16D^2\right)} \\ C_1 &= \frac{4}{3\pi}K_1\left[2L^2+\left(6-L+3HL^2+H^2L^2\right)D^2+\left(12H-6H^2-H^2L\right)D^4\right] \\ F_1 &= \frac{4}{3\pi}K_1\left[\left(L+2L^2-3HL^2\right)D+\left(-6+12H+H^2L+H^2L^2\right)D^3+6H^2D^5\right] \\ C_3 &= \frac{-4}{15\pi}K_3\begin{bmatrix} 2L^3+\left(38L+7L^2-16HL^2+11HL^3-9H^2L^3\right)D^2\ldots \\ +\left(88-304H-126H^2L+164HL-9H^2L^2\right)D^4-216H^2D^6 \end{bmatrix} \\ F_3 &= \frac{-4}{5\pi}K_3\begin{bmatrix} \left(-L^2+L^3-3HL^3\right)D\ldots \\ +\left(-24+14L-52HL-8HL^2+7H^2L^2-2H^2L^3\right)\mathrm{D}^3\ldots \\ +\left(-112H+88H^2-38H^2L\right)D^5 \end{bmatrix} \end{aligned}} \tag{193}$$

Figure 25 shows the analytical expressions for the intrinsic Chebyshev coefficients of the stress-kinetic model in LAOStress coplotted with data from numerical simulation of the same model. Agreement between the two data sets is near perfect at all De, with all deviations within the expected variation that comes from data simulation.

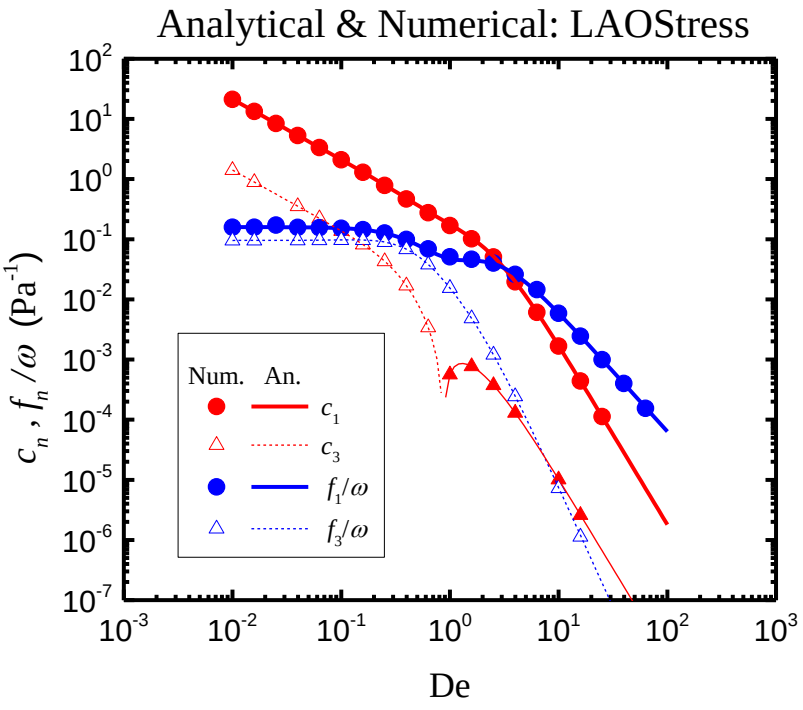

Figure 25 Comparison of analytical solution to data from simulation as verification of the analytical expressions for the stress-kinetic model in LAOStress. Data shown are for $\lambda\kappa_A = 1, H = 0.5$.